Tucholke, B.E., Sibuet, J.-C., Klaus, A., et al., 2004
Proceedings of the Ocean Drilling Program, Initial Reports Volume 210

2. EXPLANATORY NOTES[1]

Shipboard Scientific Party[2]

INTRODUCTION

The "Explanatory Notes" chapter documents the primary procedures and methods employed by the various shipboard laboratories during Leg 210. This information concerns only shipboard methods described in site reports of the Leg 210 *Initial Reports* volume of the *Proceedings of the Ocean Drilling Program* (ODP). Methods for shore-based analysis of Leg 210 samples and data will be described in individual scientific contributions to be published in scientific journals and in the *Scientific Results* volume.

Shipboard Scientific Procedures

Numbering of Sites, Holes, Cores, and Samples

Drill sites are numbered consecutively from the first site drilled by the *Glomar Challenger* in 1968. Multiple holes may be drilled at a single site. For all ODP drill sites, a letter suffix distinguishes each hole drilled at one site. The first hole drilled is assigned the site number modified by the suffix "A," the second hole takes the site number and suffix "B," and so forth.

The cored interval is measured in meters below seafloor (mbsf). The depth below seafloor is determined by subtracting the water depth estimated from the initial drill pipe measurement, which gives the length of pipe from the rig floor to the seafloor (meters below rig floor [mbrf]), from the total drill pipe measurement. Each cored interval is generally 9.5 to 9.6 m long, which is the length of a core barrel. Coring intervals may be shorter and may not necessarily be adjacent if they are separated by drilled intervals.

A recovered core is typically divided into 1.5-m sections that are numbered serially from the top. When full recovery is obtained, the

[1] Examples of how to reference the whole or part of this volume.
[2] Shipboard Scientific Party addresses.

Ms 210IR-102

sections are numbered from 1 through 7, with the last section generally being shorter than 1.5 m (Fig. F1); rarely, an unusually long core may require more than seven sections. When less than full recovery is obtained, there will be as many sections as needed to accommodate the length of the core recovered. By convention, material recovered from the core catcher of a sedimentary core is treated as a separate section during the core description, is labeled core catcher (CC), and is placed below the last section recovered in the liner. The core catcher is assigned to the top of the cored interval in cases where material is recovered only in the core catcher.

When recovered core is shorter than the cored interval, the top of the core by convention is equated to the top of the cored interval to achieve consistency in reporting depth-in-core. Any sample removed from a core is designated by distance measured in centimeters from the top of the section to the top and bottom of the sample removed. A full identification number for a sample consists of the following information: leg, site, hole, core number, core type, section number, piece number (for hard rock), and interval in centimeters measured from the top of section. For example, a sample identification of "210-1276A-3R-3, 80–85 cm" represents a sample removed from the interval 80 to 85 cm below the top of Section 3, Core 3R (R designates that this core was taken with the rotary core barrel coring system) of Hole 1276A during Leg 210 (Fig. F1).

All ODP core identifiers indicate core type. The following abbreviations are used:

R = rotary core barrel.
H = advanced piston corer.
X = extended core barrel.
W = wash core.

Core Handling

Sedimentary Cores

As soon as a core is retrieved on deck, it goes through a sequence of processing steps. Usually a sample is first taken from the core catcher and given to the paleontological laboratory for initial age assessment. The core is then placed on a long horizontal rack outside the laboratory. For safety monitoring, small (~5 cm^3) plugs of sediment are also usually taken from the end of a few sections per core for headspace gas analysis. Gas samples may also be taken by piercing the core liner, typically at voids, and withdrawing gas into a syringe (referred to as vacutainer samples). Next, the core is marked into section lengths, each section is labeled, and the core is cut into sections. If whole-round samples for interstitial water and microbiology are taken, they are removed at this time. For some cores that contain gas, several small holes are drilled into the core liners to allow gas to escape. Each section is then sealed at the top and bottom by attaching color-coded plastic caps—blue to identify the top of a section and clear at the bottom. A yellow cap is placed on section ends where a whole-round sample has been removed, and the sample code is written on the yellow cap. Caps are usually secured to liners by coating the liner ends and inside rims of caps with acetone before attaching the caps. The core sections are then carried into the laboratory, where individual sections are permanently labeled with an engraver. The length of the core in each section and the core catcher

F1. Core, section, and sample numbering, p. 42.

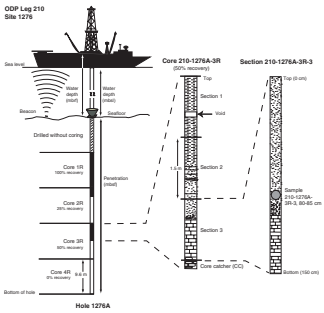

sample are measured to the nearest centimeter; this information is logged into the ODP Janus database.

Once they are in the laboratory and labeled, the whole-round core sections are first run through an X-ray computed tomography (CT) scan imager (see "Whole-Core X-Ray CT Scans," p. 8, in "Lithostratigraphy"). After a core equilibrates to room temperature (~1–3 hr), each core section is run through the multisensor track (MST) and thermal conductivity measurements are made on soft-sediment cores. Whole-round samples for shore-based studies (e.g., consolidation, shear strength, permeability, structure, etc.) may be taken at this stage.

Cores are then split lengthwise into working and archive halves. Softer cores are split with a wire or saw, depending on the degree of induration. Harder cores are split with a band saw or diamond saw. Wire-cut cores are split from bottom to top, so investigators should be aware that older material can be dragged up the core on the split face of each section.

Igneous Cores

Igneous rock cores are handled differently from sediment cores. Once on deck, the core catcher sample is placed at the bottom of the core liner and total core recovery is calculated by pushing the rock pieces together and measuring to the nearest centimeter. The core then is cut into 1.5-m-long sections and transferred into the laboratory. The contents of each section are transferred into 1.5-m-long sections of split core liner, where the bottoms of oriented pieces (i.e., pieces that clearly could not have rotated top to bottom about a horizontal axis in the liner) are marked with red wax pencil. This is done to ensure that orientation is not lost during the splitting and labeling processes. Macroscopic description of the core surface can be performed at this time. Plastic spacers are used to separate individual pieces and/or reconstruct contiguous groups of pieces in the core liner. These spacers may represent substantial intervals of no recovery. The length of each section is then recorded and entered into the database as the curated length. The curated length will commonly differ by a few centimeters from that measured on the catwalk. Each piece of core is then split into archive and working halves, with the positions of spacers maintained for both halves. Each piece is numbered sequentially from the top of each section, beginning with number 1; reconstructed groups of pieces are assigned the same number, but they are lettered sequentially from top to bottom. Pieces are labeled only on the outer, cylindrical surfaces of the core. If the piece is oriented, an arrow is added to the label pointing to the top of the section.

All Cores

For both sedimentary and igneous cores, the archive half is described visually. Smear slides are made from small sediment samples taken from the archive half (all shipboard samples are analyzed on board and then either archived at the ODP core repositories or made available to shipboard scientists for postcruise research). Digital images of the archive halves are made with a digital imaging system (DIS). Most archive sections are run through the archive multisensor track (AMST) for color reflectance spectroscopy measurements and magnetic susceptibility measurements with a point susceptibility meter, and then they are passed through the cryogenic magnetometer for magnetic remanence measurements. The archive half is photographed using both black-and-white and color film. Close-up photographs (both color and black and

white) are taken of particular features for illustrations in the summary of each site, where requested by individual scientists.

The working half of the core is sampled for both shipboard and shore-based laboratory studies. Each sample is logged into the sampling database program by location and by name of the investigator receiving the sample. The ODP curator maintains information about all samples taken. Samples are sealed in plastic vials, cubes, or bags and are labeled. Samples are routinely taken for shipboard physical properties and paleomagnetic, thin section, and geochemistry analyses as described in the sections below.

Following initial shipboard scientific measurements and sampling, both halves of igneous cores are shrink-wrapped in plastic to prevent rock pieces from vibrating out of sequence during subsequent handling. Working and archive halves of both sedimentary and igneous cores are put into labeled plastic "D" tubes, sealed, and transferred to cold-storage space aboard the drilling vessel. During Leg 210, the cores were kept in cold storage until the ship arrived in Galveston, Texas. They were then shipped in refrigerated containers to cold storage at the ODP Bremen Core Repository in Bremen, Germany.

LITHOSTRATIGRAPHY

Lithostratigraphic procedures used during Leg 210 are described under the following headings: Sediment Classification, Visual Core Descriptions, Smear Slide and Thin Section Analyses, Whole-Core X-Ray CT Scans, Digital Imaging, Point Magnetic Susceptibility and Color Reflectance, and X-Ray Diffraction Analysis. In addition, the reader is referred to "Geochemistry," p. 25, for an explanation of carbonate, major element, and trace element analysis of sedimentary rocks.

Sediment Classification

The Leg 210 lithologic classification (Fig. F2) is based on three end-member grain components (biogenic silica, carbonate, and terrigenous or volcanic grains), the grain size of the terrigenous component (i.e., proportions of clay, silt, and sand), and the degree of sediment induration (e.g., chalk vs. limestone). The terms "conglomerate" and "breccia" are the principal names for consolidated gravels with well-rounded and angular clasts, respectively. A sedimentary rock composed of 65% gravel and 35% sand is termed a sandy conglomerate.

Many Leg 210 cores have borderline textures between claystone and mudstone, so different describers might use a different name for the same sediment. In such cases and to de-emphasize minor textural differences, the informal name "mudrock" is used widely in this volume as a synonym for undifferentiated claystone and mudstone. This informal name permits general features of all fine-grained facies to be described together but does not prevent the separate description, where appropriate, of particular features of the claystones or mudstones.

The rock name "grainstone" is utilized to describe a matrix-poor, silt- to sand-grade carbonate (Dunham, 1962). A significant number of the deepwater, coarse silt- to sand-grade turbidites cored at Site 1276 have a carbonate composition or a predominance of carbonate detritus (e.g., peloids, foraminifers, echinoderm fragments, ostracodes, and mollusk fragments) in a mixed carbonate-siliciclastic rock. To clearly distinguish these from siliciclastic siltstones and sandstones, the name grainstone is

F2. Sedimentary rock classification, p. 43.

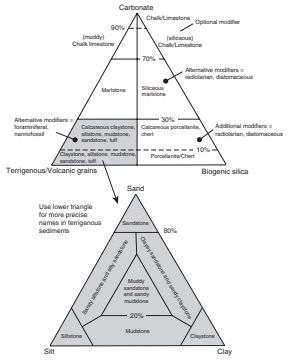

used for these rocks. This term is used even for sediment with a clay-sized matrix (either clay minerals or micrite) of several percent.

Coring during Leg 210 began at ~800 mbsf in lithified sediments, so sedimentary rock names are used throughout. Percentages of end-member grain components, as well as siliciclastic textures used to define lithologies reported on the visual core descriptions (VCDs), were determined with a hand lens, binocular microscope, or smear slide examination of disaggregated core material. Thin sections and carbonate analyses were used to refine or modify lithology designations made at the description table.

Many deposits encountered during Leg 210 are not end-member lithologies but instead grade from one lithology to another. A shorthand notation is used throughout this volume for such upward transitions within single gravity-flow deposits. This notation takes the form of an arrow (→), which indicates that one lithology gradually passes upward into another. Such transitions generally include sediments of intermediate grain size (e.g., sandstone → mudstone usually means a gradual upward change through the various grades of sandstone, through silt-grade material, and eventually into mudstone through progressive fining).

Visual Core Descriptions

Information from macroscopic and microscopic examination of each core section was recorded by hand on a primary description form ("barrel sheet"). This information was then condensed and entered into the AppleCORE program (version 8.1m) to generate simplified VCD forms (Fig. F3). Site, hole, and the depth interval in mbsf are given at the top of each VCD, with section intervals provided along the left margin. Copies of the original barrel sheets, which contain additional detailed core description, are available from the program data librarian by request. The columns depicted on the VCDs are discussed below.

F3. VCD example, p. 44.

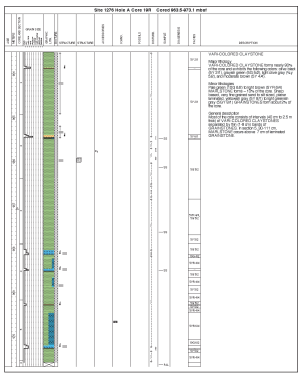

Text Description

The lithologic description on the right side of each VCD consists of five parts: (1) a heading that lists the sediment lithologies in the core; (2) a listing of the major lithologies in the core, together with adjectives to describe the color, state of bioturbation, and nature of bedding; (3) a listing of minor lithologies in the core with adjectives to describe the color, state of bioturbation, and nature of bedding; (4) an overall description of the core including details of facies present and their spatial relationships; and (5) a brief summary of structural features, where appropriate (see "Structural Geology," p. 14).

Age

Core ages are based on shipboard micropaleontological analyses, which are described in "Biostratigraphy," p. 16.

Grain Size

A strip log of grain size is presented to the left of the Graphic Lithology column. This log is based on the estimated grain size of all terrigenous and biogenic components using the Wentworth (1922) scale. The reader should review the text description on each form to ascertain

whether there are interbedded sedimentary rocks or simply mixed sedimentary rock types. Interbedded deposits have one or more vertical lines between the symbols for the separate rock types in the Graphic Lithology column (see below).

Graphic Lithology

The key for rock types (or components in biogenic/terrigenous mixtures) and facies contacts is shown in Figure F4. Lithologic symbols for mixtures of biogenic and terrigenous particles are arranged in the Graphic Lithology column with, from left, terrigenous components from coarsest to finest, carbonate, and biogenic silica components. The exception to this rule is grainstone, which, although a carbonate, is plotted to the far left with sandstone. For interbedded sediments, a single vertical bar between patterns indicates thick bedding (30–100 cm), two vertical lines indicate medium bedding (10–30 cm), and three vertical lines indicate thin bedding (3–10 cm).

A common lithologic style observed in sediment cores during Leg 210 and conjugate-margin Legs 149 and 173 is upward-darkening "motifs," as much as several tens of centimeters thick, consisting of a relatively coarse grained and light-colored calcareous sediment at the base (e.g., calcareous sandy siltstone), overlain by fine-grained, light-colored calcareous claystone to marlstone, and capped by dark claystone or mudstone. The motifs are mostly interpreted as turbidites. Two-component, three-component, and four-component motifs are illustrated elsewhere in this volume (see Fig. F12, p. 135, in the "Site 1276" chapter). Over intervals in which the motifs are too thin to be shown individually (in Cores 210-1276A-9R, 10R, 11R, 23R, and 24R), they are represented in the Graphic Lithology column by parallel columns scaled to reflect the proportion of each component lithology. Over the same interval, in the Sedimentary Structure column, symbols for "graded bedding" and "interbedding" (as very thin to thin or thin to medium alternations) are used to emphasize the interbedded nature of the deposits.

F4. Graphic lithology pattern key, p. 45.

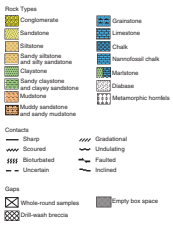

Sedimentary and Tectonic Structures, Accessory Components, and Trace and Body Fossils

Bioturbation is shown by the darkness of a vertical bar to the right of the Graphic Lithology column (Fig. F5). The shades shown in this bar have the AppleCORE names that follow, corresponding to the numerical classification of Droser and Bottjer (1986):

1 = barren.
2 = rare.
3 = moderate.
4 = common.
5 = abundant (pervasive).

The bar is left empty for structureless intervals that appear to be barren but might contain undetected burrows. The locations and types of sedimentary and tectonic structures, lithologic accessories, ichnofossils, body fossils, and diagenetic features are summarized in other columns to the right. Symbols for these features and components are presented in Figure F5.

F5. VCD symbol key, p. 46.

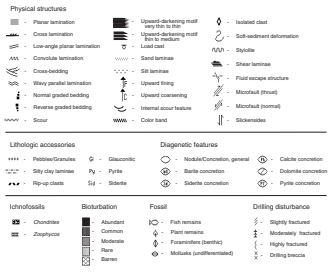

Drilling Disturbance

Different types of drilling disturbance are recorded graphically on each VCD; symbols for the types and degrees of disturbance are shown in Figure F5. Drilling disturbance of lithified sediments is classified into four categories:

1. Slightly fractured: Core pieces are in place with cracks across the core every few centimeters. Some pieces may not be stratigraphically continuous with adjacent pieces where core recovery was incomplete.
2. Moderately fractured: Core pieces are probably in correct stratigraphic sequence but may not represent the entire section. The core is more fractured than in the preceding category.
3. Highly fractured: Core pieces are probably in correct stratigraphic sequence but are strongly fractured and might be rotated. Such intervals are difficult to describe because the fracturing obscures primary features.
4. Breccia: Core pieces have completely lost their original orientation and stratigraphic position and might include cavings from uphole. Descriptions for these intervals have little stratigraphic value.

Over some intervals, no fractures were present at the time the descriptions were made—in such cases, the Drilling Disturbance column is left blank. It was noted while using the computed tomography (CT) scanner (see "Whole-Core X-Ray CT Scans," p. 8) that some cores consisted of long pieces of unbroken rock, whereas after splitting with the saw they were slightly fractured throughout. Clearly, fractures seen in split cores do not all result from drilling and may in part be produced during other stages of core handling.

Samples

Only the positions of smear slides (SS), micropaleontology samples (PAL), microbiology samples (MBIO), and whole-core samples (WHC) are indicated in the Sample column of the VCDs. The locations of other shipboard samples can be found by searching the Janus database on the Integrated Ocean Drilling Program Web site. The appropriate sample codes are:

CARB = organic carbon and inorganic carbon (reported as calculated calcium carbonate),
TSB = thin section,
PP = physical properties,
XRD = X-ray diffraction,
ICP = inorganic geochemistry determined by inductively coupled plasma–atomic emission spectroscopy (ICP-AES), and
SBA = shipboard analysis (inorganic carbon reported as calculated calcium carbonate).

Color

Color was determined by comparison with the Rock Color Chart published by the Geological Society of America in 1984. Color codes are presented in the "Colour" column of the VCDs.

Smear Slide and Thin Section Analyses

Smear slides could be prepared from the moderately consolidated sedimentary rocks and even from some of the fully lithified ones. For each smear slide, a small amount of archive-half sediment was gently crushed and dispersed in a dilute Calgon solution or deionized water on a 22 mm × 40 mm coverslip and then dried on a hot plate at a low setting. A drop of Norland optical adhesive was applied to a prelabeled 25 mm × 75 mm glass microscope slide, after which the coverslip was transferred onto the slide. The slide and coverslip were then cured in an ultraviolet light box. This procedure is different from most preparations, in that the sediment dispersion is prepared on the coverslip rather than on the glass slide. The advantage is that small particles like nannofossils and clay minerals adhere directly to the coverslip and can be viewed at high magnification because they are very close to the top of the slide. Some scientific party members preferred to prepare smear slides directly on the more robust glass slide, otherwise following the procedure outlined above.

Smear slides were examined with a transmitted-light petrographic microscope equipped with a standard eyepiece micrometer to assess the proportions and presence of biogenic and mineral components. Thin sections were described using the same petrographic microscope. Digital photographs were acquired using a Nikon CoolPIX 990 camera with an adapter tube.

Smear slide and thin section data are included in data tables in **"Core Descriptions."** In these tables, components are assigned to one of the following categories:

T = trace (0%–2%).
R = rare (2%–10%).
C = common (10%–25%).
A = abundant (25%–50%).
D = dominant (>50%).

The reader should be aware that quartz and feldspar often cannot be distinguished in smear slides. X-ray Diffraction (XRD) analysis of Leg 210 samples shows considerably higher feldspar content than was estimated from smear slides.

Whole-Core X-Ray CT Scans

An X-ray CT scanner provides rapid acquisition of X-ray images without destruction of samples (e.g., Soh, 1997; Shipboard Scientific Party, 2002). An X-ray beam passes through the sample material, in this case a core and its liner, and is attenuated by interaction with the various constituents in the sample. First, a set of two-dimensional (2-D) X-ray images is acquired at different orientations relative to the core axis; these show integrated densities across the entire thickness of the core. The 2-D image set is then stacked to provide a three-dimensional (3-D) representation of the density variation in the core. This can be sliced in any orientation for later study. These 2-D slices through a 3-D X-ray data cube lack the blurring found in traditional 2-D X-radiographs and are caused by the thickness of the sample. For slices through the data cube, the density distribution is integrated over a thickness of 1 mm or less and it therefore gives a spatially precise map of density variation in the core. The processed 3-D CT images can be viewed using free software,

IMAGEJ, available from the U.S. National Institutes of Health. During Leg 210, only vertical and horizontal slices were examined.

The same portable X-ray CT system used during Leg 204 was installed on the *JOIDES Resolution* for Leg 210. The unit was manufactured by Lawrence Berkeley National Laboratory and is described in detail by Freifeld et al. (2003). During scanning, the core is rotated around its vertical axis. The gantry holding the X-ray source and detector is raised and lowered by a belt-driven actuator to image selected regions of the core. The X-ray source has a tungsten target and a 250-µm beryllium window, delivering as much as 130 kV at 65 W. It has a variable focal-spot size that increases from 5 µm at 4 W to 100 µm at 65 W. A 15-cm image intensifier with a cesium iodide phosphor input screen is coupled to a digital camera for image capture (a Sony XC-75 with a resolution of 768 pixels × 494 pixels and a signal-to-noise ratio of 56 dB). Ten frames of the same image are acquired and averaged to reduce camera noise. A high-resolution monochrome monitor provides real-time viewing of the X-ray images.

During routine core handling, as time permitted, a variable proportion of the sections from recovered cores were viewed in a "quick-scan" mode by rapidly raising the gantry through the 150-cm section without rotation. This streamed 2-D X-ray images to a video monitor. Interesting 9-cm-long intervals that showed sufficient density contrast were then selected for detailed scanning. In these intervals, high-resolution images were obtained and stored digitally for subsequent 3-D reconstruction. The resolution of individual images is ~0.1 mm; 180 separate scans were collected during each rotation about the vertical axis of the section (i.e., a scan for each 2° rotational step).

Many of the sets of high-resolution images could not be used for 3-D reconstruction because the core pieces wobbled in the plastic liner during 360° rotation of the gantry. This was a problem with many of the rotary core barrel (RCB) cores because they were undersized.

Digital processing of the high-resolution images was performed with a National Instruments PCI–409 10-bit frame grabber installed on a personal computer. Image reconstruction software, Imgrec (developed at Lawrence Livermore National Laboratory), was employed to perform convolution backprojection and Feldkamp reconstructions of the acquired cone-beam radiographs. The Feldkamp algorithm corrects for the divergent cone beam angles and can provide an accurate reconstruction of 180 images of a 10-cm section of core in 20 min using a 2.4-GHz Pentium IV processor.

Digital Imaging

All archive halves were scanned using a Geotek DIS. The DIS uses an interference filter and three line-scan charge-coupled device arrays (1024 pixels each) to continuously record the three red-green-blue (RGB) color channels at an 8-bit dynamic range. The standard DIS configuration acquires 300 dpi on an 8-cm-wide core. Synchronization and track control is better than 0.02 mm. A framestore card contains 48 MB of RAM for image acquisition. The camera aperture was set to maximize contrast for the lightest-colored sediment of each core. Each archive section, along with a neutral gray color chip and identification bar-code label, was DIS scanned to produce TIFF (no compression) and SID (compressed) versions. Using the Geotek Image Tools utilities, the SID files were resampled to produce a JPEG file with a resolution of ~300 dpi. The JPEG files are viewable using the Web browser as "photo table"

composite images. Profiles for each RGB channel were produced by averaging pixels in 3 cm × 0.5 cm rectangles along the central axis of the core. The DIS was calibrated for black and white whenever deemed necessary by ODP technical staff. The individual SID images were routinely viewed using MrSID Standalone Viewer (version 2.0). This capability was essential for reviewing previous cores and for preparation of draft figures for site reports.

Point Magnetic Susceptibility and Color Reflectance

Archive-half sections were measured at 2-cm intervals on the AMST with a Bartington MS2 magnetic susceptibility meter at a sensitivity setting of 0.1 instrument units.

Color was measured on the split-core surface of the archive half of selected cores using diffuse-reflected spectrophotometry, available on the AMST. Light reflected from the material was collected in an integration sphere normalized to the source light of the reflectance and calibrated with the measurement of a pure white standard (100% reflection) and a black box (0% reflection) over the entire wavelength spectrum of visible light. Shipboard reflectance was measured using an automated Minolta photospectrometer (CM-2002), which measures the spectral reflectance of surfaces with a diameter >8 mm. To ensure accuracy, the CM-2002 uses a double-beam feedback system, monitoring the illumination on the specimen at the time of measurement and automatically compensating for any changes in the intensity of spectral distribution of the light.

Color is reported using the L*a*b* system. This can be visualized as a cylindrical coordinate system in which the axis of the cylinder is the lightness component L*, ranging from 0% to 100%, and the radii are the chromaticity components a* and b*. Component a* is the green (negative) to red (positive) axis, and component b* is the blue (negative) to yellow (positive) axis.

X-Ray Diffraction Analysis

Selected samples were taken for qualitative mineral analysis by XRD using a Philips diffractometer with CuK_α radiation generated at 40 kV and 35 mA and with a focusing graphite monochromator. The settings were as follows:

Focus = fine.
Irradiated length = 12 mm.
Divergence slit = automatic.
Receiving slit = 0.2 mm.
Step size = 0.02°2θ.
Count time per step = 1 s.
Scanning rate = 2°2θ/min.
Ratemeter time constant = 0.2 s.
Spinner = off.
Monochromator = on.
Scan = continuous.

Bulk samples were freeze-dried, ground with an agate mortar and pestle, and tightly packed in sample holders. The packing, together with the ship's movement, probably imparted some orientation to the mineral powder. These samples were scanned from 2° to 70°2θ. MacDiff software

(version 4.2.5 PPC, freeware distributed by Rainer Petschick) was used to display diffractograms and to identify the minerals. Most diffractograms were corrected to match the main peaks of quartz and calcite at 3.343 and 3.035 Å, respectively. Identifications are based on multiple peak matches with the mineral database provided with the MacDiff software. Relative abundances reported in the site chapters and data tables are useful for general characterization of the sediments, but they are not quantitative concentration data.

IGNEOUS AND METAMORPHIC PETROLOGY

All igneous and metamorphic descriptions and measurements during Leg 210 were made on the archive halves of the cores except where otherwise noted.

The methods used here were designed following the "Explanatory Notes" chapters of the *Initial Reports* volumes for earlier ODP legs, mainly 149 (Shipboard Scientific Party, 1994), 173 (Shipboard Scientific Party, 1998), and 209 (Shipboard Scientific Party, in press). Modifications were made as appropriate in order to meet the specific needs and problems encountered during Leg 210.

Core Curation and Shipboard Sampling

Prior to splitting igneous and metamorphic rock cores, the whole cores were examined for structural features. Each contiguous "piece" was then numbered sequentially from the top of each core section and labeled. Broken core fragments that could be fit together were reassembled into composite pieces; each fragment was lettered consecutively from the top down (e.g., 1A, 1B, 1C, etc.). Composite pieces sometimes occupied more than one core section. Plastic spacers were placed between pieces with different numbers. If it was evident that an individual piece or fragment had not rotated about a horizontal axis during drilling, an arrow was added to the label pointing to the top of the section. The pieces were split with a diamond saw into archive and working halves. Cores were split so as to allow important features and structures to be represented in both the working and archive halves.

Visual Core Descriptions of Igneous and Metamorphic Rocks

A VCD form was designed to record petrology and structural observations of both igneous and metamorphic rocks (Fig. F6). The left column is a graphic representation of the archive half of the core. A horizontal line across the entire width of the Graphic Representation column denotes a plastic spacer. Pieces that could be oriented vertically are indicated on the form by an arrow pointing upward to the right of the piece. Symbols were designed to graphically illustrate the mineralogy and structures observed in the cores (Fig. F7). During core description, representative samples of the main lithologies were taken from the working half for XRD analysis to confirm mineral identities. For each lithologic unit, representative samples were examined in the working half of the core (where recovery permitted) for shipboard physical property analysis, magnetic studies, ICP-AES, and polished thin section studies. Samples were oriented with respect to the core face. Where feasible, cubes or minicores for physical property measurements were

F6. Igneous and metamorphic rock VCD forms, p. 47.

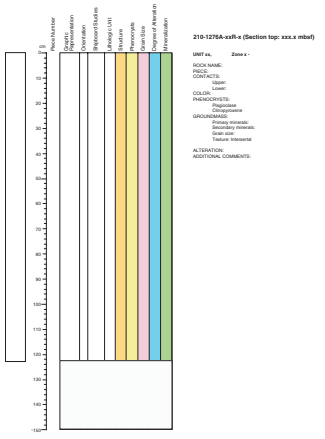

F7. Key to VCD symbols, p. 48.

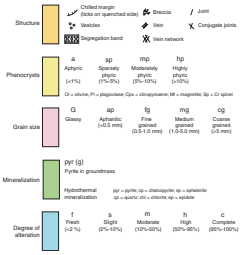

taken immediately adjacent to samples used for chemical analyses and polished thin sections.

Shipboard samples and studies are indicated in the column headed Shipboard Studies, using the following notation:

XRD = X-ray diffraction analysis.
ICP = inductively coupled plasma–atomic emission spectroscopy.
TS = petrographic thin section.
PP = physical property measurements.
PM = paleomagnetic measurement.
SS = smear slide.

Digital core images were recorded for all archive halves, and images were used to aid petrological description. For VCDs of igneous and metamorphic rocks, see the **"Visual Core Descriptions"** for each site.

Rock Classification

The classification of igneous and metamorphic rocks is based on texture, grain size, mineral occurrence and abundance, rock composition, and rock clast type. When modal analyses could be reliably obtained, igneous rocks were classified according to essential primary minerals and/or chemical analyses following standard International Union of Geodesy and Geophysics nomenclature (Streckeisen, 1976; Le Bas et al., 1986). Rocks for which the protolith is completely obscured by metamorphism or alteration processes were given separate lithologic names. If the original rock type was discernible, the prefix "meta" or the term "altered" was used as a modifier with the name of the protolith. Any postemplacement changes in mineralogy or structure associated with elevated temperatures or pressures were classified as "metamorphic." We reserved the term "altered" for rocks that have undergone low-temperature hydrothermal alteration or seafloor weathering. Igneous minerals were termed "primary." Minerals affected by hydrothermal alteration or metamorphic processes were termed "secondary." Rock classification and description of mafic and ultramafic rocks are referenced to the "Igneous Petrology" and "Metamorphic Petrology" sections in the "Explanatory Notes" chapter of the Leg 209 *Initial Reports* volume (Shipboard Scientific Party, in press). Modifications were made as appropriate in order to meet the specific needs and problems encountered during Leg 210.

The primary and secondary rock-forming minerals were recorded in a short description added to the VCD. The primary rock-forming minerals found at Sites 1276 and 1277 include olivine, orthopyroxene, clinopyroxene, spinel, Fe-Ti oxide, plagioclase, and amphibole. Mica, apatite, oxide and sulfide minerals, and other minerals of magmatic origin such as zircon were recorded as accessory minerals. Secondary minerals include clay minerals (smectite, kaolinite, chlorite, and serpentine), analcime, pyrite, calcite, and quartz. For each rock type, the following data were recorded in a log accompanying the VCD:

1. Rock name;
2. Piece belonging to the same "rock type;"
3. Place and nature of contacts;
4. Color;
5. Composition and type of phenocrysts;
6. Composition, grain size, and texture of groundmass; and
7. Alteration/veins/structures and additional comments.

On the VCD forms the modal percentage of the mineral includes both the fresh and altered parts of the mineral recorded in the piece. Grain size is recorded for the primary minerals and refers to the average long dimension of the minerals and is given in millimeters, as are the minimum and maximum crystal sizes. The crystal shape of the primary minerals describes the aspect ratio of the grains and is used when the deformation has modified the original crystal morphology. The aspect ratio is the ratio of the long to the short dimension of the crystal. The terms euhedral, subhedral, anhedral, and interstitial are used to describe the shapes of crystals preserving an igneous morphology. The shapes are divided into four classes: (1) equant (<2:1 aspect ratio), (2) subequant (2:1–3:1 aspect ratio), (3) tabular (3:1–5:1 aspect ratio), and (4) elongate (>5:1 aspect ratio).

When describing the texture and structure of the igneous cores, a separate description is required for diabase and gabbroic rocks and for basaltic rocks. In diabase and gabbroic rocks, the texture is defined by the grain size and the extent of igneous foliation that is developed. Diabases have grain sizes that range from too small to be discerned by the unaided eye to fine grained; microgabbros are fine grained; gabbros are medium grained or coarser. The textural distinction between diabases and microgabbros is based on the modal homogeneity of the sample. Diabases are defined as having a felty texture with randomly distributed plagioclase laths throughout and are modally homogeneous. Microgabbros can have felty textured plagioclase with distinctive modal segregations of plagioclase laths into a framework in the sample, or they can be more massive.

When describing basaltic rocks, the proportions and characters of phenocrysts and vesicles define the following textures:

1. Aphyric (phenocrysts occupy <1%),
2. Porphyritic (phenocrysts occupy >1% and are surrounded by finer-grained groundmass),
3. Seriate (the crystals of the principal minerals show a continuous range of sizes),
4. Poikilitic (relatively large crystals of one mineral "oikocryst" enclose smaller crystals of one or more other minerals ["chadacrysts"]),
5. Glomerocrystic (a porphyritic texture where the phenocrysts are clustered), and
6. Vesicular (vesicles occupy >10%).

Where segregations, bands, and veins were observed in the cores, the orientation, frequency, and mineralization were recorded on the VCD. The word "vein" was used to describe features formed by precipitation from nonmagmatic fluids, and the abundance, connectivity, and dimension of the veins was noted. Segregation bands are formed by different chemistries of the magma as it flowed through the igneous intrusive unit.

The terms metamorphism, metasomatism, and hydrothermal alteration are used loosely and synonymously without making implications about open- vs. closed-system behavior. The VCDs (alteration log) provide information on the degree of hydrothermal mineral alteration seen in the pieces and in thin section. This takes into account the extent of replacement of igneous minerals by secondary minerals and the nature and approximate modes of secondary mineral assemblages. These data were merged with the estimated primary modes to calculate

the total extent of rock alteration. Further, the extent to which metamorphic minerals contribute to any subsolidus fabric was recorded in the comments on the VCD. Alteration intensity was classified as follows: fresh (<2%), slight (2%–10%), moderate (10%–40%), high (40%–80%), very high (80%–95%), and complete (>95%).

Thin Section Descriptions

Thin sections were examined to complement and refine the hand specimen observations. The same terminology used for megascopic descriptions was used for thin section descriptions. The percentages and textural descriptions of individual phases are reported. Thin section descriptions are included in the "Core Descriptions" contents list.

STRUCTURAL GEOLOGY

Structural studies performed on the cores from Leg 210 were designed to

1. Document all deformation structures in a systematic and quantitative way,
2. Establish the relative timing (overprinting relations) and probable range of pressure-temperature conditions under which individual structures formed,
3. Record the orientations of all structures observed on the core surface in three dimensions in a core reference frame (Fig. F8), and
4. Assess the role of fluids and compaction in deformation processes.

F8. ODP core reference frame, p. 49.

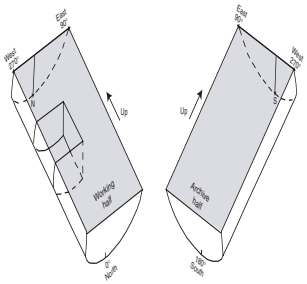

The methods used here were designed following the "Explanatory Notes" chapters of the *Initial Reports* volumes for earlier ODP legs, mainly Legs 141 (Shipboard Scientific Party, 1992), 149 (Shipboard Scientific Party, 1994), 160 (Shipboard Scientific Party, 1996), and 173 (Shipboard Scientific Party, 1998). Modifications were made as appropriate in order to meet the specific needs and problems encountered during Leg 210.

An important consideration is that commonly only part of the cored interval is actually recovered. This leads to a sampling bias that for structural purposes can be acute. In particular, in cases of incomplete recovery, material from fault zones may be missing. When faulted or fractured rock from such zones is recovered, it is often highly disturbed and its original orientation has changed. Further limitations are created by drilling-induced deformation and rotation in cores. Features are considered to be drilling induced if their origin is doubtful.

Graphical Representation and Terminology

The structures on the cut face of the archive half of the core were included on the VCD form where deformation structures were considered to be either important or common (see "Visual Core Descriptions," p. 5). Details that could not be included on the VCDs are available on the handwritten barrel sheets from the program data librarian. The descriptive terminology we used for deformation structures in hard and soft rocks follows Ramsay and Huber (1983, 1987), and terminology

more particular to sediments follows Maltman (1994). For microstructures, we applied the terminology of Passchier and Trouw (1996).

Structural Measurements

Determining the orientation of observed structures (and intrusive dikes) in the geographical reference frame is difficult. Therefore, structures were oriented with respect to the core reference frame. The core reference frame was chosen according to the conventions used for ODP magnetic measurements to allow direct comparison with the paleomagnetic results (Fig. **F8;** also see Fig. **F12**). The plane perpendicular to the long axis of the core was taken as the horizontal. "North," "south," "east," and "west" were defined in this plane in the following manner. South (azimuth = 180°) is the direction perpendicular to the cut surface of the archive half, pointing toward the cylindrical outer surface of the archive half. Consequently, north (azimuth = 000°) is the opposite direction, pointing into the cut face of the working half. With the archive half oriented top up, west (270°) is directed toward the right side of the surface of the archive half and east (090°) is toward the left side. The orientations of planar and linear elements in the core were documented using dip azimuth and dip angle (Fig. **F9**). The orientation is always expressed by two numbers; the first indicates the dip azimuth, expressed by three digits, and the second indicates the dip angle, expressed by two digits (i.e., 090/45 means a plane or a line dipping or plunging east at an angle of 45°).

F9. Azimuth and dip measuring convention, p. 50.

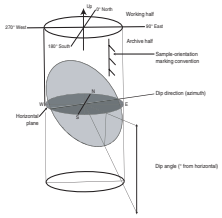

Measurements of orientations of planar structures observed in the cores were made using a protractor. For planar elements, the apparent dip on the core face was measured as either dipping toward the east or toward the west. The orientation of the planar element was then further constrained using an additional measurement either from the horizontal plane (top or bottom of core piece) or from the cylindrical outer surface of the core half, as shown in Figure **F9.** The two measurements yielded the orientations of two lines contained within the planar element. The orientation of the planar element itself was then determined from the orientation of the two lines using a stereonet. This procedure provided the working azimuth and dip of the observed structure (i.e., the azimuth and dip within the core reference frame). The dip is "true," as long as the core axis is approximately vertical. The orientations of linear structures were recorded as "working trends." These were measured using dip azimuth and dip angle and referred to the core reference frame in the same way as planar surfaces (Fig. **F8**). If cut surfaces were parallel to azimuth of lineations and perpendicular to azimuth of faults, dips could be measured directly. Mineral and/or mylonitic foliations and lineations were measured in much the same way as faults and veins.

The sense of fault displacement was recorded and referred to as normal, reverse, sinistral strike-slip, or dextral strike-slip. The apparent displacement was measured on the core face and/or on the top or bottom side of pieces. In cases where the direction of slip was visible, offset was measured in a plane normal to the fault and parallel to slip direction, as straight-line separation between displaced markers.

Geographic Orientation of Structures

At this stage, structures were oriented in the core reference frame shown in Figure **F8,** but they were not oriented with respect to geo-

graphic ordinates. In some cases, viscous remanent magnetization (VRM), considered to be parallel to the present-day magnetic field, can be used to orient cores to the geographic frame. Unfortunately, the VRM was dominated by drilling effects during Leg 210 (see "Paleomagnetism," p. 22), so it was generally not possible to reorient structural features in cores.

No downhole logging was conducted during Leg 210 because of poor hole conditions, so no Formation MicroScanner data were available for core reorientation.

Thin Section Description

Thin sections of sedimentary, igneous, and metamorphic rocks recovered during Leg 210 were examined in order to

1. Document each type of macroscopic deformation structure in a systematic and quantitative way,
2. Characterize the microstructure of the rocks,
3. Provide information on the kinematics of ductile and brittle deformation,
4. Assess the role of fluids in contributing to deformation, and
5. Document major structural zones and downhole variations.

For the description of microstructures, we applied the terminology of Passchier and Trouw (1996). Shipboard thin sections were oriented, except when they were made from small pieces whose orientation with respect to the rest of the core was unknown. Orientation was in the core reference frame and was marked on each thin section by an arrow pointing upward and a short tick pointing toward west from the base of the arrow. Marking two directions is necessary in order to achieve complete orientation of thin sections, which are cut parallel to the split surface of the core.

BIOSTRATIGRAPHY

Preliminary age assignments were based on biostratigraphic analyses of calcareous nannofossils, planktonic foraminifers, radiolarians, and palynomorphs. Paleodepth interpretations were based on benthic foraminifers. All core catcher samples were analyzed for calcareous nannofossils, planktonic foraminifers, benthic foraminifers, and radiolarians, and select core catcher samples were analyzed for palynomorphs. Additional samples were examined for calcareous nannofossils and planktonic foraminifers, including thin sections for the latter group, in order to refine the biostratigraphy where appropriate and to focus on unconformities and other critical intervals. The preservation, abundance, and zonal assignment for each sample and for each microfossil group were recorded in the stratigraphic site summary sheets (see Table **T7,** p. 331, in the "Site 1276" chapter). The timescale of Berggren et al. (1995b) is applied in the Cenozoic, and timescales of Gradstein et al. (1995) and Channell et al. (1995) are used for the Cretaceous (Figs. **F10, F11**).

Calcareous Microfossil Datums

Ages of Cenozoic calcareous nannofossil and planktonic foraminifer first occurrence (FO or datum base) and last occurrence (LO or datum

F10. Calcareous microfossil timescale, p. 51.

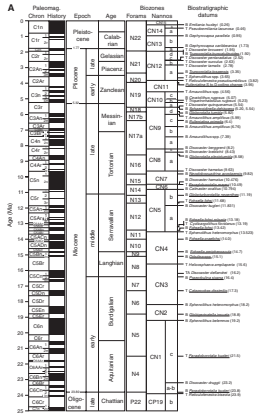

F11. Calcareous and siliceous microfossil timescale, p. 56.

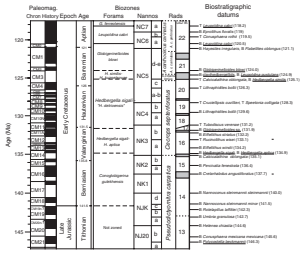

top) older than 14 Ma follow Berggren et al. (1995b); younger datums are astrochronologically tuned ages from several sources (Shackleton et al., 1995; Backman and Raffi, 1997; Chaisson and Pearson, 1997). Ages for Cenozoic datums are presented in Tables T1 and T2. Age estimates for Cretaceous calcareous nannofossil and planktonic foraminiferal datums are from Erba et al. (1995), Bralower et al. (1997), Premoli Silva and Sliter (1999), and Gardin et al. (2001). Cretaceous datums are presented in Tables T3 and T4.

T1. Cenozoic calcareous nannofossil datums, p. 58.

T2. Cenozoic planktonic foraminiferal datums, p. 60.

T3. Cretaceous calcareous nannofossil datums, p. 62.

T4. Cretaceous planktonic foraminiferal datums, p. 63.

Zonal Schemes

Calcareous Nannofossil Zonal Scheme and Taxonomy

The zonal scheme of Bukry (1973, 1975; zonal code numbers CN and CP added and modified by Okada and Bukry, 1980) is used for Cenozoic calcareous nannofossil biostratigraphy (Table T1). The zonal schemes of Sissingh (1977; CC zones), as modified by Perch-Nielsen (1985), Applegate and Bergen (1988; Lower Cretaceous subzones), and Burnett (1999; UC zones) are used for the Late Cretaceous, and those of Roth (1973, 1983; NC zones), with subdivisions by Bralower et al. (1993), are used for the Early Cretaceous (Table T3). The zonal scheme of Bralower et al. (1989; NK and NJK zones) is applied for the Jurassic/Cretaceous boundary interval. All of these zonations represent a general framework for the biostratigraphic classification of mid- to low-latitude nannofloral assemblages and are presented in Figures F10 and F11. Cenozoic and Cretaceous nannofossil taxonomy is in accordance with that cited in Perch-Nielsen (1985), Firth and Wise (1992), and Bown (1998), where full taxonomic lists can be found.

Planktonic Foraminiferal Zonal Scheme and Taxonomy

The tropical planktonic foraminiferal zonal scheme (N and P zones) used for the Cenozoic follows Berggren et al. (1995b) (Table T2). The zonation used for Cretaceous planktonic foraminifers is based on the tropical zonal schemes of Caron (1985) and Sliter (1989; KS zones), with modifications by Bralower et al. (1993, 1995, 1997) and Premoli Silva and Sliter (1994, 1999) (Table T4; Fig. F10). Cenozoic taxonomic concepts follow Postuma (1971), Kennett and Srinivasan (1983), Bolli and Saunders (1985), Toumarkine and Luterbacher (1985), Spezzaferri and Premoli Silva (1991), Chaisson and Leckie (1993), Leckie et al. (1993), Spezzaferri (1994), Pearson (1995), Berggren and Norris (1997), Chaisson and Pearson (1997), Pearson and Chaisson (1997), Norris (1998), and Olsson et al. (1999). Genus-species combinations generally follow those used by Berggren et al. (1995b) with few modifications. Cretaceous taxonomic concepts are based on Longoria (1974), Robaszynski and Caron (1979), Leckie (1984), Robaszynski et al. (1984), Caron (1985), Nederbragt (1990, 1991), Coccioni and Premoli Silva (1994), and Petrizzo (2000, 2001).

Benthic Foraminiferal Taxonomy and Paleodepth Determination

At suprageneric levels, the classification scheme of Loeblich and Tappan (1988) is followed. Cenozoic (Paleogene) benthic foraminiferal taxonomic concepts are mainly based on Tjalsma and Lohmann (1983), van Morkhoven et al. (1986), Kaiho (1992), and Bolli et al. (1994). Cre-

taceous taxonomic concepts follow Luterbacher (1973), Sliter (1977, 1980), Gradstein (1978), Bolli et al. (1994), Holbourn and Kaminski (1997), and Kuhnt and Urquhart (2001).

Cenozoic paleodepth estimates are based on the work of Pflum and Frerichs (1976), Woodruff (1985), and van Morkhoven et al. (1986). For the Cretaceous section, estimates are mainly based on the studies of Nyong and Olsson (1984), Holbourn et al. (2001), and backtracked paleodepth curves from Deep Sea Drilling Project (DSDP) and ODP data of Kaiho (1999). The following paleodepth terminology is applied (after van Morkhoven et al., 1986):

Neritic = 0–200 m.
Upper bathyal = 200–600 m.
Middle and lower bathyal = 600–2000 m.
Abyssal = >2000 m.

Radiolarian Zonal Scheme and Taxonomy

Radiolarian biostratigraphy studied during Leg 210 is based largely on the radiolarian zonation and code numbers tied to the global polarity timescale of Cande and Kent (1995) and documented by Sanfilippo and Nigrini (1998). Supplemental markers, also derived from Sanfilippo and Nigrini (1998), are used whenever possible and correlate with the data supplied by calcareous nannofossils and planktonic foraminifers.

The taxonomy of Early Cretaceous radiolarians is based on Baumgartner et al. (1995b). Eleven radiolarian Unitary Association Zones (UAZ) characterize the uppermost Jurassic and Lower Cretaceous and can be used for biostratigraphic correlation (Baumgartner et al., 1995a). A Unitary Association is a "maximal set of mutually compatible taxa" (Baumgartner et al., 1995a, p. 1014). The age correlation of radiolarian UAZs in the upper Barremian–Aptian interval follows Erba et al. (1999), and the uppermost Jurassic–lower Barremian interval is correlated to the Mesozoic polarity chronozones (Gradstein et al., 1995) by Baumgartner et al. (1995a).

Palynomorph Zonal Scheme and Taxonomy

Leg 210 palynomorph biostratigraphy is based largely on the work of Powell (1992) and Williams et al. (unpubl. data [N1]) for the Paleogene and Stover et al. (1996), Duxbury (2001), and Williams et al. (unpubl. data [N1]) for the Cretaceous. Absolute ages for FO and LO datums of selected taxa are after Williams et al. (unpubl. data [N1]) (Table T5). Dinoflagellate cyst taxonomy is in accordance with that cited in Williams et al. (1998).

T5. Paleogene and Late Cretaceous dinocyst datums, p. 64.

Methods of Study

Calcareous Nannofossils

Calcareous nannofossils were examined in smear slides using standard light-microscope techniques, under cross-polarized, transmitted, and phase-contrast light at 1250×. The following abbreviations are used to describe nannofossil preservation:

VG = very good (no evidence of dissolution and/or recrystallization; no alteration of primary morphological characteristics, and

specimens appear diaphanous; specimens are identifiable to the species level).
G = good (little or no evidence of dissolution and/or recrystallization; primary morphological characteristics only slightly altered; specimens are identifiable to the species level).
M = moderate (specimens exhibit some etching and/or recrystallization; primary morphological characteristics are somewhat altered; however, most specimens are identifiable to the species level).
P = poor (specimens are severely etched or overgrown; primary morphological characteristics are largely destroyed; fragmentation has occurred; specimens often cannot be identified at the species and/or generic level).

Five calcareous nannofossil relative abundance levels are recorded as follows:

VA = very abundant (>100 specimens per field of view).
A = abundant (11–100 specimens per field of view).
C = common (2–10 specimens per field of view).
F = frequent (1 specimen per 1–10 fields of view).
R = rare (<1 specimen per 10 fields of view).

Foraminifers

Unlithified sediment was soaked in a 3% solution of hydrogen peroxide (H_2O_2) with a small amount of Calgon added, warmed on a hot plate, and then washed with tap water over a 63-µm or 45-µm sieve (Lower Cretaceous interval). H_2O_2 was used in the interest of time efficiency and to keep pace with drilling operations. As a consequence, some of the agglutinated foraminiferal taxa, which incorporate organic cement into their tests, may have been eliminated from the processed residues.

Semilithified claystone, mudstone, and shale were first partially fragmented by hand and then soaked in hydrogen peroxide and Calgon before washing; lithified samples were first crushed using a Carver laboratory press in order to facilitate disaggregation. After every use, the sieve was dipped in a dilute solution of methyl blue dye to identify contaminants from previous samples. All samples (residues >63 or 45 µm) were dried on filter paper placed on a hot plate at ~50°C.

Samples within 0.5 m above the Cretaceous/Tertiary boundary were treated the same as other unlithified sediment samples, except that a 38-µm sieve was used to catch the dwarf microfossil assemblages.

Species identifications for planktonic foraminifers were generally made on the >63-µm fraction, although the >250- and >150-µm size fractions were carefully scanned for larger age-diagnostic taxa and other constituents of the sand-sized residues. In addition to planktonic foraminiferal species, other biotic (e.g., radiolarians, sponge spicules, echinoid spines, fish bone/teeth, ostracodes, and inoceramid prisms) and mineral (glauconite, pyrite, and phosphate pellets) constituents were noted in each of the core catcher residues. Two picking trays per sample from the >63-µm fraction were examined to identify benthic foraminifers and estimate their abundance.

The following abundances of species (in relation to total foraminifers) were estimated from visual examination of dried samples of planktonic foraminifers:

D = dominant (>30%).
A = abundant (10%–30%).
F = few (5%–10%).
R = rare (1%–5%).
P = present (<1%).

The following abundance categories were used for relative benthic foraminiferal abundance based on the number of benthic foraminifers encountered in two picking trays:

A = abundant (>100 specimens).
C = common (51–100 specimens).
F = few (21–50 specimens).
R = rare (10–20 specimens).
T = trace (<10 specimens).

The preservation status of the planktonic and benthic foraminifers was estimated as follows:

VG = very good (no evidence of overgrowth, dissolution, or abrasion).
G = good (little evidence of overgrowth, dissolution, or abrasion).
M = moderate (common calcite overgrowth, dissolution, abrasion, or minor fragmentation).
P = poor (substantial overgrowth, dissolution, or extensive fragmentation).

Radiolarians

The presence/absence of radiolarians in core catcher samples was evaluated from the foraminiferal residue and in slides prepared for palynology.

Total radiolarian abundance was determined based on strewn-slide evaluation at 100×, using the following convention:

A = abundant (>100 specimens per slide traverse).
C = common (51–100 specimens per slide traverse).
F = few (11–50 specimens per slide traverse).
R = rare (1–10 specimens per slide traverse).
T = trace (<1 specimen per slide traverse).
B = barren (no radiolarians in sample).

The abundance of individual radiolarian species was estimated as a fraction of the total assemblages as follows:

A = abundant (>10% of the total assemblage).
C = common (5%–10% of the total assemblage).
F = few (<5% of the total assemblage).
R = rare (a few or more specimens per slide).
T = trace (present in slide).
B = barren (absent).

Radiolarian preservation was recorded as follows:

G = good (majority of specimens complete, with minor dissolution, recrystallization, and/or breakage).

M = moderate (minor but common dissolution, with a small amount of breakage of specimens).
P = poor (strong dissolution, recrystallization, or breakage; many specimens unidentifiable).

Palynomorphs

Up to 20 cm^3 of sample was processed following standard palynological techniques (e.g., Pross, 2001). Samples composed of fine-grained, dark-colored detrital material were selected wherever possible. Briefly, the processing procedure included digestion by HCl and HF, with centrifuging and rinsing through a stainless steel 20-µm mesh after each step. If necessary, the recovered residue was then treated with nitric acid to partially oxidize the organic matter and with potassium hydroxide solution to remove humic acids. For some samples from quartz-rich sediments, heavy-liquid separation using a $ZnCl_2$ solution was completed. Residues were partly stained with Safranine to improve palynomorph visibility. Finally, residues from each sample were strew mounted on glass slides using glycerine jelly. For biostratigraphic purposes, a minimum of two slides were prepared and evaluated.

Preservation was classified as one of the following:

G = good.
M = moderate.
P = poor.

Sedimentation Rates

To determine sedimentation rates, one must first generate an age-depth relationship. Paleomagnetic stratigraphy with unambiguously defined chrons can be a prime tool in this determination, but, unfortunately, a polarity-reversal history was not well resolved in Leg 210 holes. Instead, we had to rely on biostratigraphic data.

Where biostratigraphic datums are used, the chief uncertainty in determining sedimentation rates arises from the fact that with a limited amount of time for study, many datums are determined to lie between widely separated samples. During many ODP legs, it has been necessary to reconstruct sedimentation rates using datums determined only from core catcher samples (i.e., within 9.5 m). The amount of uncertainty in each sedimentation-rate estimate derived in this way is defined by the thickness of the interval over which the rate is averaged, divided by the combined age uncertainty in the top and bottom controls.

A second source of uncertainty is the accuracy with which datums can be picked in the cores. This depends on fossil abundance, preservation, and reworking, as well as the fossil assemblage (one or several groups) that is available for study. Finally, there is uncertainty in the absolute ages of the datums as defined by the timescale that is used.

Sedimentation rates (in meters per million years) were estimated from age-depth plots by drawing best-fit lines through all the biostratigraphic data over successive depth intervals (i.e., by drawing straight-line segments through discrete intervals of data). Sedimentation rates were calculated using midpoints in the observed range of uncertainty in sample age or datum depth.

PALEOMAGNETISM

Paleomagnetic studies conducted aboard the *JOIDES Resolution* during Leg 210 consisted of routine measurements of natural remanent magnetization (NRM) and magnetic susceptibility of sediments and rocks. NRM was measured on all archive halves of recovered sediments and rocks and on discrete samples taken from the working halves. Stepwise alternating-field (AF) demagnetization was conducted on all archive halves and on some discrete samples in an attempt to isolate stable components of remanence. A few discrete samples were thermally demagnetized in an effort to obtain their primary remanent magnetization and to identify magnetic carriers. Magnetic susceptibility was measured on archive halves and, in a few cases, on discrete samples.

Laboratory Instruments

The remanence of archive halves and oriented discrete samples from working halves was measured using a 2G Enterprises pass-through cryogenic direct-current superconducting quantum-interference-device rock magnetometer (model 760R). This magnetometer is equipped with an in-line AF demagnetizer (2G model 2G600) that allows for demagnetization of samples up to peak fields of 80 mT with a 200 Hz frequency. The practical limit on the resolution of natural remanence of core samples is imposed by the magnetization of the core liner itself (~0.01 mA/m). The magnetometer and AF demagnetizer are interfaced to a computer and are controlled by the 2G Long Core software by National Instruments. A Molspin spinner magnetometer was also available on the ship for measuring the remanence of discrete samples. For stepwise demagnetization of discrete samples, the laboratory contains an AF demagnetizer (model D-2000 by DTech Inc.) and a thermal demagnetizer (model TSD-1 by Schonstedt Instrument Co.) capable of demagnetizing specimens to 200 mT and 700°C, respectively. An Analytical Services Company model IM-10 impulse magnetizer (capable of pulsed fields from 0.02 to 1.35 T) and a PARM-2 system by DTech Inc. were available for anhysteretic and isothermal remanent magnetization (IRM) acquisition studies of discrete samples. A Geofyzika Brno Kappabridge KLY-2 magnetic susceptibility meter was available for magnetic susceptibility measurements of discrete samples.

Core Orientation and Sampling Method

The standard ODP core orientation convention was applied for paleomagnetic work during Leg 210. This convention is described as follows. The positive z-axis direction is downhole, parallel to the core. The x-axis forms a line perpendicular to the split face of the core and is directed into the working half (Fig. **F12**). The positive x-axis direction is used as the reference "geomagnetic north" (also "north" in the structural geologists' reference frame) for the definition of magnetic declination values. The positive y-axis direction is left along the split surface of the archive half when looking upcore (see Fig. **F12**).

Discrete samples of the softer sediments were taken using oriented standard plastic boxes (7 cm^3), with an arrow pointing in the uphole direction (Fig. **F12**). In order to reduce the deformation of the sediment, the core was cut using a thin stainless steel spatula before pressing the plastic boxes into the sediment. Minicores (10 cm^3) were drilled from

F12. Magnetic orientation convention, p. 57.

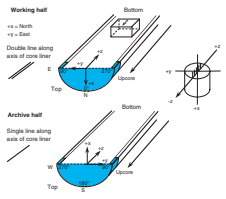

lithified sedimentary and crystalline rocks using a water-cooled nonmagnetic drill bit attached to a standard drill press. Minicores were oriented as for the samples just described, with an arrow pointing in the uphole direction. Discrete samples used in pilot demagnetization studies were typically taken in increments of one or two per section. However, discrete samples were taken at smaller increments (as little as every 10 cm) to examine geomagnetic reversals, key geologic boundaries, or other intervals of interest.

Remanent Magnetization Measurements

Tests conducted during previous legs (e.g., Leg 131) indicate that in cases where the core is not uniformly magnetized, either because of natural processes or artifacts (voids in the core or differential rotation of segments within the core liner [biscuiting]), the values of declination, inclination, and intensity need careful evaluation. For this reason, at least one discrete shipboard paleomagnetic sample was taken from each section and from each representative lithology for progressive AF and/or thermal demagnetization to characterize the magnetic behavior.

The NRM and remanence after progressive AF demagnetization were routinely measured on all archive halves at 2-cm intervals. For shipboard analyses, measurements within 10 cm of the ends of each section were disregarded because of end effects. Progressive AF demagnetization steps, incremented by 10 mT, were typically 10, 20, 30, 40, 50, and 60 mT, as required, to remove drilling overprints and to resolve the characteristic remanent magnetization. To isolate stable remanence, stepwise thermal demagnetization up to 580°C was also applied to some discrete samples using the Schonstedt thermal specimen demagnetizer. The magnetic susceptibility of the samples was monitored between each temperature step to assess any irreversible mineralogical changes associated with heating.

Perturbations by Drilling

Mechanical disturbance of unconsolidated sediments can occur during rotary coring, which complicates the interpretation of measurements made by the pass-through cryogenic magnetometer. Another persistent problem is the pervasive remagnetization associated with drilling. As noted during previous legs, discrete samples taken from the center of the working half of the core tend to show shallower inclinations. This indicates that the intensity of the drilling-induced overprint increases radially from the center to the edge of the core, and it suggests that the core barrel is the most significant source of the overprint. Isolation of the primary component of magnetization in the discrete samples generally required AF demagnetization of 20 to 30 mT. Thus, the drilling-induced remagnetization can be considered as a viscous remanence, or it may be comparable to a strong-field (>20 mT) IRM.

Starting with Core 210-1276A-59R, a nonmagnetic RCB was used for all odd-numbered cores, whereas even-numbered cores were recovered with a regular RCB. Sedimentary rocks from Cores 210-1276A-58R through 68R in Unit 5 (see **"Lithostratigraphy,"** p. 20, in the "Site 1276" chapter) have uniform lithology and composition, and these sediments all have a single normal polarity. Thus, we could test the effects of the regular vs. nonmagnetic RCBs on remanence intensity of these cores. The results clearly indicate that cores obtained with a regular core

barrel are more strongly magnetized than those obtained with the nonmagnetic core barrel.

Magnetostratigraphy

Where magnetic cleaning successfully isolated the primary component of remanence, paleomagnetic inclinations were used to assign a magnetic polarity to the stratigraphic column. The revised polarity timescale of Cande and Kent (1995), as presented in Berggren et al. (1995a, 1995b), was used as a reference for the ages of Cenozoic polarity chrons. The timescale of Gradstein et al. (1995) was used for Mesozoic rocks and sediments (Table T6).

T6. Cenozoic and Cretaceous normal polarity intervals, p. 66.

Magnetic Susceptibility Measurements and the Königsberger Ratio

Magnetic susceptibility was measured for each whole-core section as part of the MST analysis (see "Multisensor Track Measurements," p. 29). Susceptibility was measured on the MST using a Bartington MS2 meter coupled to a MS2C sensor coil with a diameter of 88 cm operating at 0.565 kHz. The sensor was set on SI units, and the data were stored in the Janus database in raw meter units. The sensor coil is sensitive over an interval of ~4 cm (half-power width of the response curve), and the width of the sensing region corresponds to a volume of 166 cm^3 of cored material. To convert to true SI volume susceptibilities, these values should be multiplied by 10^{-5} and then multiplied by a correction factor to account for the actual volume of material that passed through the susceptibility coils. Except for measurements near the ends of each section, the correction factor for a standard full ODP core is ~0.66 (= 1/1.5). The end effect of each core section is not adequately corrected using this procedure.

The magnetic susceptibility of archive halves was also routinely measured using the AMST at 2-cm intervals. The measurements were automatically recorded by the AMST, which permits measurements only at evenly spaced intervals along each section of core. For the two types of susceptibility measurements (MST and AMST), the same type of magnetic susceptibility meter (Bartington Instruments model MS2) was used but with a different sensor.

MST susceptibility measurements made on the whole core are directly comparable with the AMST measurements of archive halves, correcting for the final curated positions and placement of spacers. The susceptibility response is a function of the mineralogy as well as the shape and volume of the magnetic particles within the rocks. Susceptibility provides an indication of the amount of magnetic material in the core and was used to consider locations for taking discrete samples for further paleomagnetic measurements. The volume susceptibility was used in conjunction with the NRM intensity to calculate the Königsberger ratio (Q, the ratio of remanent to induced magnetization) of the samples. The International Geomagnetic Reference Field value at the Leg 210 sites (49,412 nT = 39.59 A/m) was used for calculating Q.

$$Q = \text{NRM [A/m]} / (k \text{ [SI]} \times H \text{ [A/m]}),$$

where H is the local geomagnetic field and k is the susceptibility. In general, the Königsberger ratio is used as a measure of stability to indicate a

rock's capability of maintaining a stable remanence. At Leg 210 sites, the Königsberger ratio is a useful parameter to evaluate how much the effective magnetization that results from the susceptibility of the rocks contributes to the regional magnetic anomalies; the Königsberger ratio is a linear function of NRM/induced magnetization.

GEOCHEMISTRY

The shipboard geochemistry program for Leg 210 included (1) real-time monitoring of volatile hydrocarbons in cores as required by ODP safety regulations; (2) measurement of sediment carbonate content; (3) elemental analysis of total carbon (TC), nitrogen, and hydrogen contents of sediment; (4) characterization of bulk organic matter by Rock-Eval pyrolysis; and (5) elemental analysis of major and trace elements by ICP-AES.

Laboratory procedures and instruments employed during Leg 210 are described in Pimmel and Claypool (2001) and Murray et al. (2000). The procedures and instruments are primarily those used during the most recent ODP legs.

Hydrocarbon Gas Analysis

Compositions and concentrations of gases in sediment were monitored for safety and pollution prevention with an average sample interval of two per core. Headspace (HS) gas samples were collected immediately after core retrieval. On deck, 5-cm^3 sediment samples were obtained using a borer tool, placed in a glass serum vial, and sealed with a septum and metal crimp cap. For consolidated or lithified sediment, chips of material were sampled. Each vial was then heated at 60°C for 30 min, and a 5-cm^3 subsample of the HS gas was extracted using a glass syringe.

Gas obtained by HS sampling was analyzed using a Hewlett-Packard (HP) 6890 gas chromatograph (GC) equipped with a flame ionization detector (FID). Chromatographic responses were calibrated using Scotty IV gas mixtures, and the results were reported as component parts per million by volume (ppmv) relative to the analyzed gas. This system determines concentrations of C_1–C_3 (methane, ethane, ethene, propane, and propene) hydrocarbons.

Gas samples were also analyzed with a natural gas analyzer (NGA) when high concentrations of C_{2+} hydrocarbons or nonhydrocarbon gases such as H_2S or CO_2 were anticipated. The NGA system consists of an HP 6890 GC equipped with both FID and thermal conductivity detectors. Detectable gases are N_2, O_2, CO_2, H_2S, and hydrocarbons in the range of C_1–C_6.

To the extent that sampling procedures are uniform, the differences in the HS results reflect differences in the amounts of gas remaining in the cores.

Carbonate Analysis

Inorganic carbon (IC) and carbonate contents were determined by a titration method. Amounts of CO_2 evolved from sediment samples were measured by a spectrophotometer through a colorimetric reaction, using a Coulometrics 5011 CO_2 coulometer equipped with a System 140

carbonate analyzer. Aliquots of 10 mg of freeze-dried, ground sediment were reacted with 2-N HCl to liberate CO_2. Carbonate content (in weight percent) was then calculated from the IC content using the following equation:

$$CaCO_3\ (wt\%) = IC\ (wt\%) \times 8.33.$$

This method assumes that the CO_2 evolved from the sediment was derived solely from dissolution of calcium carbonate. No corrections were made to account for the possible presence of other carbonate minerals.

Elemental Analysis

TC, nitrogen, and hydrogen were determined using a Carlo Erba NA 1500 CHNS analyzer. The analytical procedure employs a 10-mg subsample of freeze-dried, ground sediment. The amount of total organic carbon (TOC) was calculated as the difference between TC and IC (determined by coulometry on the same sample),

$$TOC\ (wt\%) = TC\ (wt\%) - IC\ (wt\%).$$

Organic Matter Characterization and Maturity Determination

The type of organic matter was characterized by programmed pyrolysis using a Delsi Nermag Rock-Eval II system. Aliquots of 100 mg of freeze-dried, ground sediment are employed in this technique. The amount of volatile hydrocarbons released by heating organic matter at 300°C for 3 min is S_1. The quantity of hydrocarbons subsequently released by thermal cracking of kerogen as the temperature is increased to 550°C at a rate of 25°C/min is S_2. The nominal temperature at which the kerogen yields the maximum amount of hydrocarbons (top of the S_2 peak) is T_{max}, which is used to assess the thermal maturity of the organic matter. The amount of CO_2 released from thermal degradation of organic matter (between 300° and 390°C) is S_3. S_1, S_2, and S_3 are reported in milligrams per gram of dry sediment.

Rock-Eval analysis provides the following calculated parameters: S_2/S_3 ratio and hydrogen, oxygen, and production indexes (HI, OI, and PI, respectively). These parameters are calculated using the following equations:

$$HI = S_2/TOC \times 100.$$

$$OI = S_3/TOC \times 100.$$

$$PI = S_1/(S_1+S_2).$$

Samples with <0.5 wt% TOC may not give reliable results because of the small size of the S_1, S_2, and S_3 signals.

Elemental Analysis of Bulk Sediment by ICP-AES

Sediments and Sedimentary Rocks

Mainly fine grained sediments were routinely analyzed for elemental composition using ICP-AES. The main objective was to highlight downhole trends in bulk geochemistry that could help indicate changes in sediment provenance, diagenesis, and organic productivity. Additional samples were taken as appropriate to highlight finer-scale variations and to help with lithostratigraphic identifications. Samples from Cretaceous black shales were analyzed to help characterize paleoceanographic conditions during oceanic anoxic events.

Elemental composition of bulk sediment was determined using a Jobin-Yvon 2000 Ultrace ICP-AES using a type-C Meinhard concentric nebulizer. Our analytical approach followed the general procedure outlined by Murray et al. (2000) and the constraints indicated by Quintin et al. (2002). Analytical blanks were prepared using 400 mg of lithium metaborate ($LiBO_2$) flux to ensure matrix matching. Samples analyzed by ICP-AES were ignited before dissolution by heating 1 g of freeze-dried, ground sediment at 900°C for 4 hr to determine weight loss on ignition (LOI), to release volatile phases (H_2O, CO_2, and S), and to fully oxidize all iron to ferric iron.

Aliquots of 100 mg of ignited sediment and standards were mixed with 400 mg of $LiBO_2$ flux. Subsequently, 10 µL of a wetting agent, 0.172-mM lithium bromide (LiBr), was added to the samples, standards, and blanks. This mixture was fused at 1050°C for 3 min in a NT-2100 Bead Sampler prior to dissolution in 50 mL of 10% HNO_3. For complete dissolution, 1 hr of shaking with a Burrell wrist-action shaker was required. Aliquots of 5 mL of the resulting solutions were filtered (0.45 µm) and diluted with 35 mL of 10% HNO_3, resulting in a 4000× dilution of the original sediment.

A range of standards was initially selected to cover the entire range of expected sediment compositions, and their suitability was monitored during the leg. These standards were as follows: Cody shale (SCO-1), pahoehoe basalt lava flow (BHVO-2), marine mud (MAG-1), Green River shale (SGR-1), Glass Mountain rhyolite (RGM), dolomitic limestone (NBS-88), and argillaceous limestone (NBS-1c). The Cody shale (SCO-1) was also selected as both the drift and the consistency standard.

We decided to analyze a range of major and trace elements that would be useful for interpretation. The major elements are Si, Al, Fe, MgO, CaO, Na, K, Ti, Mn, and P, and the trace elements are Ba, V, La, Ce, Nd, Cr, Cd, Ni, Cu, Zn, Pb, Rb, Sr, Y, Zr, Nb, and Mo. Major elements were expressed as weight percent oxide and trace elements as parts per million. LOI values were determined routinely. Samples were analyzed in duplicate. There was insufficient time at the end of the cruise for the analysis of some chemical constituents, and thus some values are not included in the database.

Basement Rocks

Selected representative samples were cut with a diamond-impregnated saw blade and were wet ground on a diamond abrasive wheel to remove surface contamination. Samples were washed in an ultrasonic bath with methanol for 10 min, followed by three consecutive 10-min washes in an ultrasonic bath containing nanopure deionized water. Samples were then dried for 12 hr in an oven at 110°C. They were sub-

sequently reduced to fragments <1 cm in diameter by crushing between two disks of Delrin plastic in a hydraulic press, followed by grinding to a fine powder for 5 min in a Spex 8510 shatterbox with a tungsten carbide barrel. Approximately 1 g of sample powder was ignited at 1025°C for 4 hr.

Sample dissolution and analyses followed procedures described for sediment samples (see **"Sediments and Sedimentary Rocks,"** p. 27).

Interstitial Water Sampling and Chemistry

Interstitial water analyses were performed on 10-cm whole-round sections cut on deck immediately after core retrieval. After extrusion from the core liner, the surface of each whole-round sample was scraped with a spatula to remove potential contamination. Interstitial waters were collected using a titanium squeezer, modified after Manheim and Sayles (1974). Pressure up to 45,000 lb was applied using a hydraulic press. Pore waters were double filtered through prewashed 0.45-µm Acrodisk filters fitted above a titanium screen and subsequently extruded through Whatman number 1 filters into a plastic syringe attached to the bottom of the squeezer assembly.

Interstitial water samples were analyzed for salinity as total dissolved solids with a Goldberg optical handheld refractometer. Sulfate (SO_4^{2-}) was analyzed by nephelometry using a spectrophotometer (Gieskes et al., 1991). Results are reported in molar units. International Association of Physical Sciences of the Oceans seawater was used as standard.

PHYSICAL PROPERTIES

Physical property measurements made during Leg 210 provided (1) sediment properties (density, porosity, natural gamma radiation [NGR], and magnetic susceptibility) to compare with composition, diagenesis, and consolidation history and to help constrain the location of unconformities, sediment fracturing, and fluid migration and expulsion; (2) compressional wave (*P*-wave) velocity and bulk density to calculate synthetic seismograms and integrated traveltime curves; and (3) near-continuous records of density, velocity, NGR, and magnetic susceptibility to help define lithologic composition and stratigraphic cyclicity.

Physical properties were measured on unsplit cores, undisturbed parts of split cores, rock cubes selected from the split cores, and cylinders prepared from the rock cubes. For rock cores (e.g., indurated sediment and basement samples), the liners were split and the curated lengths of the whole cores were determined prior to measurement on the MST. The MST was used on whole-core RCB sections for nondestructive measurements of wet bulk density, magnetic susceptibility, and NGR. Thermal conductivity measurements were conducted on split rock cores. Three-directional *P*-wave velocity was measured on rock cubes. Wet and dry mass and dry volume were measured from rock cylinders prepared from the rock cubes, and moisture content, bulk density, porosity, grain density, and void ratio were calculated.

Core Handling and Measurement Sequence

The first measurement station was the MST, which combines four sensors on an automated track. The sensors are the magnetic susceptibility loop (MSL), the gamma ray attenuation (GRA) bulk densiometer,

the *P*-wave logger (not used), and the NGR detector. MST sampling intervals and measurement times for each core section were selected so that physical properties could be accurately characterized in 20 min for a 1.5-m-long section without hindering the flow of core processing through the laboratories (Table T7). After MST analysis, the cores were split and thermal conductivity measurements were conducted on half-core samples.

T7. MST data acquisition parameters, p. 67.

The working half of each section was used for further physical property measurements of *P*-wave velocity, water content, and grain volume. Water content and grain volume were used to calculate bulk density, porosity, grain density, and related parameters using the moisture and density (MAD) method C for lithified sediment and rock samples. A summary of each of the physical property measurement procedures for Leg 210 is outlined below. Blum (1997) provides a detailed description of the physical principles underlying the methods.

Multisensor Track Measurements

In order to collect measurements, individual unsplit core sections were placed on the MST, which automatically moved the core section through the four sensors on a fiberglass boat. MST data are not continuous as a function of depth because of incomplete recovery, drilling-disturbed intervals, and removal (in places) of whole-round sections immediately following core arrival on deck. The quality of these data is also degraded in RCB sections where the core may be undersized with respect to the liner diameter and/or disturbed. Nevertheless, the general downhole trends and peak amplitudes may be useful for stratigraphic correlations or comparison with logging data.

GRA bulk density, magnetic susceptibility, and NGR were measured on all cores that exceeded a minimum length of ~0.5 m. The top and bottom 5 cm of each section were not included in the MST measurements to avoid using data from disturbed parts of the core. *P*-wave velocity was not measured on the MST because of degraded core continuity and volume caused by RCB drilling.

Magnetic Susceptibility Loop Sensor

High-amplitude magnetic susceptibility primarily indicates the presence and concentration of ferro- and ferrimagnetic minerals such as magnetite, hematite, goethite, and titanomagnetite in sediment. This material may be associated with the coarse sediment fraction of, for example, proximal turbidites and/or with single-domain magnetic material in the clay fraction. In contrast, low-amplitude magnetic susceptibility is induced by paramagnetic and diamagnetic minerals such as clays, evaporites, and various precipitates. Because magnetic susceptibility reflects changes in magnetic mineralogy, it is widely used as a proxy for lithologic variations and thus depositional processes. Sampling was conducted at 2.5-cm intervals with three data acquisitions per interval (Table T7). The technical details of the MSL are presented in "Magnetic Susceptibility Measurements and the Königsberger Ratio," p. 24, in "Paleomagnetism".

The MSL is set to SI units, and data are stored in the Janus database in raw meter units (instrument units). To convert to true SI volume susceptibilities, magnetic susceptibility instrument units are multiplied first by 10^{-5} and then by a correction factor to take into account the volume of material that passed through the susceptibility coils. Except for

measurements near the end of each section, the correction factor for a standard full ODP core is ~0.66. No correction was applied to the magnetic susceptibility values for reduced core volume.

Gamma Ray Attenuation Bulk Density

GRA bulk density was estimated for unsplit core sections using the GRA densiometer every 2.5 cm over a sampling period of 10 s (Table T7). The GRA bulk density is an independent estimate that has a shorter sampling interval than the bulk density determined using the MAD method. Measurement of GRA density is based on the principle that the attenuation, mainly by Compton scattering, of a collimated beam of gamma rays produced by a ^{137}Ce source passing through a known volume of sediment is related to material density (Evans, 1965). GRA bulk density is therefore volume dependent, and the quality of GRA bulk density measurements is compromised because of RCB-induced core disruption and size variation.

Natural Gamma Radiation

NGR emissions are a function of the random and discrete decay of radioactive isotopes, predominantly those of U, Th, and K, and they are measured through scintillation detectors arranged at 90° angles to each other and perpendicular to the core. NGR count typically correlates positively with increasing clay/mudrock content and/or diagenesis where uranium is sequestered from seawater and organic matter. Sand-prone units usually tend to be characterized by low NGR counts and vice versa (although this relationship can be reversed or confused by peculiarities of the eroding source region). Ideally, these relationships can be used to define the locations of mudrock- and sand-prone formations downhole. For siliciclastic units, mudrock- and sand-prone units relate primarily to changes in relative sea level or to individual turbidite sequences. In particular, upward-coarsening and upward-fining sedimentary sequences are expressed as overall decreasing and increasing NGR signatures, respectively. NGR was measured for 10 s at 2.5-cm intervals (Table T7). NGR calibration was performed at the beginning of the leg.

Thermal Conductivity

Thermal conductivity was measured during Leg 210 using the TK04 system described by Blum (1997). This system employs a single-needle probe (Von Herzen and Maxwell, 1959), heated continuously, in a half-space configuration for hard rock. The needle probe is a thin metal tube that contains a thermistor and a heater wire. The needle is assumed to approximate an infinitely long, continuous medium; the temperature near the line source is measured as a function of time. If it is assumed that the sediment or rock sample to be measured can be represented as solids in a fluid medium, it is then possible to determine a relationship between thermal diffusivity and thermal conductivity. With this assumption, the change in temperature of the probe as a function of time is given to a good approximation by (Von Herzen and Maxwell, 1959)

$$T(t) = (q/4\times k)\ \ln(4\alpha t/\mathrm{B}a^2),$$

where

T = temperature [°C],
q = heat input per unit time per unit length [W/m],
k = thermal conductivity of the sediment or rock sample [W/m·°C],
t = time after the initiation of the heat [s],
α = thermal diffusivity of the sample [m^2/s],
B = a constant (1.7811), and
a = the probe radius [m].

This relationship is valid when t is large compared with a^2/α. A plot of T vs. ln(t) will then give a straight line, the slope of which determines k (Von Herzen and Maxwell, 1959).

Half-core rock specimens were measured for thermal conductivity using the half-space configuration. A needle probe was secured onto the flat surface of the half core. The samples and needles were then immersed in seawater for ~30 min prior to measurement. After immersion of the rock sample, the probe was heated at 3 W/m and the temperature rise was monitored. The optimal integration time for each conductivity measurement was calculated by an algorithm in the TK04 program.

The half-space method works well on unfractured sections of core that are at least ~5 cm long. In Leg 210 cores, mudrock sections were rarely preserved in unfractured sections longer than ~2 cm after core splitting, whereas sandstones often remained intact. Therefore, to avoid a sampling bias, a technique was devised for conducting thermal conductivity measurements on the mudrock lithologies with the half-space method. Several consecutive (i.e., well-fitting; separated by cracking rather than by drilling disturbance) pieces of mudrock from a given section were extracted and clamped together with a C-clamp to help close the fractures between the pieces and to simulate an unfractured sample. The probe was then secured to the sample, and the usual method was applied. A similar method of wrapping mudrock pieces in heat-wrap plastic was attempted, but the rock reconstruction was not as strong as that for the C-clamp approach. Perhaps more importantly, the thermal conductivity measurements on the heat-wrapped samples showed considerable scatter for each sample. Thus, the C-clamp technique was the preferred method for thermal conductivity measurements on shales and mudrocks.

In general, one thermal conductivity measurement was taken per core. The reported thermal conductivity measurement for each sample was the average of four repeated measurements using the half-space method. Data are reported in watts per meter degree Kelvin with a stated error of ~5% and precision of 2%.

Thermal conductivity typically varies with bulk density and porosity. A direct inverse relationship should exist between porosity (ϕ) and thermal conductivity because of the power-law dependence of bulk thermal conductivity (k_{bulk}) on the solid-matrix grain thermal conductivity (k_{grain}) and the thermal conductivity of the interstitial fluid (k_w) (Keen and Beaumont, 1990). This equation can be expressed as

$$k_{bulk} = k_w^{\phi} \times k_{grain}^{(1-\phi)}.$$

The observed relationship between the thermal conductivity and porosity can be compared with calculated bulk thermal conductivity using the measured porosity values and grain thermal conductivity values summarized in Table T8 (Keen and Beaumont, 1990).

T8. Sediment grain thermal conductivity, p. 68.

Moisture and Density Measurements

MAD quantities (water content, wet and dry bulk density, grain density, and porosity) were routinely measured from cylinders prepared from cubes (~8 cm^3) that initially were cut from consolidated sediment and/or basement rocks. The cubes were prepared for triaxial *P*-wave velocity measurements. Routine measurements were made on one sample per section to characterize all significant lithologies in a core. This is particularly important if downhole logging proves problematic or is not possible. Particular care was taken to sample undisturbed parts of the core and to avoid drilling slurry from RCB cores, which frequently showed a biscuiting-type disturbance.

Immediately after the rock cubes were cut, the *P*-wave velocity measurements were made and then the cubes were recut into cylinders to fit into 10-mL beakers for measurement of wet and dry mass and dry volume. Wet sediment mass was measured. Dry sediment mass and dry sediment volume were measured for samples after they had dried in a convection oven for 24 hr at a temperature of 105° ± 5°C. After drying and prior to measuring dry mass and volume, the samples were stored in a desiccator for at least 20 min to cool. Sample mass was determined to a precision of 0.01 g using two Scientech 202 electronic balances to compensate for the ship's motion. Grain volumes were determined using a helium Quantachrome penta-pycnometer with a precision of ±0.02 cm^3. The determination of water content followed the methods of the American Society for Testing and Materials (ASTM) designation (D) 2216 (ASTM, 1980). Blum (1997) discusses the assumptions and fundamental interrelationships between the various MAD properties, summarized below:

1. Consolidated sediment and rock samples (method C). Mass and volume calculations: Wet mass (M_{wet}), dry mass (M_{dry}), and dry volume (V_{dry}) are measured in the laboratory. Salt precipitated in the rock and sediment pore space during the drying process is included in the dry mass and dry volume values. The mass of the pore water (M_{pw}) and the salt (M_{salt}) in the sample are given by

$$M_{pw} = (M_{wet} - M_{dry})/(1 - s) \text{ and}$$

$$M_{salt} = M_{pw} \times s,$$

where s is the assumed saltwater salinity (0.035) corresponding to a pore water density (ρ_{pw}) of 1.024 g/cm^3 and a salt density (ρ_{salt}) of 2.257 g/cm^3. In order to determine the bulk and grain densities and porosity, the corrected mass of pore water (M_{pw}), volume of pore water (V_{pw}), mass of solids excluding salt (M_{solid}), volume of salt (V_{salt}), volume of solids excluding salt (V_{solid}), and wet volume (V_{wet}) need to be defined.

For the consolidated sediment and basement rock cylinders, the above parameters are calculated from the following:

$$V_{pw} = M_{pw}/\rho_{pw},$$

$$V_{salt} = M_{salt}/\rho_{salt},$$

$$V_{solid} = V_{dry} - V_{salt},$$

$$V_{wet} = V_{bulk} = V_{solid} + V_{pw}, \text{ and}$$

$$M_{solid} = M_{dry} - M_{salt}.$$

2. Calculation of MAD parameters. For all sediment and basement samples, wet water content (w_{wet}) is expressed as the ratio of the mass of pore water to the wet sediment (total) mass, and the dry water content (w_{dry}) is the ratio of the mass of pore water to the mass of solids (excluding salt):

$$w_{wet} = M_{pw}/M_{wet} \text{ and}$$

$$w_{dry} = M_{pw}/M_{solid}.$$

In turn, bulk density (ρ_{wet}), dry bulk density (ρ_{dry}), sediment grain (solid) density (ρ_{solid}), porosity (ϕ), and void ratio (e) are calculated from

$$\rho_{wet} = M_{wet}/V_{wet},$$

$$\rho_{dry} = M_{solid}/V_{wet} \text{ or } M_{solid}/V_{bulk},$$

$$\rho_{solid} = M_{solid}/V_{solid},$$

$$\phi = V_{pw}/V_{wet}, \text{ and}$$

$$e = V_{pw}/V_{solid}.$$

Porosity-Depth Behavior

Porosity behavior as a function of depth is often described in terms of Athy's law (Athy, 1930). This empirical relationship presumes a negative exponential relationship between depth and porosity:

$$\phi(z) = \phi_0\, e^{-kz},$$

where $\phi(z)$ is the porosity as a function of depth z, ϕ_0 is the surface porosity, and k controls the rate of decay of porosity with depth. A linear regression of $\ln(\phi[z])$ vs. z can be used to estimate the natural logarithm of ϕ_0 and k. Obtained results are compared with the predicted porosity-depth curve. Variations from the predicted curve are often diagnostic of grain size and composition, facies variations, and interstitial fluid pressure disequilibrium.

P-Wave Velocity on Split Cores, Consolidated Sediment, and Basement Samples

Velocity was measured using the *P*-wave sensor 3 (PWS3) modified Hamilton Frame velocimeter (Boyce, 1976). The PWS3 system uses a vertically oriented transducer pair that can be used with or without a liner correction. Using cube samples cut from cores, the *P*-wave velocity can be measured in each of the coordinate axis directions. An acoustic

signal of 500 kHz was transmitted and received by the two transducers. Analog-to-digital transformation of the signal allows the seismic signal to be displayed on a digital oscilloscope so that the first-arrival waveform can be picked automatically and the velocity can be calculated. Cube thickness was measured directly by a digital caliper. If the received signal was weak, the transmitter voltage was manually increased. To improve the coupling between the transducer and sample, deionized water was applied to the transducer/receiver heads. Additionally, if the received signal waveform was complicated, the first arrival was manually selected and velocity was calculated.

Calibration of the system was performed in accordance with Blum (1997). The separation between transducers was calibrated with four polycarbonate standards with varying thicknesses (20–50 mm). The delay time was determined by a linear regression of traveltime vs. thickness (15.4–57.5 mm) of seawater.

Anisotropy was determined using the difference between the average horizontal (x- and y-directions) and vertical (z-direction) velocity using the following equation:

$$\text{Anisotropy} = 2(V_{Pt} - V_{Pl})/(V_{Pt} + V_{Pl}),$$

where V_{Pt} is the average (horizontal or traverse) *P*-wave velocity and V_{Pl} is the vertical or longitudinal velocity.

REFERENCES

Applegate, J.L., and Bergen, J.A., 1988. Cretaceous calcareous nannofossil biostratigraphy of sediments recovered from the Galicia margin, ODP Leg 103. *In* Boillot, G., Winterer, E.L., et al., *Proc. ODP, Sci. Results,* 103: College Station, TX (Ocean Drilling Program), 293–348.

ASTM, 1980. Standard method for laboratory determination of water (moisture) content of soil, rock and soil-aggregate mixtures. In *Annual Book of ASTM Standards:* Philadelphia (Am. Soc. Testing and Mater.).

Athy, L.F., 1930. Density, porosity, and compaction of sedimentary rocks. *AAPG Bull.,* 14:1–24.

Backman, J., and Raffi, I., 1997. Calibration of Miocene nannofossil events to orbitally tuned cyclostratigraphies from Ceara Rise. *In* Shackleton, N.J., Curry, W.B., Richter, C., and Bralower, T.J. (Eds.), *Proc. ODP, Sci. Results,* 154: College Station, TX (Ocean Drilling Program), 83–99.

Baumgartner, P.O., Bartolini, A., Carter, E.S., Conti, M., Cortese, G., Danelian, T., De Wever, P., Dumitrica, P., Dumitrica-Jud, R., Gorican, S., Guex, J., Hull, D.M., Kito, N., Marcucci, M., Matsuoka, A., Murchey, B., O'Dogherty, L., Savary, J., Vishnevskaya, V., Widz, D., and Yao, A., 1995a. Middle Jurassic to Early Cretaceous radiolarian biochronology of Tethys based on Unitary Associations, Middle Jurassic to Lower Cretaceous radiolaria of Tethys: occurrences, systematics, biochronology. *In* Baumgartner, P.O., O'Dogherty, L., Gorican, S., Urquhart, E., Pillevuit, A., and De Wever, P. (Eds.), *Middle Jurassic to Lower Cretaceous Radiolaria of Tethys: Occurrences, Systematics, Biochronology.* Mem. Geol. (Lausanne), 23:1013–1048.

Baumgartner, P.O., O'Dogherty, L., Gorican, S., Dumitrica-Jud, R., Dumitrica, P., Pillevuit, A., Urquart, E., Matsuoka, A., Danelian, T., Bartolini, A., Carter, E.S., De Wever, P., Kito, N., Marcucci, M., and Steiger, T., 1995b. Radiolarian catalogue and systematics of Middle Jurassic to Early Cretaceous Tethyan genera and species. *In* Baumgartner, P.O., O'Dogherty, L., Gorican, S., Urquhart E., Pillevuit, A., and De Wever, P. (Eds.), *Middle Jurassic to Lower Cretaceous Radiolaria of Tethys: Occurrences, Systematics, Biochronology.* Mem. Geol. (Lausanne), 23:37–685.

Berggren, W.A., Hilgen, F.J., Langereis, C.G., Kent, D.V., Obradovich, J.D., Raffi, I., Raymo, M.E., and Shackleton, N.J., 1995a. Late Neogene chronology: new perspectives in high-resolution stratigraphy. *Geol. Soc. Am. Bull.,* 107:1272–1287.

Berggren, W.A., Kent, D.V., Swisher, C.C., III, and Aubry, M.-P., 1995b. A revised Cenozoic geochronology and chronostratigraphy. *In* Berggren, W.A., Kent, D.V., Aubry, M.-P., and Hardenbol, J. (Eds.), *Geochronology, Time Scales and Global Stratigraphic Correlation*. Spec. Publ.—SEPM (Soc. Sediment. Geol.), 54:129–212.

Berggren, W.A., and Norris, R.D., 1997. Biostratigraphy, phylogeny and systematics of Paleocene trochospiral planktic foraminifera. *Micropaleontology, Suppl. 1,* 43:1–116.

Blum, P., 1997. Physical properties handbook: a guide to the shipboard measurement of physical properties of deep-sea cores. *ODP Tech. Note,* 26 [Online]. Available from World Wide Web: <http://www-odp.tamu.edu/publications/tnotes/tn26/INDEX.HTM>. [Cited 2003-09-05]

Bolli, H.M., Beckmann, J.-P., and Saunders, J.B., 1994. *Benthic Foraminiferal Biostratigraphy of the South Caribbean Region:* Cambridge (Cambridge Univ. Press).

Bolli, H.M., and Saunders, J.B., 1985. Oligocene to Holocene low latitude planktic foraminifera. *In* Bolli, H.M., Saunders, J.B., and Perch-Nielsen, K. (Eds.), *Plankton Stratigraphy:* Cambridge (Cambridge Univ. Press), 155–262.

Bown, P.R. (Ed.), 1998. *Calcareous Nannofossil Biostratigraphy:* London (Chapman-Hall).

Boyce, R.E., 1976. Definitions and laboratory techniques of compressional sound velocity parameters and wet-water content, wet-bulk density, and porosity parameters by gravimetric and gamma-ray attenuation techniques. *In* Schlanger, S.O.,

Jackson, E.D., et al., *Init. Repts. DSDP,* 33: Washington (U.S. Govt. Printing Office), 931–958.

Bralower, T.J., Fullagar, P.D., Paull, C.K., Dwyer, G.S., and Leckie, R.M., 1997. Mid-Cretaceous strontium-isotope stratigraphy of deep-sea sections. *Geol. Soc. Am. Bull.,* 109:1421–1442.

Bralower, T.J., Leckie, R.M., Sliter, W.V., and Thierstein, H.R., 1995. An integrated Cretaceous microfossil biostratigraphy. *In* Berggren, W.A., Kent, D.V., Aubry, M.-P., and Hardenbol, J. (Eds.), *Geochronology, Time Scales and Global Stratigraphic Correlation.* Spec. Publ.—SEPM (Soc. Sediment. Geol.), 54:65–79.

Bralower, T.J., Monechi, S., and Thierstein, H.R., 1989. Calcareous nannofossil zonation of the Jurassic–Cretaceous boundary interval and correlation with the geomagnetic polarity timescale. *Mar. Micropaleontol.,* 14:153–235.

Bralower, T.J., Sliter, W.V., Arthur, M.A., Leckie, R.M., Allard, D.J., and Schlanger, S.O., 1993. Dysoxic/anoxic episodes in the Aptian–Albian (Early Cretaceous). *In* Pringle, M.S., Sager, W.W., Sliter, W.V., and Stein, S. (Eds.), *The Mesozoic Pacific: Geology, Tectonics, and Volcanism.* Geophys. Monogr., 77:5–37.

Bukry, D., 1973. Low-latitude coccolith biostratigraphic zonation. *In* Edgar, N.T., Saunders, J.B., et al., *Init. Repts. DSDP,* 15: Washington (U.S. Govt. Printing Office), 685–703.

————, 1975. Coccolith and silicoflagellate stratigraphy, northwestern Pacific Ocean, Deep Sea Drilling Project Leg 32. *In* Larson, R.L., Moberly, R., et al., *Init. Repts. DSDP,* 32: Washington (U.S. Govt. Printing Office), 677–701.

Burnett, J.A., 1999. Upper Cretaceous. *In* Bown, P.R. (Ed.), *Calcareous Nannofossil Biostratigraphy:* Dordrecht, The Netherlands (Kluwer Academic Publ.), 132–199.

Cande, S.C., and Kent, D.V., 1995. Revised calibration of the geomagnetic polarity timescale for the Late Cretaceous and Cenozoic. *J. Geophys. Res.,* 100:6093–6095.

Caron, M., 1985. Cretaceous planktic foraminifera. *In* Bolli, H.M., Saunders, J.B., and Perch-Nielsen, K. (Eds.), *Plankton Stratigraphy:* Cambridge (Cambridge Univ. Press), 17–86.

Chaisson, W.P., and Leckie, R.M., 1993. High-resolution Neogene planktonic foraminifer biostratigraphy of Site 806, Ontong Java Plateau (western equatorial Pacific). *In* Berger, W.H., Kroenke, L.W., Mayer, L.A., et al., *Proc. ODP, Sci. Results,* 130: College Station, TX (Ocean Drilling Program), 137–178.

Chaisson, W.P., and Pearson, P.N., 1997. Planktonic foraminifer biostratigraphy at Site 925: middle Miocene–Pleistocene. *In* Shackleton, N.J., Curry, W.B., Richter, C., and Bralower, T.J. (Eds.), *Proc. ODP, Sci. Results,* 154: College Station, TX (Ocean Drilling Program), 3–31.

Channell, J.E.T., Erba, E., Nakanishi, M., and Tamaki, K., 1995. Late Jurassic–Early Cretaceous time scales and oceanic magnetic anomaly block models. *In* Berggren, W.A., Kent, D.V., Aubry, M.-P., and Hardenbol, J. (Eds.), *Geochronology, Time Scales and Global Stratigraphic Correlation.* Spec. Publ.—SEPM (Soc. Sediment. Geol.), 54:51–63.

Coccioni, R., and Premoli Silva, I., 1994. Planktonic foraminifera from the Lower Cretaceous of Rio Argos sections (southern Spain) and biostratigraphic implications. *Cretaceous Res.,* 15:645–687.

Droser, M.L., and Bottjer, D.J., 1986. A semiquantitative field classification of ichnofabric. *J. Sediment. Petrol.,* 56:558–559.

Dunham, R.J., 1962. Classification of carbonate rocks according to depositional texture. *In* Ham, W.E. (Ed.), *Classification of Carbonate Rocks.* AAPG Mem., 108–121.

Duxbury, S., 2001. A palynological zonation scheme for the Lower Cretaceous–United Kingdom Sector, central North Sea. *In* Luterbacher, H., Pross, J., and Wille, W. (Eds.), *Studies in Dinoflagellate Cysts in Honour of Hans Gocht.* Neues Jahrb. Mineral., Abh., 219:95–137.

Erba, E., Channell, J.E.T., Claps, M., Jones, C., Larson, R., Opdyke, B., Premoli Silva, I., Riva, A., Salvini, G., and Torricelli, S., 1999. Integrated stratigraphy of the Cismon

APTICORE (southern Alps, Italy): a "reference section" for the Barremian–Aptian interval at low latitudes. *J. Foraminiferal Res.,* 29:371–391.

Erba, E., Premoli Silva, I., and Watkins, D.K., 1995. Cretaceous calcareous plankton biostratigraphy of Sites 872 through 879. *In* Haggerty, J.A., Premoli Silva, I., Rack, F., and McNutt, M.K. (Eds.), *Proc. ODP, Sci. Results,* 144: College Station, TX (Ocean Drilling Program), 157–169.

Evans, H.B., 1965. GRAPE—a device for continuous determination of material density and porosity. *Trans. SPWLA 6th Ann. Logging Symp.:* Dallas, 2:B1–B25.

Firth, J.V., and Wise, S.W., Jr., 1992. A preliminary study of the evolution of *Chiasmolithus* in the middle Eocene to Oligocene of Sites 647 and 748. *In* Wise, S.W., Jr., Schlich, R., et al., *Proc. ODP, Sci. Results,* 120: College Station, TX (Ocean Drilling Program), 493–508.

Freifeld, B.M., Kneafsey, T.J., Tomutsa, L., and Pruess, J., 2003. Development of a portable X-ray computed tomographic imaging system for drill-site investigation of recovered core. *Proc. Int. Symp. Soc. Core Anal., September 21–24, 2003, Pau, France,* 581–586.

Gardin, S., Del Panta, F., Monechi, S., and Pozzi, M., 2001. A Tethyan reference section for the Campanian and Maastrichtian stages: the Bottaccione section (Central Italy). Review of the data and new calcareous nannofossil results. *In* Odin, G.S. (Ed.), *The Boundary between the Campanian and the Maastrichtian Stages: Characterisation and Correlation from Tercis-les-Bains to Europe and Other Continents*. Dev. Palaeontol. Stratigr., 19:820–833.

Gieskes, J.M., Gamo, T., and Brumsack, H., 1991. Chemical methods for interstitial water analysis aboard *JOIDES Resolution*. *ODP Tech. Note,* 15 [Online]. Available from World Wide Web: <http://www-odp.tamu.edu/publications/tnotes/tn15/f_chem1.htm>. [Cited 2003-09-05]

Gradstein, F.M., 1978. Biostratigraphy of Lower Cretaceous Blake Nose and Blake Bahama Basin foraminifera, DSDP Leg 44, western North Atlantic Ocean. *In* Benson, W.E., Sheridan, R.E., et al., *Init. Repts. DSDP,* 44: Washington (U.S. Govt. Printing Office), 663–702.

Gradstein, F.M., Agterberg, F.P., Ogg, J.G., Hardenbol, J., van Veen, P., Thierry, J., and Huang, Z., 1995. A Triassic, Jurassic and Cretaceous time scale. *In* Berggren, W.A., Kent, D.V., Aubry, M.P., and Hardenbol, J. (Eds.), *Geochronology, Time Scales and Global Stratigraphic Correlation*. Spec. Publ.—SEPM (Soc. Sediment. Geol.), 54:95–126.

Hilgen, F.J., 1991a. Astronomical calibration of Gauss to Matuyama sapropels in the Mediterranean and implication for the geomagnetic polarity time scale. *Earth Planet. Sci. Lett.,* 104:226–244.

Hilgen F.J., 1991b. Extension of the astronomically calibrated (polarity) time scale to the Miocene/Pliocene boundary. *Earth Planet. Sci. Lett.,* 107:349–368.

Holbourn, A., and Kaminski, M.A., 1997. Lower Cretaceous deep-water benthic foraminifera of the Indian Ocean. *Gzybowski Found., Spec. Publ.,* 4:1–175.

Holbourn, A., Kuhnt, W., and Soeding, E., 2001. Atlantic paleobathymetry, paleoproductivity and paleocirculation in the late Albian: the benthic foraminiferal record. *Palaeogeogr., Palaeoclimatol., Palaeoecol.,* 170:171–196.

Kaiho, K., 1992. Eocene to Quaternary benthic foraminifers and paleobathymetry of the Izu-Bonin arc, Legs 125 and 126. *In* Taylor, B., Fujioka, K., et al., *Proc. ODP, Sci. Results,* 126: College Station, TX (Ocean Drilling Program), 285–310.

————, 1999. Evolution in the test size of deep-sea benthic foraminifera during the past 120 million years. *Mar. Micropaleontol.,* 37:53–65.

Kameo, K., and Bralower, T.J., 2000. Neogene calcareous nannofossil biostratigraphy of Sites 998, 999, and 1000, Caribbean Sea. *In* Leckie, R.M., Sigurdsson, H., Acton, G.D., and Draper, G. (Eds.), *Proc. ODP, Sci. Results,* 165: College Station, TX (Ocean Drilling Program), 3–17.

Keen, C., and Beaumont, C., 1990. Geodynamics of rifted continental margins. *In* Keen, M.J., and Williams, G.L. (Eds.), *Geology of the Continental Margin of Eastern Canada*. Geol. Soc. Am., 1:391–472.

Kennett, J.P., and Srinivasan, M.S., 1983. *Neogene Planktonic Foraminifera: A Phylogenetic Atlas:* Stroudsburg, PA (Hutchinson Ross).

Kuhnt, W., and Urquhart, E., 2001. Tethyan flysch-type benthic foraminiferal assemblages in the North Atlantic: Cretaceous to Paleogene deep-water agglutinated foraminifers from the Iberia Abyssal Plain (ODP Leg 173). *Rev. Micropaleontol.,* 44:27–59.

Le Bas, M.J., Le Maitre, R.W., Streckeisen, A., and Zanettin, B., 1986. A chemical classification of volcanic rocks based on the total alkali-silica diagram. *J. Petrol.,* 27:745–750.

Leckie, R.M., 1984. Mid-Cretaceous planktonic foraminiferal biostratigraphy off central Morocco, DSDP Leg 79, Sites 545 and 547. *In* Hinz, K., Winterer, E.L., et al., *Init. Repts. DSDP,* 79: Washington (U.S. Govt. Printing Office), 579–620.

Leckie, R.M., Farnham, C., and Schmidt, M.G., 1993. Oligocene planktonic foraminifer biostratigraphy of Hole 803D (Ontong Java Plateau) and Hole 628A (Little Bahama Bank), and comparison with the southern high latitudes. *In* Berger, W.H., Kroenke, L.V., and Mayer, L.A. (Eds.), *Proc. ODP, Sci. Results,* 130: College Station, TX (Ocean Drilling Program), 113–136.

Loeblich, A.R., Jr., and Tappan, H., 1988. Foraminiferal evolution, diversification, and extinction. *J. Paleontol.,* 62:695–714.

Longoria, J.F., 1974. Stratigraphic, morphologic and taxonomic studies of Aptian planktonic foraminifera. *Rev. Esp. Micropaleontol.,* Num. Extraordinario.

Luterbacher, H., 1973. Early Cretaceous foraminifera from the northwestern Pacific: Leg 32 of the Deep Sea Drilling Project. *In* Larson, R.L., Moberly, R., et al., *Init. Repts. DSDP,* 32: Washington (U.S. Govt. Printing Office), 703–718.

Maltman, A. (Ed.), 1994. *The Geological Deformation of Sediments:* London (Chapman and Hall).

Manheim, F.T., and Sayles, F.L., 1974. Composition and origin of interstitial waters of marine sediments, based on deep sea drill cores. *In* Goldberg, E.D. (Ed.), *The Sea* (Vol. 5): *Marine Chemistry: The Sedimentary Cycle:* New York (Wiley), 527–568.

Murray, R.W., Miller, D.J., and Kryc, K.A., 2000. Analysis of major and trace elements in rocks, sediments, and interstitial waters by inductively coupled plasma–atomic emission spectrometry (ICP-AES). *ODP Tech. Note,* 29 [Online]. Available from World Wide Web: <http://www-odp.tamu.edu/publications/tnotes/tn29/INDEX.HTM>. [Cited 2003-09-05]

Nederbragt, A.J., 1990. Biostratigraphy and paleoceanographic potential of the Cretaceous planktic foraminifera Heterohelicidae [Ph.D. thesis]. Centrale Huisdrukkerij Vrije Univ., Amsterdam.

————, 1991. Late Cretaceous biostratigraphy and development of Heterohelicidae planktic foraminifera. *Micropaleontology,* 37:329–372.

Norris, R.D., 1998. Planktonic foraminifer biostratigraphy: eastern equatorial Atlantic. *In* Mascle, J., Lohmann, G.P., and Moullade, M. (Eds.), *Proc. ODP, Sci. Results,* 159: College Station, TX (Ocean Drilling Program), 445–479.

Nyong, E.E., and Olsson, R.K., 1984. A paleoslope model of Campanian to lower Maestrichtian foraminifera in the North American Basin and adjacent continental margin. *Mar. Micropaleontol.,* 8:437–477.

Okada, H., and Bukry, D., 1980. Supplementary modification and introduction of code numbers to the low-latitude coccolith biostratigraphic zonation (Bukry, 1973; 1975). *Mar. Micropaleontol.,* 5:321–325.

Olsson, R.K., Hemleben, C., Berggren, W.A., and Huber, B.T. (Eds.), 1999. *Atlas of Paleocene Planktonic Foraminifera*. Smithson. Contrib. Paleobiol., Vol. 85.

Passchier, C.W., and Trouw, R.A.J., 1996. *Microtectonics:* Berlin (Springer-Verlag).

Pearson, P.N., 1995. Planktonic foraminifer biostratigraphy and the development of pelagic caps on guyots in the Marshall Islands group. *In* Haggerty, J.A., Premoli

Silva, I., Rack, F., and McNutt, M.K. (Eds.), *Proc. ODP, Sci. Results,* 144: College Station, TX (Ocean Drilling Program), 21–59.

Pearson, P.N., and Chaisson, W.P., 1997. Late Paleocene to middle Miocene planktonic foraminifer biostratigraphy of the Ceara Rise. *In* Shackleton, N.J., Curry, W.B., Richter, C., and Bralower, T.J. (Eds.), *Proc. ODP, Sci. Results,* 154: College Station, TX (Ocean Drilling Program), 33–68.

Perch-Nielsen, K., 1985. Mesozoic calcareous nannofossils. *In* Bolli, H.M., Saunders, J.B., and Perch-Nielsen, K. (Eds.), *Plankton Stratigraphy:* Cambridge (Cambridge Univ. Press), 329–426.

Petrizzo, M.R., 2000. Upper Turonian–lower Campanian planktonic foraminifera from southern mid-high latitudes (Exmouth Plateau, NW Australia): biostratigraphy and taxonomic notes. *Cretaceous Res.,* 21:479–505.

————, 2001. Late Cretaceous planktonic foraminifera from the Kerguelen Plateau (ODP Leg 183): new data to improve the Southern Oceans biozonation. *Cretaceous Res.,* 22:829–855.

Pflum, C.E., and Frerichs, W.E., 1976. *Gulf of Mexico Deep-Water Foraminifers*. Spec. Publ.—Cushman Found. Foraminiferal Res., 14:1–122.

Pimmel, A., and Claypool, G., 2001. Introduction to shipboard organic geochemistry on the *JOIDES Resolution. ODP Tech. Note,* 30 [Online]. Available from World Wide Web: <http://www-odp.tamu.edu/publications/tnotes/tn30/INDEX.HTM>. [Cited 2003-09-05]

Postuma, J.A., 1971. *Manual of Planktonic Foraminifera:* Amsterdam (Elsevier).

Powell, A.J., 1992. Dinoflagellate cysts of the Tertiary System. *In* Powell, A.J. (Ed.), *A Stratigraphic Index of Dinoflagellate Cysts:* London (Chapman and Hall), 155–251.

Premoli Silva, I., and Sliter, W.V., 1994. Cretaceous planktonic foraminiferal biostratigraphy and evolutionary trends from the Bottaccione Section, Gubbio, Italy. *Palaeontogr. Ital.,* 82:2–90.

————, 1999. Cretaceous paleoceanography: evidence from planktonic foraminiferal evolution. *In* Barrera, E., and Johnson, C.C. (Eds.), *The Evolution of Cretaceous Ocean-Climatic System.* Spec. Pap.—Geol. Soc. Am., 332:301–328.

Pross, J., 2001. Paleo-oxygenation of Tertiary epeiric seas: evidence from dinoflagellate cysts. *Palaeogeogr., Palaeoclimatol., Palaeoecol.,* 166:369–381.

Quintin, L.L., Faul, K.L., Lear, C., Graham, D., Peng, C., Murray, R.W., and Shipboard Scientific Party, 2002. Geochemical analysis of bulk marine sediment by inductively coupled plasma–atomic emission spectroscopy on board the *JOIDES Resolution*. *In* Lyle, M., Wilson, P.A., Janecek, T.R., et al., 2002. *Proc. ODP, Init. Repts.,* 199, 1–14 [CD-ROM]. Available from Ocean Drilling Program, Texas A&M University, College Station TX 77845-9547, USA.

Raffi, I., and Flores, J.-A., 1995. Pleistocene through Miocene calcareous nannofossils from eastern equatorial Pacific Ocean. *In* Pisias, N.G., Mayer, L.A., Janecek, T.R., Palmer-Julson, A., and van Andel, T.H. (Eds.), *Proc. ODP, Sci. Results,* 138: College Station, TX (Ocean Drilling Program), 233–286.

Ramsay, J.G., and Huber, M.I., 1983. *The Techniques of Modern Structural Geology* (Vol. 1): *Strain Analysis:* London (Acad. Press).

————, 1987. *The Techniques of Modern Structural Geology* (Vol. 2): *Folds and Fractures:* New York (Acad. Press).

Robaszynski, F., and Caron, M., 1979. *Atlas de Foraminiferes Planctoniques du Cretace Moyen (Mer Boreale et Tethys)* (Vols. 1 and 2). Cah. Micropaleontol.

Robaszynski, F., Caron, M., Gonzales-Donoso, J.-M., Wonders, A.A.H., and the European Working Group on Planktonic Foraminifera, 1984. Atlas of Late Cretaceous globotruncanids. *Rev. Micropaleontol.,* 26:145–305.

Roth, P.H., 1973. Calcareous nannofossils—Leg 17, Deep Sea Drilling Project. *In* Winterer, E.L., Ewing, J.I., et al., *Init. Repts. DSDP,* 17: Washington (U.S. Govt. Printing Office), 695–795.

————, 1983. Jurassic and Lower Cretaceous calcareous nannofossils in the western North Atlantic (Site 534): biostratigraphy, preservation, and some observations on

biogeography and paleoceanography. *In* Sheridan, R.E., Gradstein, F.M., et al., *Init. Repts. DSDP,* 76: Washington (U.S. Govt. Printing Office), 587–621.

Sanfilippo, A., and Nigrini, C., 1998. Code numbers for Cenozoic low latitude radiolarian biostratigraphic zones and GPTS conversion tables. *Mar. Micropaleontol.,* 33:109–156.

Shackleton, N.J., Berger, A., and Peltier, W.A., 1990. An alternative astronomical calibration of the lower Pleistocene timescale based on ODP Site 677. *Trans. R. Soc. Edinburgh: Earth Sci.,* 81:251–261.

Shackleton, N.J., Crowhurst, S., Hagelberg, T., Pisias, N.G., and Schneider, D.A., 1995. A new late Neogene time scale: application to Leg 138 sites. *In* Pisias, N.G., Mayer, L.A., Janecek, T.R., Palmer-Julson, A., and van Andel, T.H. (Eds.), *Proc. ODP, Sci. Results,* 138: College Station, TX (Ocean Drilling Program), 73–101.

Shepard, F.P., 1954. Nomenclature based on sand-silt-clay ratios. *J. Sediment. Petrol.,* 24:151–158.

Shipboard Scientific Party, 1992. Explanatory notes. *In* Behrmann, J.H., Lewis, S.D., Musgrave, R.J., et al., *Proc. ODP, Init. Repts.,* 141: College Station, TX (Ocean Drilling Program), 37–71.

————, 1994. Explanatory notes. *In* Sawyer, D.S., Whitmarsh, R.B., Klaus, A., et al., *Proc. ODP, Init. Repts.,* 149: College Station, TX (Ocean Drilling Program), 11–34.

————, 1996. Explanatory notes. *In* Emeis, K.-C., Robertson, A.H.F., Richter, C., et al., *Proc. ODP, Init. Repts.,* 160: College Station, TX (Ocean Drilling Program), 29–52.

————, 1998. Explanatory notes. *In* Whitmarsh, R.B., Beslier, M.-O., Wallace, P.J., et al., *Proc. ODP, Init. Repts.,* 173: College Station, TX (Ocean Drilling Program), 25–47.

————, 2004. Explanatory notes. *In* Kelemen, P.B., Kikawa, E., Miller, D.J., et al., *Proc. ODP, Init. Repts.,* 209, 1–75 [CD-ROM]. Available from: Ocean Drilling Program, Texas A&M University, College Station TX 77845-9547, USA.

————, 2002. Leg 204 preliminary report. *ODP Prelim. Rept.,* 104 [Online]. Available from World Wide Web: <http://www-odp.tamu.edu/publications/prelim/204_prel/204PREL.PDF>. [Cited 2003-08-30]

Sissingh, W., 1977. Biostratigraphy of Cretaceous calcareous nannoplankton. *Geol. Mijnbouw,* 56:37–65.

Sliter, W.V., 1977. Cretaceous benthic foraminifers from the western South Atlantic Leg 39, Deep Sea Drilling Project. *In* Supko, P.R., Perch-Nielsen, K., et al., *Init. Repts. DSDP,* 39: Washington (U.S. Govt. Printing Office), 657–697.

————, 1980. Mesozoic foraminifers and deep-sea benthic environments from Deep Sea Drilling Project Sites 415 and 416, eastern North Atlantic. *In* Lancelot, Y., Winterer, E.L., et al., *Init. Repts. DSDP,* 50: Washington (U.S. Govt. Printing Office), 353–427.

————, 1989. Biostratigraphic zonation for Cretaceous planktonic foraminifers examined in thin section. *J. Foraminiferal Res.,* 19:1–19.

Soh, W., 1997. Computed tomography scan analysis of Site 941 cores, western mass-transport deposit, Amazon Fan. *In* Flood, R.D., Piper, D.J.W., Klaus, A., and Peterson, L.C. (Eds.), *Proc. ODP, Sci. Results,* 155: College Station, TX (Ocean Drilling Program), 465–475.

Spezzaferri, S., 1994. Planktonic foraminiferal biostratigraphy and taxonomy of the Oligocene and lower Miocene in the oceanic record: an overview. *Palaeontographica Ital.,* 81:1–187.

Spezzaferri, S., and Premoli Silva, I., 1991. Oligocene planktonic foraminiferal biostratigraphy and paleoclimatic interpretation from Hole 538A, DSDP Leg 77, Gulf of Mexico. *Palaeogeogr., Palaeoclimatol., Palaeoecol.,* 83:217–263.

Stover, L.E., Brinkhuis, H., Damassa, S.P., de Verteuil, L., Helby, R.J., Monteil, E., Partridge, A.D., Powell, A.J., Riding, J.B., Smelror, M., and Williams, G.L., 1996. Mesozoic–Tertiary dinoflagellates, acritarchs and prasinophytes. *In* Jansonius, J., and

McGregor, D.C. (Eds.), *Palynology: Principles and Applications* (Vol. 2): Dallas, TX (Am. Assoc. Stratigr. Palynol. Found.), 641–750.

Streckeisen, A., 1976. To each plutonic rock its proper name. *Earth Sci. Rev.,* 12:1–33.

Tjalsma, R.C., and Lohmann, G.P., 1983. *Paleocene–Eocene Bathyal and Abyssal Benthic Foraminifera from the Atlantic Ocean* (Vol. 4). Micropaleontology, Spec. Publ.

Toumarkine, M., and Luterbacher, H., 1985. Paleocene and Eocene planktic foraminifera. *In* Bolli, H.M., Saunders, J.B., and Perch-Nielsen, K. (Eds.), *Plankton Stratigraphy:* Cambridge (Cambridge Univ. Press), 87–154.

van Morkhoven, F.P.C.M., Berggren, W.A., and Edwards, A.S., 1986. *Cenozoic Cosmopolitan Deep-Water Benthic Foraminifera*. Bull. Cent. Rech. Explor.—Prod. Elf-Aquitaine, 11.

Von Herzen, R.P., and Maxwell, A.E., 1959. The measurement of thermal conductivity of deep-sea sediments by a needle-probe method. *J. Geophys. Res.,* 64:1557–1563.

Wentworth, C.K., 1922. A scale of grade and class terms of clastic sediments. *J. Geol.,* 30:377–392.

Williams, G.L., Brinkhuis, H., Pearce, M.A., Fensome, R.A., and Weegink, J.W., 2004. Southern Ocean and global dinoflagellate cyst events compared: index events for the Late Cretaceous–Neogene. *In* Exon, N.F., Kennett, J.P., and Malone, M.J. (Eds.), *Proc. ODP, Sci. Results,* 189, 1–98 [Online]. Available from World Wide Web: http://www-odp.tamu.edu/publications/189_SR/VOLUME/CHAPTERS/107.PDF. [Cited 2004-04-09]

Williams, G.L., Lentin, J.K., and Fensome, R.A., 1998. *The Lentin and Williams Index of Fossil Dinoflagellate Cysts* (1998 Ed.). Am. Assoc. Stratigr. Palynol., Contrib. Ser., Vol. 34.

Woodruff, F., 1985. Changes in Miocene deep-sea benthic foraminiferal distribution in the Pacific Ocean: relationship to paleoceanography. *In* Kennett, J.P. (Ed.), *The Miocene Ocean: Paleoceanography and Biogeography.* Mem.—Geol. Soc. Am., 163:131–175.

Figure F1. Schematic illustration of core, section, and sample numbering. (mbsf = meters below seafloor, mbrf = meters below rig floor, mbsl = meters below sea level).

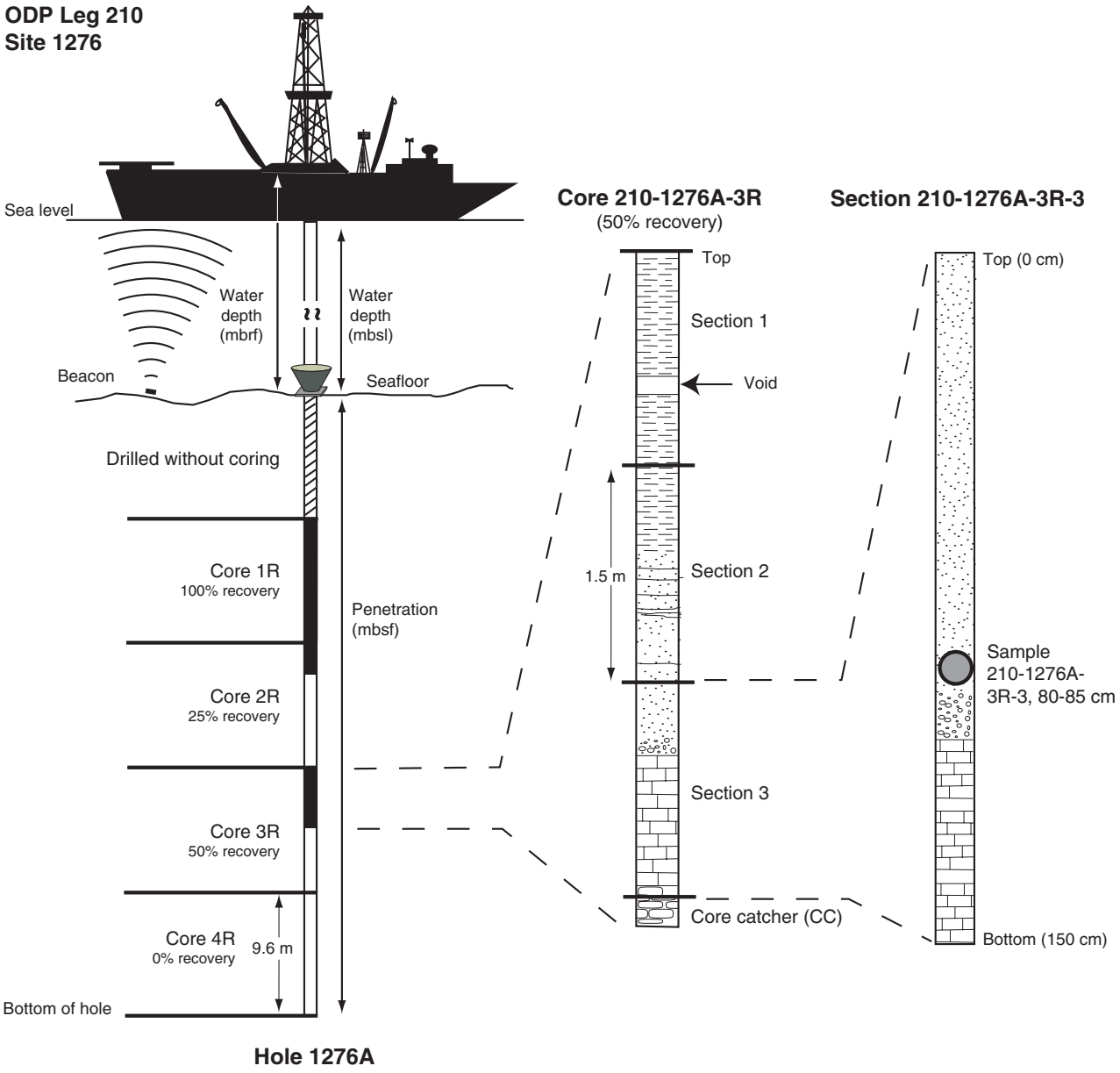

Figure F2. Ternary plots outlining the classification used to describe Leg 210 sedimentary rocks. Basic sedimentary rock types are defined using proportions of biogenic silica, carbonate, and terrigenous or volcanic components. The terrigenous scheme is expanded to allow for more detailed rock names based on the proportions of sand, silt, and clay in the rock. The lower triangle is simplified and modified from Shepard (1954). Additional rock types (e.g., conglomerate, mudrock, and grainstone) are described in the text.

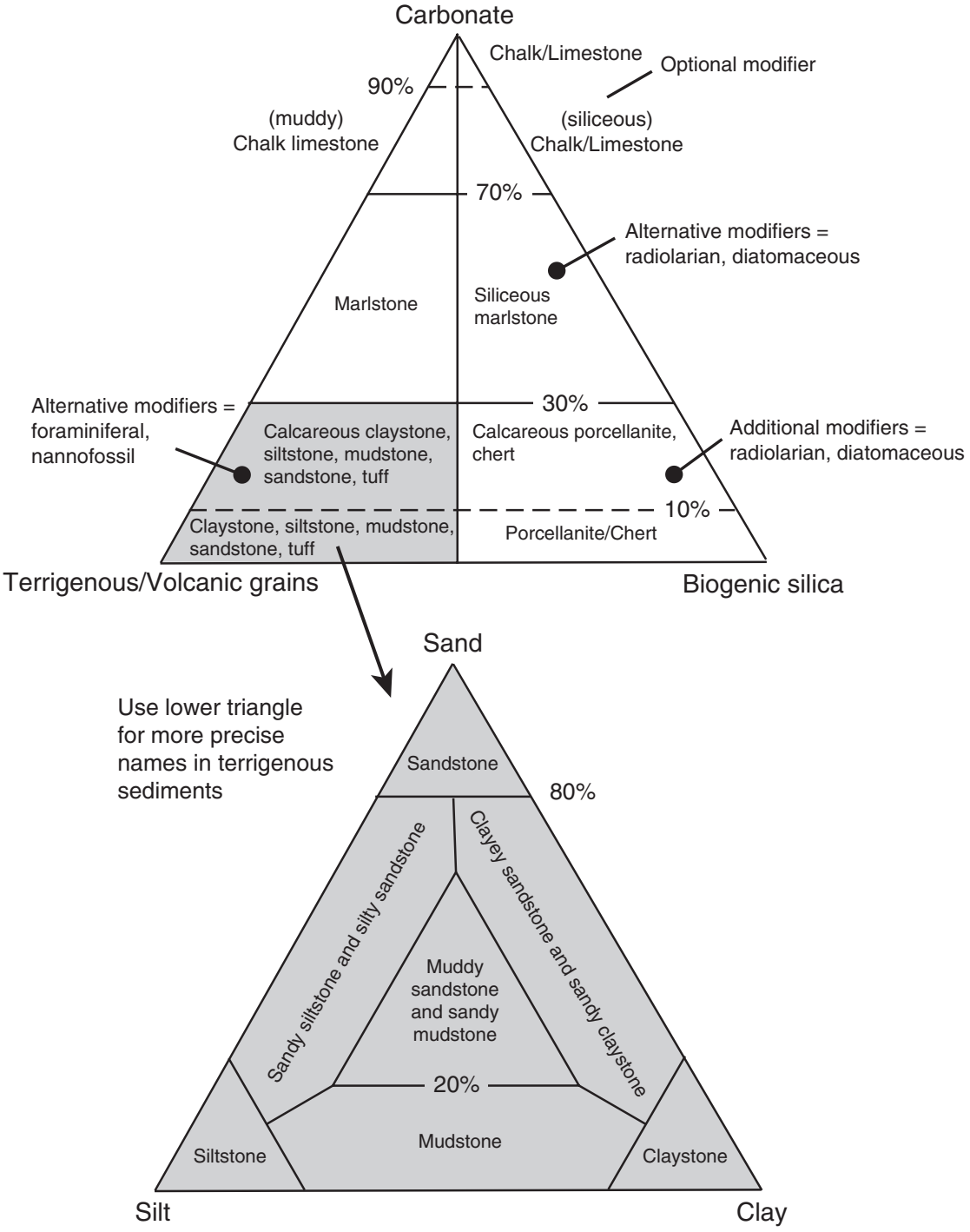

Figure F3. Example of the VCD format used during Leg 210 with the AppleCORE program. Core depths (second column from the left) are in meters below seafloor. The graphic lithology key is found in Figure F5, p. 46. See "Visual Core Descriptions," p. 5, for details.

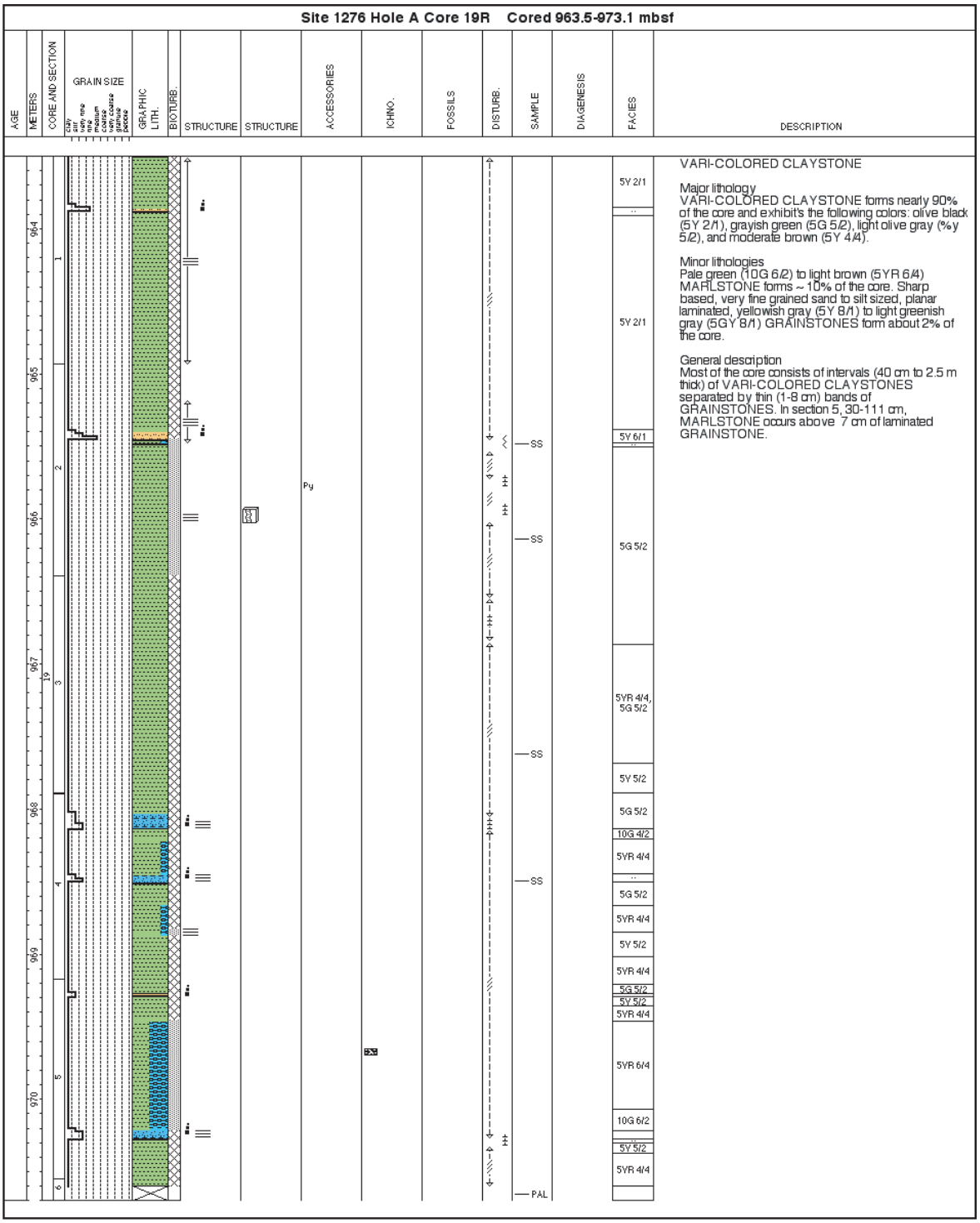

Figure F4. Key to patterns used in the AppleCORE Graphic Lithology column. These are based on the classification scheme outlined in Figure F2, p. 43, except for grainstone (see "Sediment Classification," p. 4).

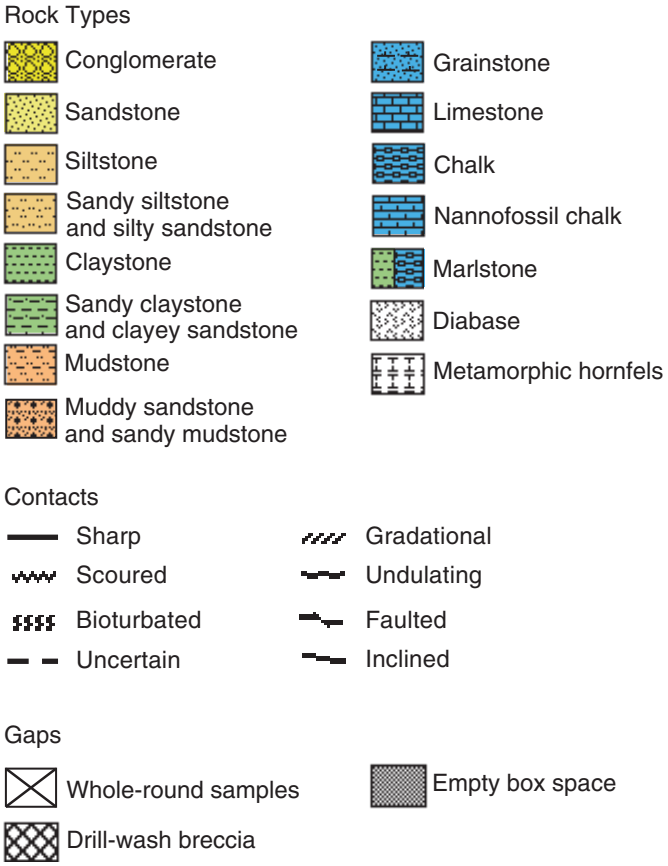

Figure F5. Key to symbols used to depict core structures, components, and other attributes within AppleCORE VCDs.

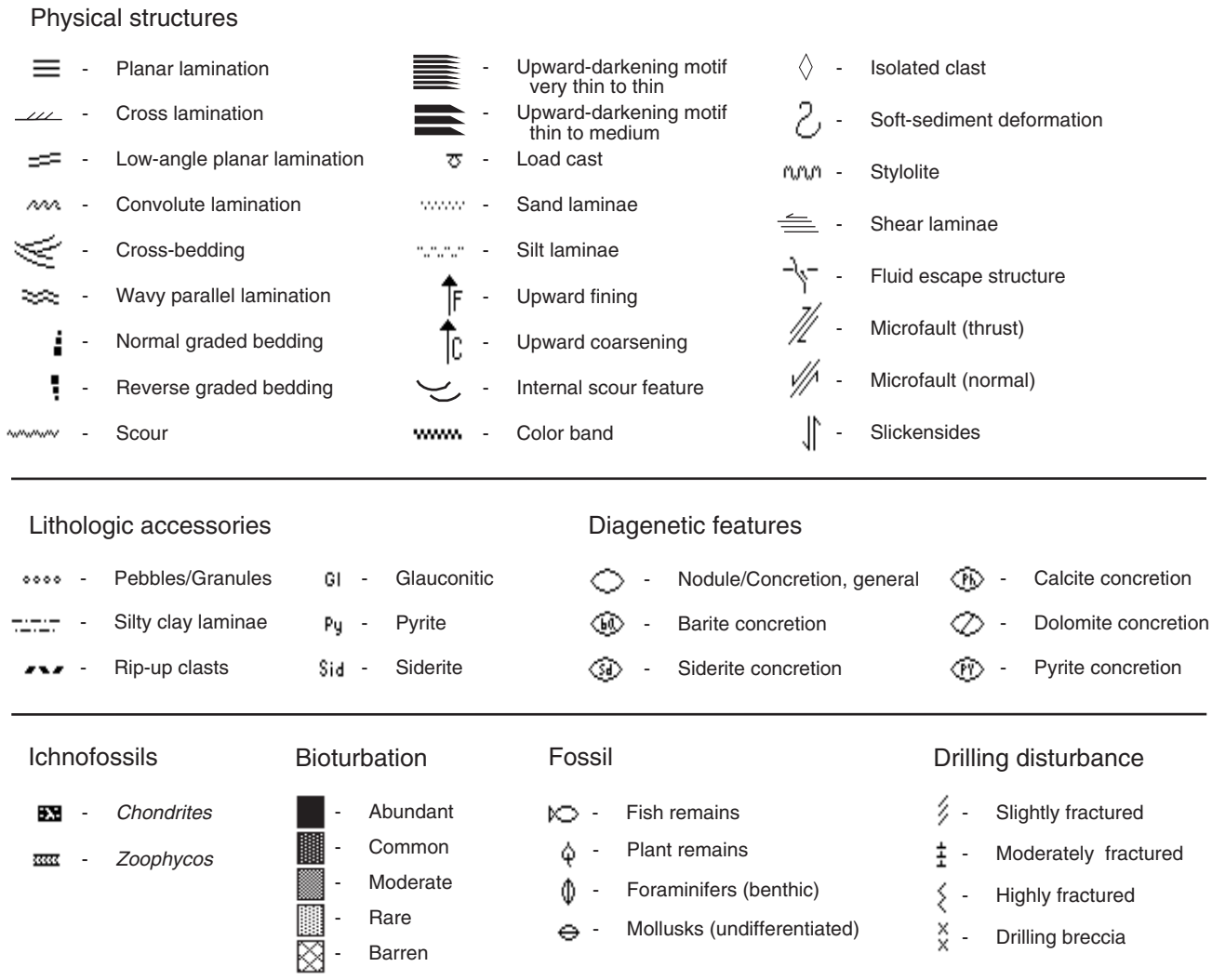

Figure F6. Blank example of the igneous and metamorphic rock VCD form.

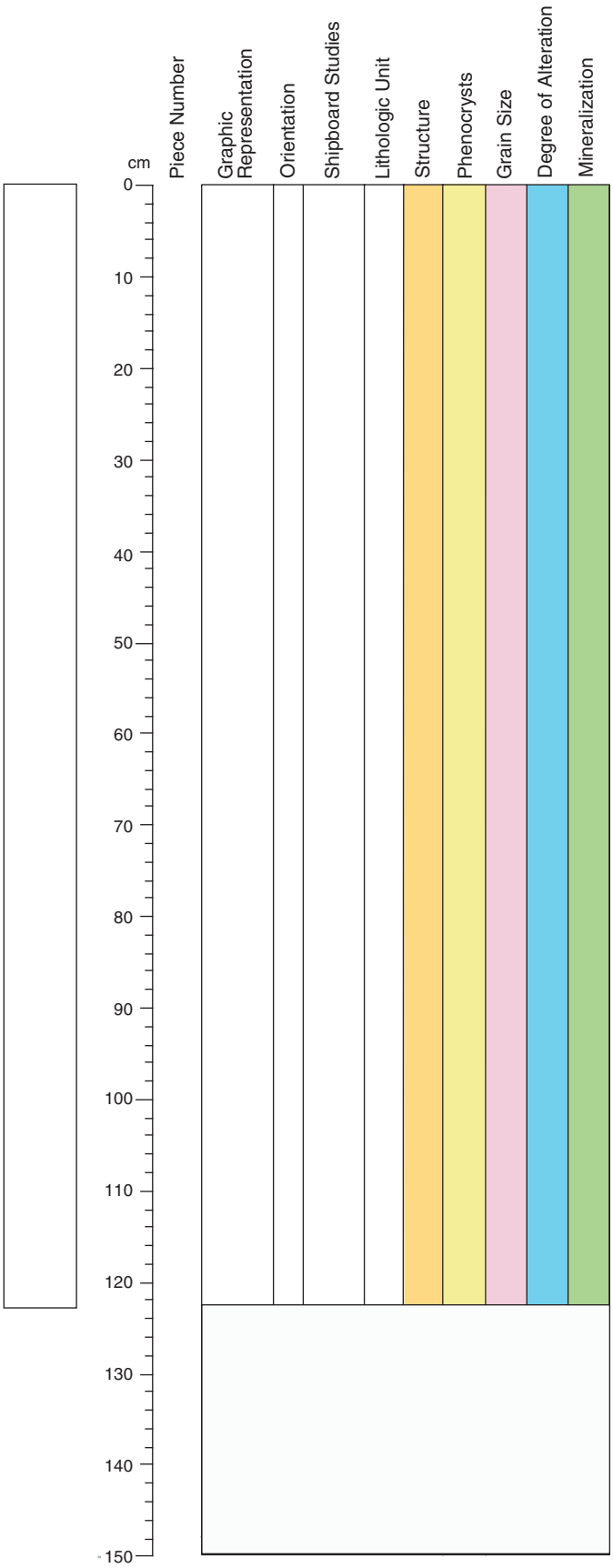

210-1276A-xxR-x (Section top: xxx.x mbsf)

UNIT xx, Zone x -

ROCK NAME:
PIECE:
CONTACTS:
Upper:
Lower:
COLOR:
PHENOCRYSTS:
Plagioclase
Clinopyroxene
GROUNDMASS:
Primary minerals:
Secondary minerals:
Grain size:
Texture: Intersertal

ALTERATION:
ADDITIONAL COMMENTS:

Figure F7. Key to the igneous and metamorphic petrology VCD form used during Leg 210.

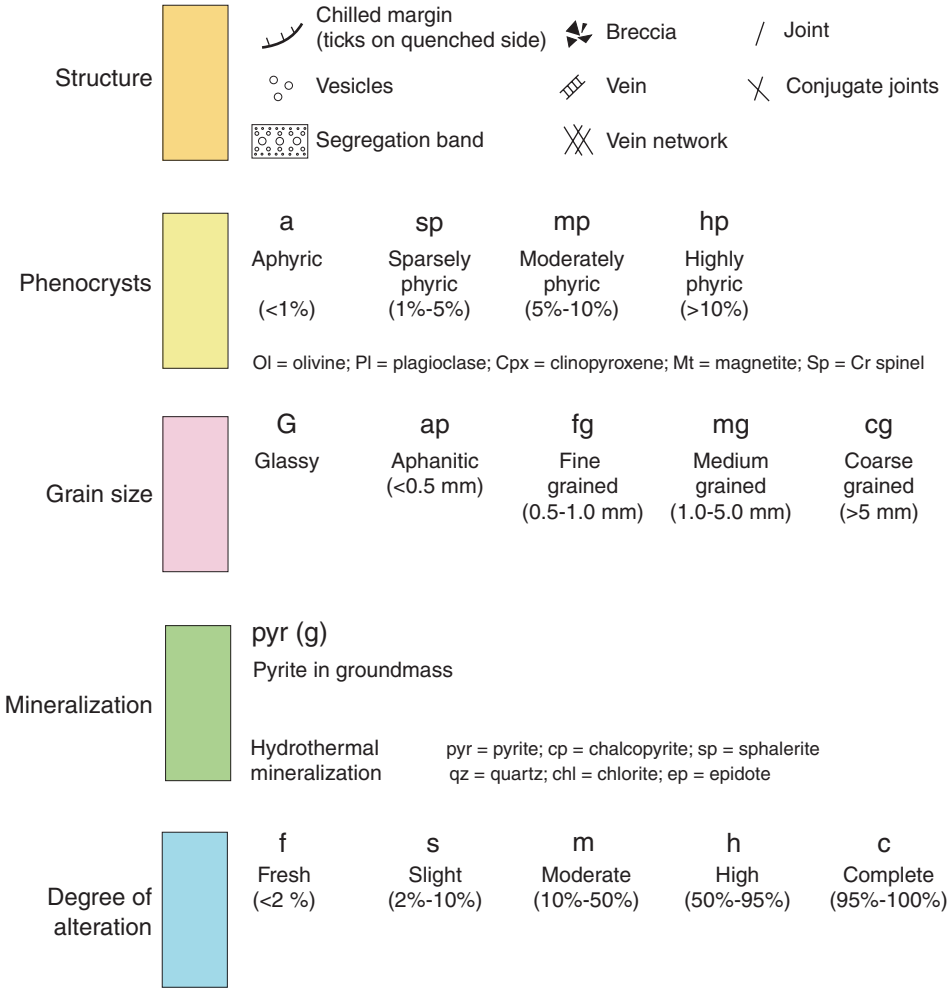

Figure F8. Core reference frame used during Leg 210 for measuring azimuths and dips of structural features in the working and archive halves of the core. See **"Structural Measurements,"** p. 15, in "Structural Geology" for an explanation.

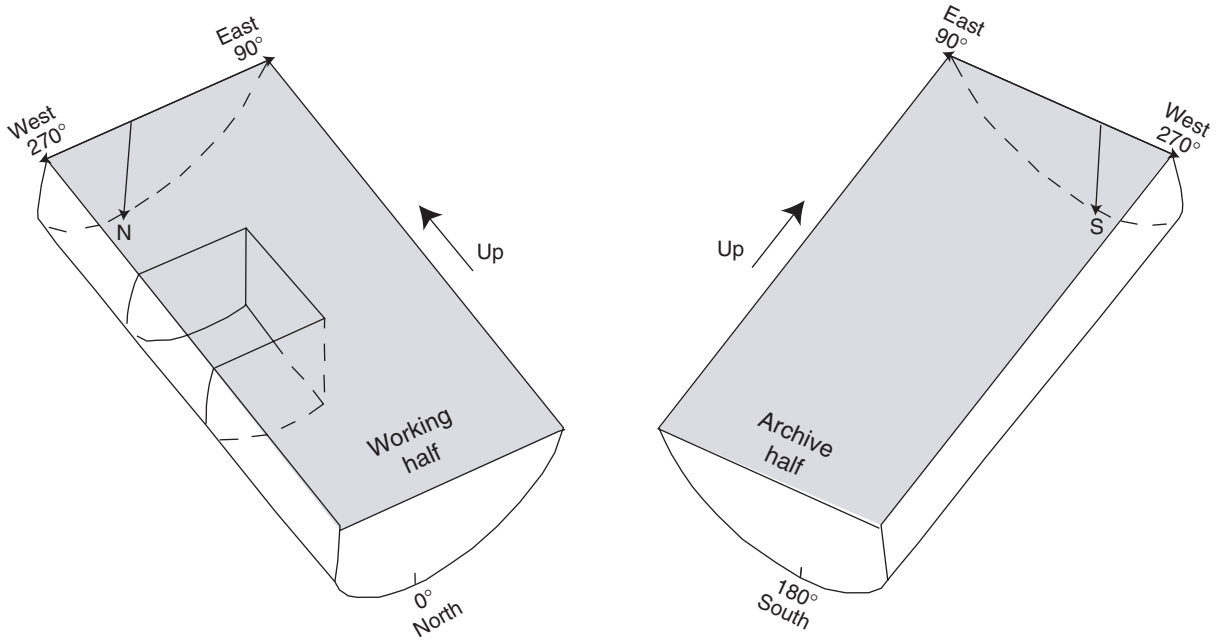

Figure F9. Conventions used for the measurement of azimuths and dips of structural features.

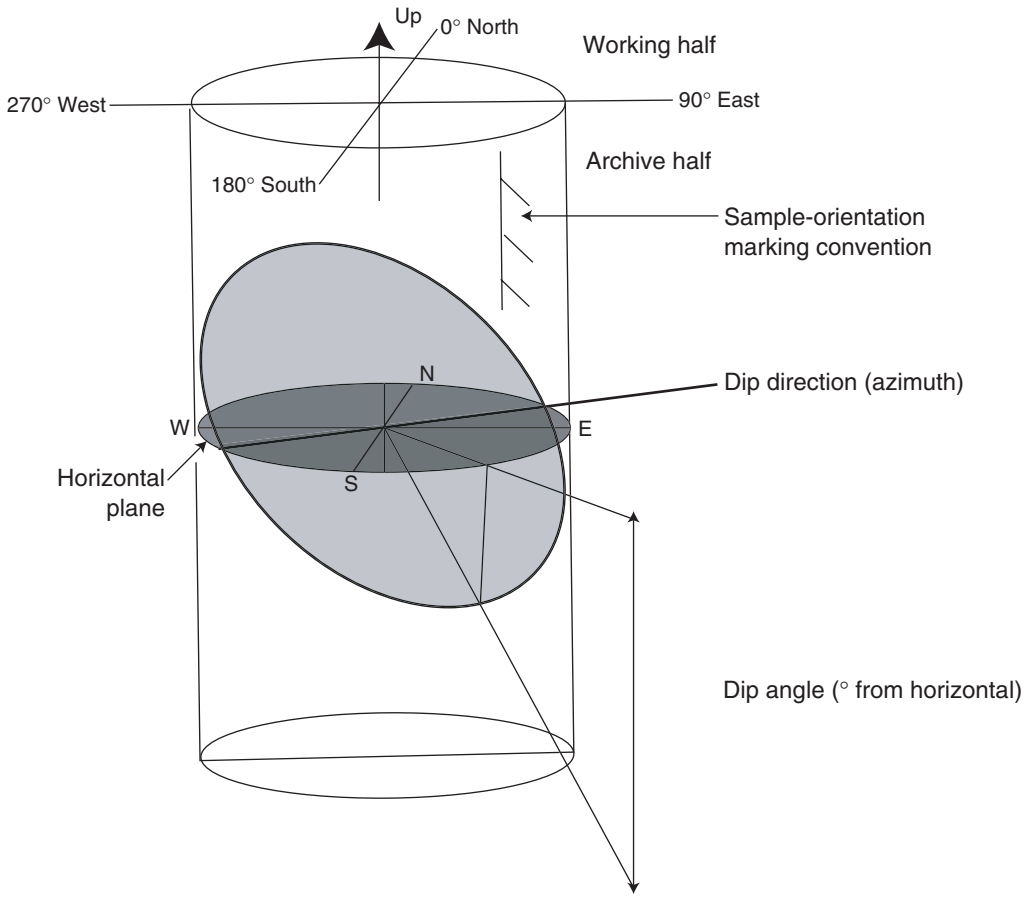

Figure F10. Leg 210 timescale and primary calcareous microfossil datums for the Cenozoic and Cretaceous. A. 0–25 Ma. Forams = foraminifers, Nannos = nannofossils. T = top (last occurrence), B = bottom (first occurrence). TA = top acme. Foraminifer datums are underlined. S = sinistral, D = dextral. Datum ages (Ma) are in parentheses. (Continued on next four pages.)

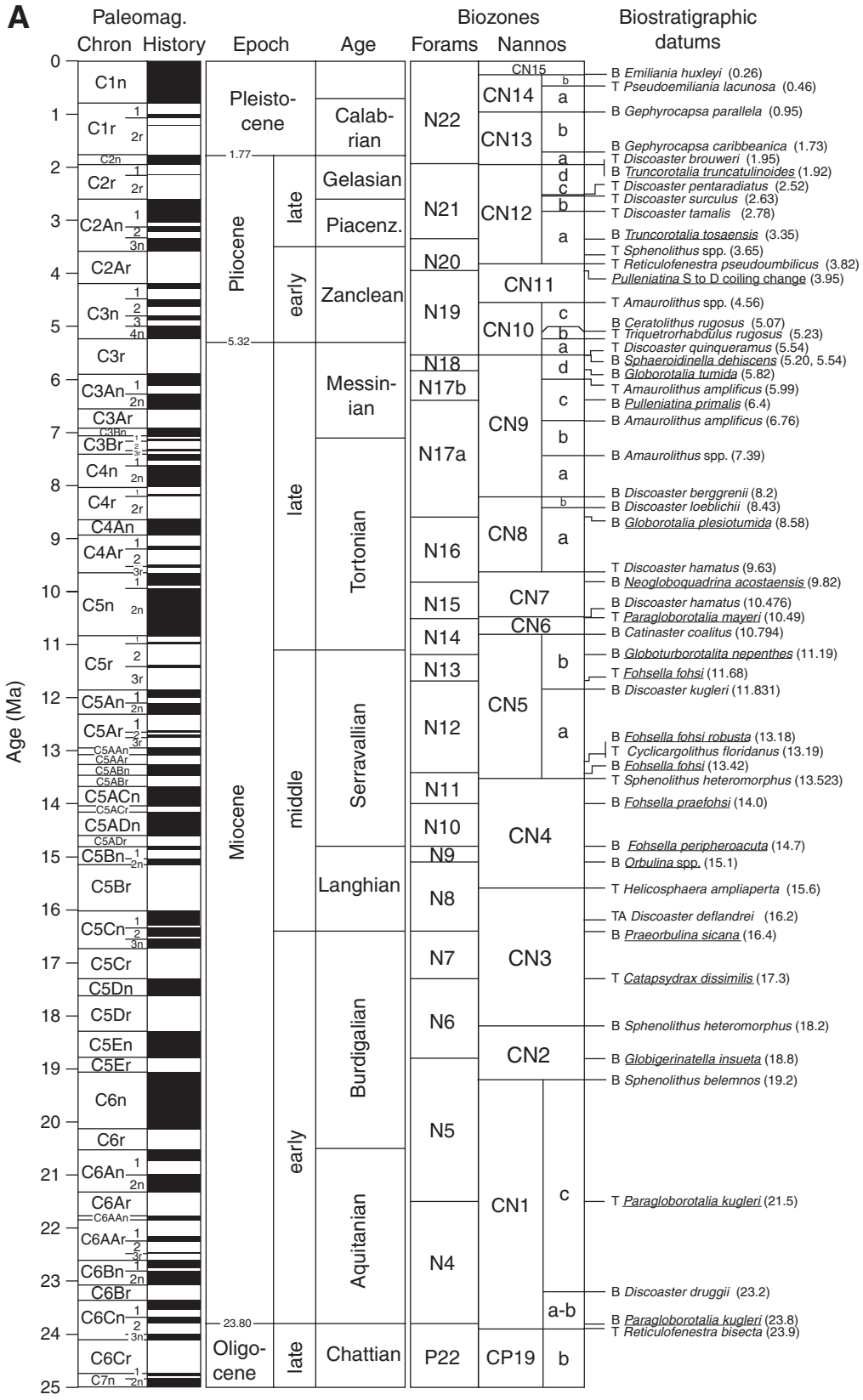

Figure F10 (continued). B. 20–45 Ma.

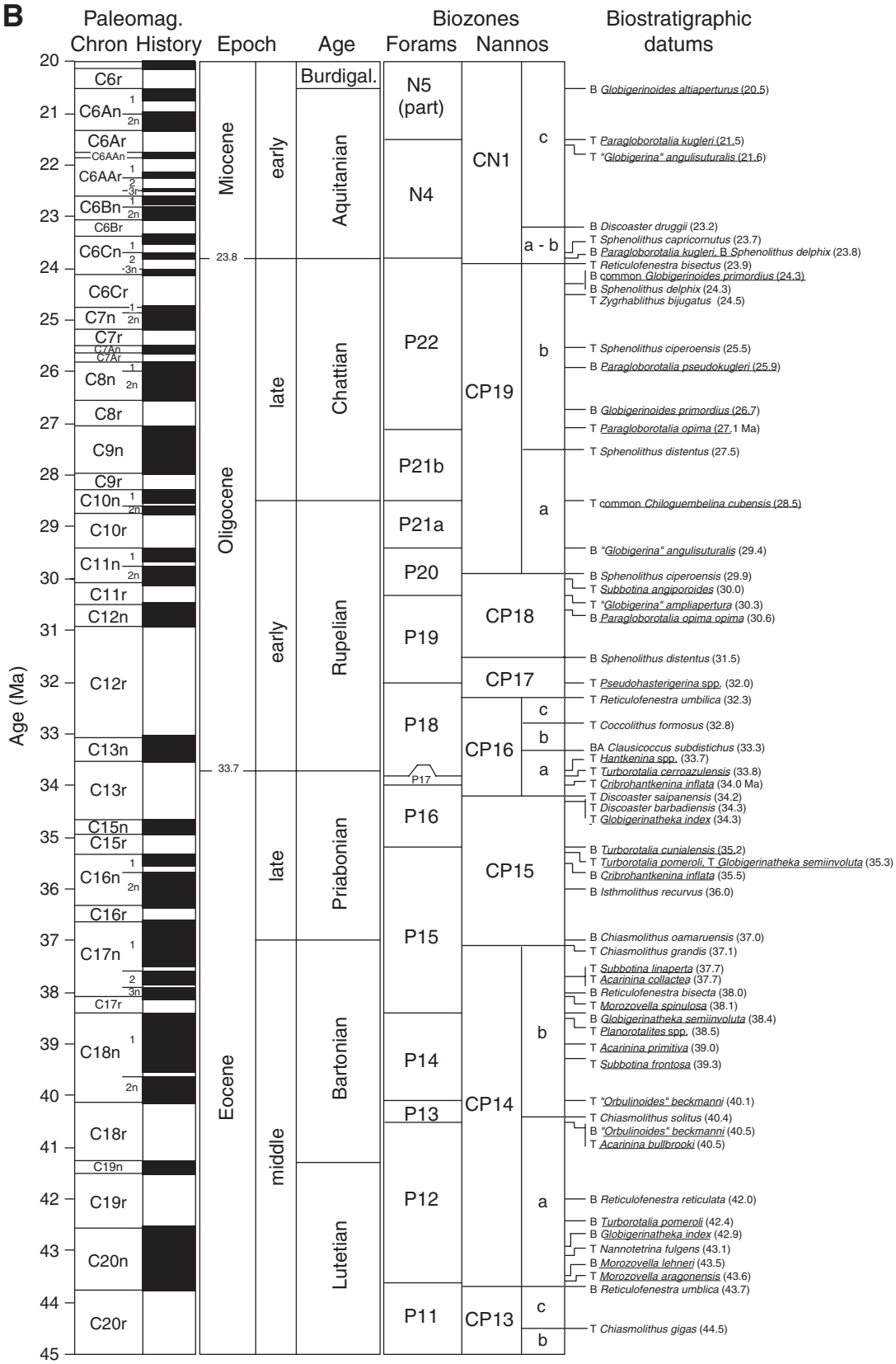

Figure F10 (continued). C. 40–65 Ma.

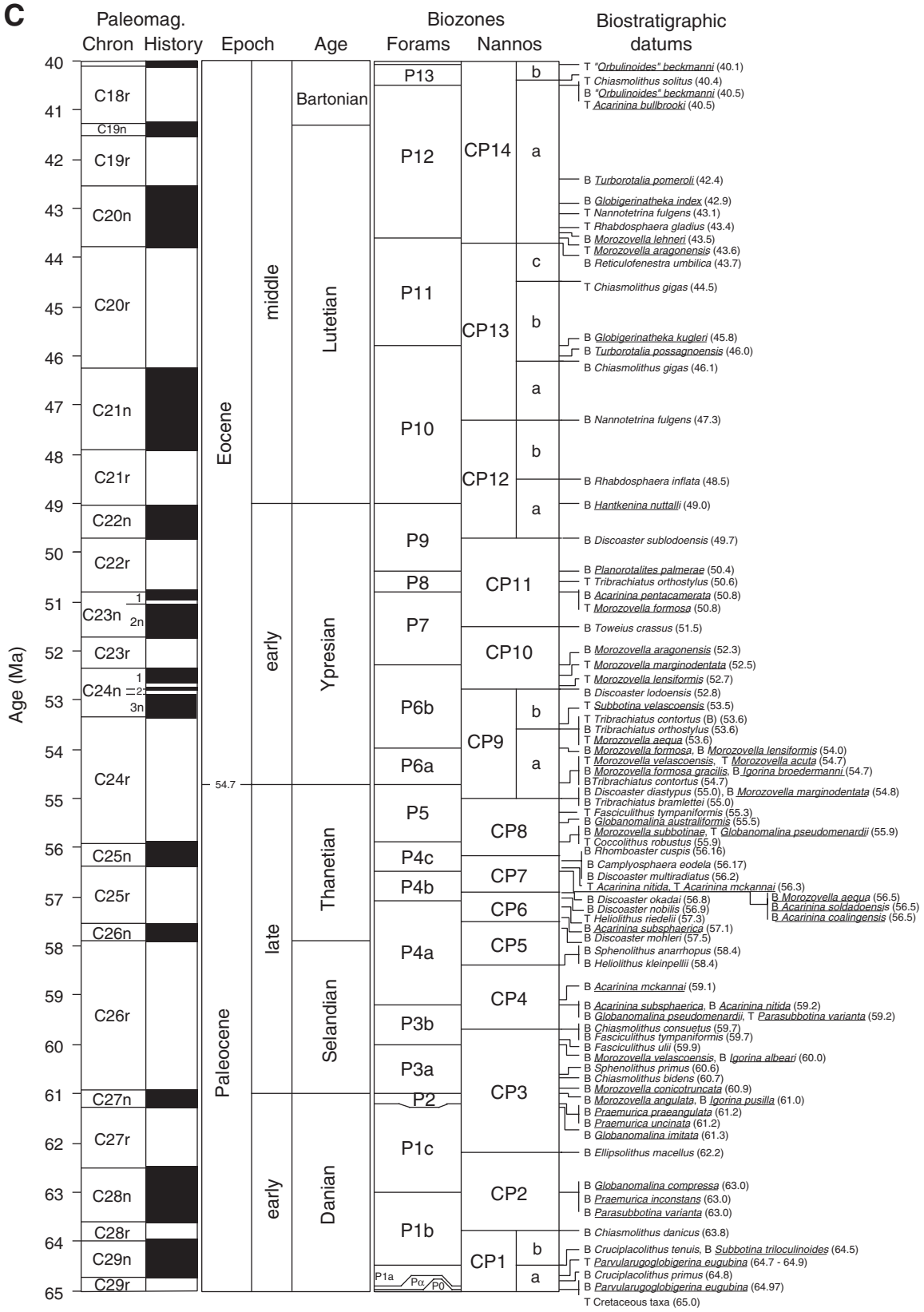

Figure F10 (continued). D. 60–85 Ma.

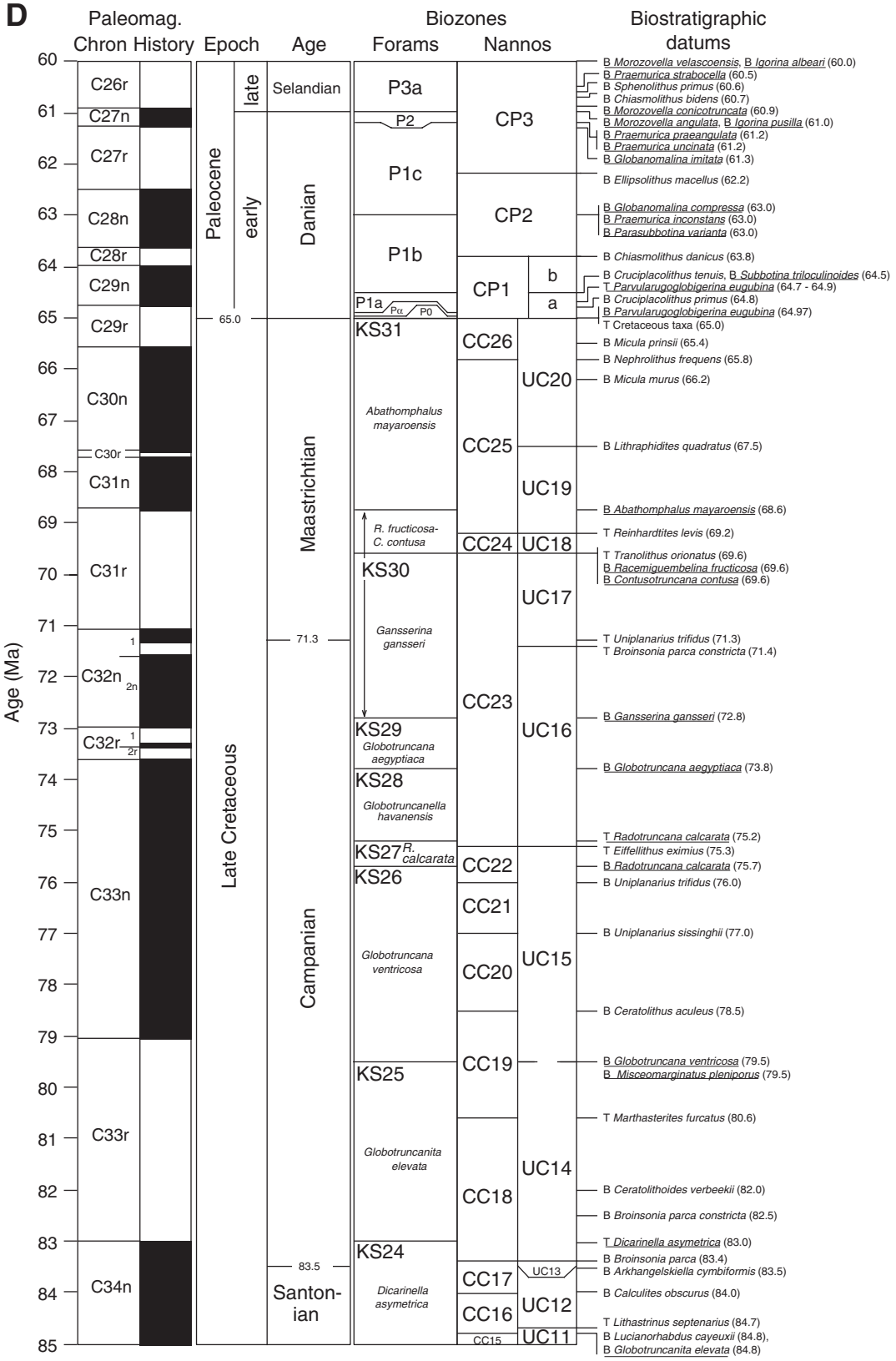

Figure F10 (continued). E. 80–130 Ma.

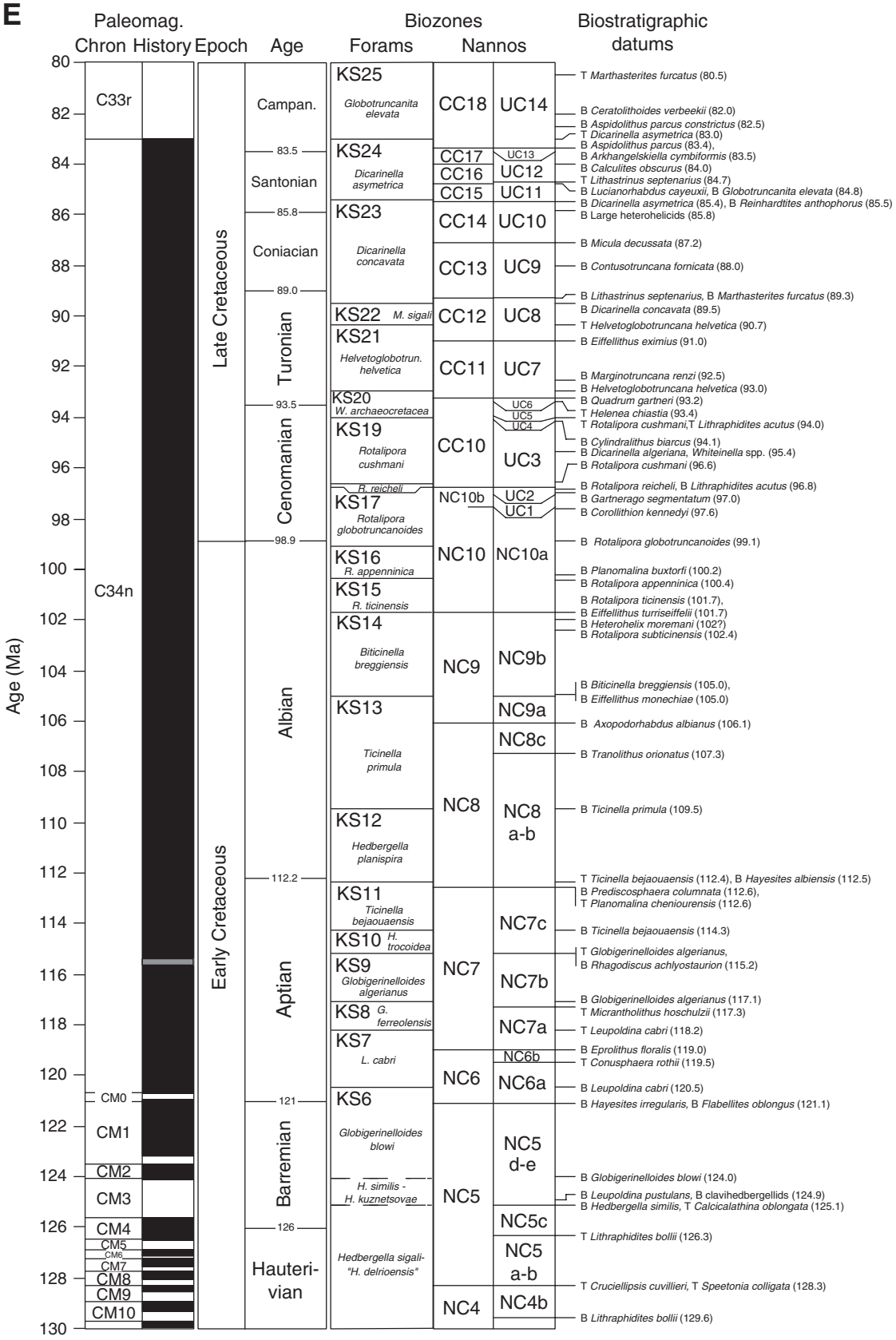

Figure F11. Leg 210 timescale and primary calcareous and siliceous microfossil datums for the latest Jurassic–Early Cretaceous. T = top (last occurrence), B = bottom (first occurrence). Forams = foraminifers, Nannos = nannofossils, Rads = radiolarians. Foraminifer datums are underlined. Datum ages (Ma) are in parentheses.

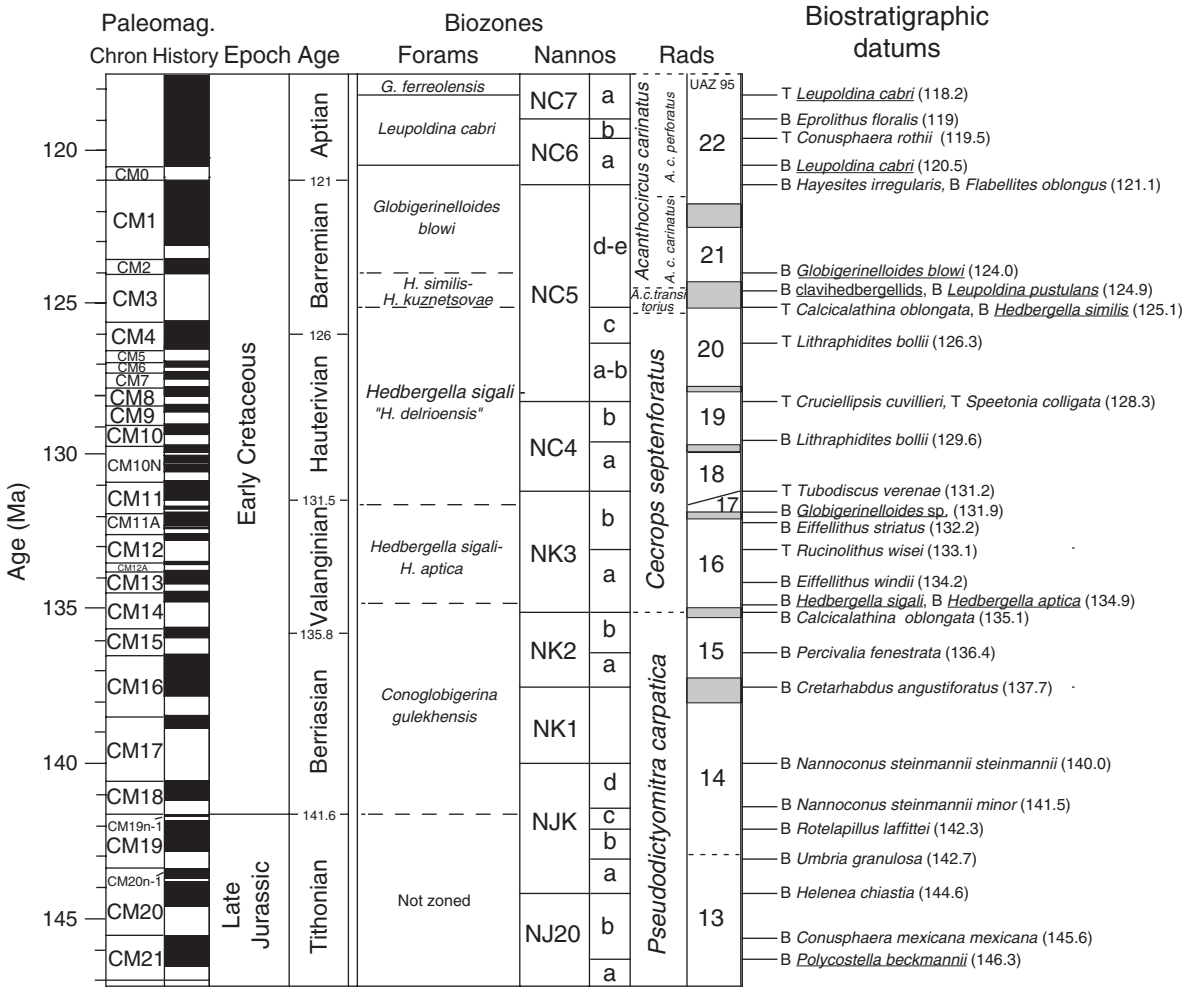

Figure F12. Magnetic orientation convention. Hachures show sample orientation marking convention, with arrows pointing up.

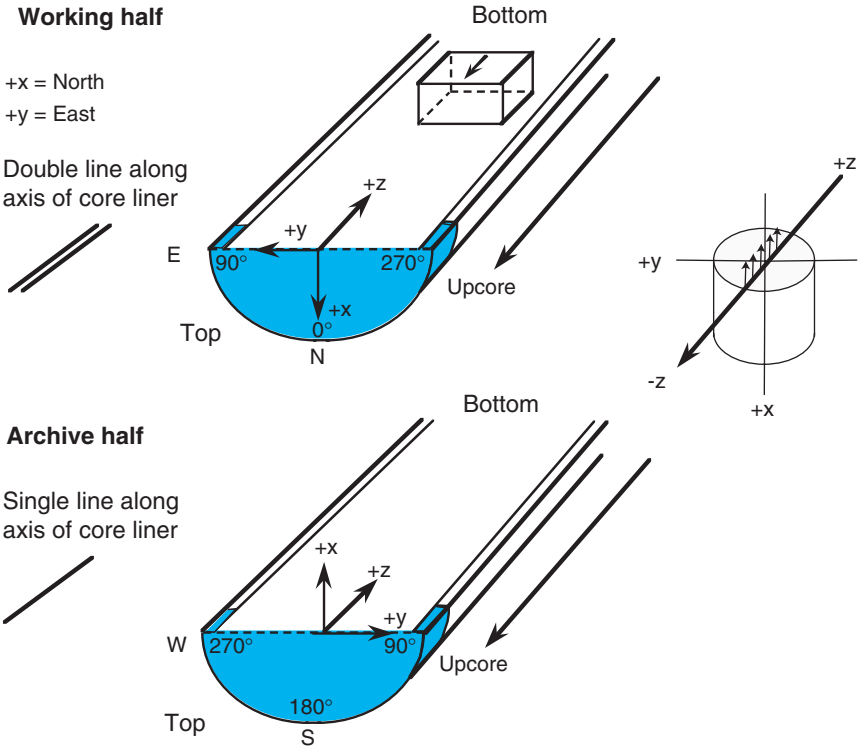

Table T1. Cenozoic calcareous nannofossil datums. (See table notes. Continued on next page.)

Datum event	Zone (base)	Age (Ma)	Reference
FO *Emiliania huxleyi*	CN15/NN21	**0.26**	1
LO *Pseudoemiliania lacunosa*	CN14b/NN20	**0.46**	1
FO *Gephyrocapsa parallela*	CN14a	0.95	2
FO *Gephyrocapsa caribbeanica*	CN13b	1.73	2
LO *Discoaster brouweri*	CN13a/NN19	**1.95**	1
LO *Discoaster pentaradiatus*	CN12d/NN18	**2.52**	3
LO *Discoaster surculus*	CN12c/NN17	**2.63**	3
LO *Discoaster tamalis*	CN12b	**2.78**	3
LO *Reticulofenestra pseudoumbilicus*	CN12a/NN16	**3.82**	3
LO *Amaurolithus primus*		**4.56**	3
LO *Ceratolithus acutus*		**5.046**	4
FO *Ceratolithus rugosus*	CN10c/NN13	**5.089**	4
LO *Triquetrorhabdulus rugosus*		**5.231**	4
LO *Discoaster quinqueramus*	CN10a/NN12	**5.537**	4
LO *Amaurolithus amplificus*	CN9d/NN11d	**5.999**	4
FO *Amaurolithus amplificus*	CN9c/NN11c	**6.84**	4
FO *Amaurolithus primus*		**7.392**	4
FO *Discoaster berggrenii*	CN9a/NN11a	**8.281**	4
FO *Discoaster loeblichii* (*Discoaster neoerectus*?)	CN8b	**8.43**	4
LO *Discoaster hamatus*	CN8a/NN10	**9.635**	4
LO *Catinaster calyculus*		**9.641**	4
LO *Catinaster coalitus*		**9.694**	4
FO *Discoaster neohamatus*		**10.45**	4
FO *Discoaster hamatus*	CN7a/NN9a	**10.476**	4
FO *Discoaster brouweri*		**10.687**	4
FO *Catinaster calyculus*		**10.705**	4
FO *Catinaster coalitus*	CN6/NN8	**10.794**	4
LO *Coccolithus miopelagicus*		**10.941**	4
LO *Discoaster kugleri*		**11.52**	4
FO *Discoaster kugleri*	CN5b/NN7	**11.831**	4
LO *Cyclicargolithus floridanus*		**13.19**	5
LO *Sphenolithus heteromorphus*	CN5a/NN6	**13.523**	4
LO *Helicosphaera ampliaperta*	CN4/NN5	15.6	1
LO Abundant *Discoaster deflandrei*		**16.2**	5
FO *Sphenolithus heteromorphus*		18.2	1
FO *Sphenolithus belemnos*	CN2/NN3	19.2	1
FO *Discoaster druggii*	CN1c/NN2	23.2	1
LO *Sphenolithus capricornutus*		23.7	1
LO *Sphenolithus delphix*		23.8	1
LO *Reticulofenestra bisectus*	CN1a–CN1b	23.9	1
FO *Sphenolithus delphix*		24.3	1
LO *Zygrhablithus bijugatus*		24.5	1
LO *Sphenolithus ciperoensis*		25.5	1
LO *Sphenolithus distentus*	CP19b/NP25	27.5	1
FO *Sphenolithus ciperoensis*	CP19a/NP24	29.9	1
FO *Sphenolithus distentus*	CP18	31.5	1
LO *Reticulofenestra umbilica*	CP17/NP23	32.3	1
LO *Coccolithus formosus*	CP16c/NP22	32.8	1
FO Acme *Clausicoccus subdistichus*	CP16b	33.3	1
LO *Discoaster saipanensis*	CP16a/NP21	34.2	1
LO *Discoaster barbadiensis*		34.3	1
FO *Isthmolithus recurvus*	NP19–NP20	36.0	1
FO *Chiasmolithus oamaruensis*		37.0	1
LO *Chiasmolithus grandis*	CP15/NP18	37.1	1
FO *Reticulofenestra bisecta*		38.0	1
LO *Chiasmolithus solitus*	CP14b/NP17	40.4	1
FO *Reticulofenestra reticulata*		42.0	1
LO *Nannotetrina fulgens*		43.1	1
FO *Reticulofenestra umbilica*	CP14a/NP16	43.7	1
LO *Chiasmolithus gigas*	CP13c/NP15c	44.5	1
FO *Chiasmolithus gigas*	CP13b/NP15b	46.1	1
FO *Nannotetrina fulgens*	CP13a/NP15a	47.3	1
FO *Rhabdosphaera inflatus*	CP12b/NP14b	48.5	1
FO *Discoaster sublodoensis*	CP12a/NP14a	49.7	1
LO *Tribrachiatus orthostylus*	CP11/NP13	50.6	1
FO *Toweius crassus*		51.5	1
FO *Discoaster lodoensis*	CP10/NP12	52.85	1
LO *Tribrachiatus contortus*	CP9b/NP11	52.85	1

Table T1 (continued).

Datum event	Zone (base)	Age (Ma)	Reference
FO *Tribrachiatus orthostylus*		53.6	1
FO *Tribrachiatus contortus*		54.7	1
FO *Discoaster diastypus*	CP9a/NP10	55.0	1
FO *Tribrachiatus bramlettei*	CP9a/NP10	55.0	1
LO *Fasciculithus tympaniformis*		55.3	1
FO *Rhomboaster cuspis*		55.16	1
FO *Campylosphaera eodela*	CP8b	55.5	1
FO *Discoaster multiradiatus*	CP8a/NP9	56.2	1
FO *Discoaster okadai*		56.8	1
FO *Discoaster nobilis*	CP7/NP9	56.9	1
FO *Heliolithus riedelii*	NP 8	57.3	1
FO *Discoaster mohleri*	CP6/NP7	57.5	1
FO *Sphenolithus anarrhopus*		58.4	1
FO *Heliolithus kleinpellii*	CP5/NP6	58.4	1
FO *Chiasmolithus consuetus*		59.7	1
FO *Fasciculithus tympaniformis*	CP4/NP5	59.7	1
FO *Fasciculithus ulii*		59.9	1
FO *Sphenolithus primus*		60.6	1
FO *Chiasmolithus bidens*		60.7	1
FO *Ellipsolithus macellus*	CP3/NP4	62.2	1
FO *Chiasmolithus danicus*	CP2/NP3	63.8	1
FO *Cruciplacolithus tenuis*	CP1b/NP2	64.5	1
FO *Cruciplacolithus primus*		64.8	1

Notes: LO = last occurrence, FO = first occurrence. Reference: 1 = Berggren et al. (1995b), 2 = Kameo and Bralower (2000), 3 = Shackleton et al. (1995), 4 = Backman and Raffi (1997), 5 = Raffi and Flores (1995). Bold = astrochronologically tuned datums.

Table T2. Cenozoic planktonic foraminifer datums. (See table notes. Continued on next page.)

Datum event	Zone (base)	Age (Ma)	Reference
LO *Truncorotalia tosaensis*	PT1b	**0.65**	1
LO *Globigerinoides fistulosus*	PT1a	**1.88**	3
FO *Truncorotalia truncatulinoides*	N22	**1.92**	3
LO *Globorotalia exilis*		**2.09**	3
LO *Globorotalia miocenica*		**2.38**	3
LO *Globorotalia pseudomiocenica* (Indo-Pacific only)	PL6	**2.3**	2
LO *Globoturborotalia woodi*		**2.33**	3
LO *Dentoglobigerina altispira*	PL5	**3.11**	3
LO *Sphaeroidinellopsis seminulina*	PL4	**3.11**	3
FO *Globigerinelloides fistulosus*		**3.33**	1
FO *Truncorotalia tosaensis*	N21	**3.35**	1
LO *Pulleniatina primalis*		**3.65**	1
FO *Globorotalia miocenica*		**3.77**	3
LO *Globorotalia margaritae*	PL3	**3.85**	3
FO *Globorotalia crassaformis*		**4.31**	3
LO *Pulleniatina spectabilis*		**4.33**	4
LO *Globoturborotalita nepenthes*	PL2	**4.39**	3
LO *Globorotalia cibaoensis*	PL1b	**4.6**	2
FO *Sphaeroidinella dehiscens* s.l.	N19	**5.54**	3
FO *Globorotalia tumida*	N18/PL1a	**5.82**	3
LO *Globorotalia lenguaensis*	M14	6.0	2
FO *Pulleniatina primalis*		6.4	2
FO *Globorotalia conomiozea*		7.12 (6.9)	2
FO *Globigerinoides extremus*		**8.58**	3
FO *Globorotalia plesiotumida*	N17/M13b	**8.58**	3
FO *Neogloboquadrina acostaensis*	N16/M13a	**9.82**	3
LO *Paragloborotalia mayeri*	N15/M12	**10.49**	3
FO *Globoturborotalita nepenthes*	N14/M11	**11.19**	3
LO *Fohsella fohsi* s.l. (incl. *fohsi lobata* and *fohsi robusta*)	N13/M10	**11.68**	3
FO *Globorotalia lenguaensis*		**12.85**	3
FO *Fohsella fohsi robusta*		**13.18**	3
FO *Fohsella fohsi* s.l.	N12/M8	**13.42**	3
FO *Fohsella praefohsi*	N11	14.0	5
FO *Fohsella peripheroacuta*	N10/M7	14.7	5
FO *Orbulina* spp.	N9/M6	15.1	5
FO *Praeorbulina glomerosa*	M5b	16.1	5
FO *Praeorbulina sicana*	N8/M5a	16.4	5
FO *Globorotalia miozea*		16.7	2
LO *Catapsydrax dissimilis*	N7/M4a	17.3	5
FO *Globorotalia praescitula*		18.5	2
FO *Globigerinatella insueta*	N6/M3	18.8	2
LO *Globoquadrina binaiensis*		19.1	5
FO *Globigerinoides altiaperturus*		20.5	2
LO *Paragloborotalia kugleri*	N5/M2	21.5	2
LO *Globigerina angulisuturalis*		21.6	2
FO *Globoquadrina dehiscens*	M1b	23.2	2
FO *Globigerinoides trilobus* s.l.		23.4	5
FO *Paragloborotalia kugleri*	N4/M1a	23.8	2
FO *Globigerinoides primordius* (common)		24.3	2
FO *Paragloborotalia pseudokugleri*		25.9	2
FO *Globigerinoides primordius*		26.7	2
LO *Paragloborotalia opima*	P22	27.1	2
LO *Chiloguembelina cubensis* (common)	P21b	28.5	2
FO *Globigerina angulisuturalis*	P21a	29.4	2
LO *Subbotina angiporoides*		30.0	2
LO *Globigerina ampliapertura*	P20	30.3	2
FO *Paragloborotalia opima*		30.6	2
LO *Pseudohastigerina* spp.	P19	32.0	2
LO *Hantkenina* spp.		33.7	2
LO *Turborotalia cerroazulensis*	P18	33.8	2
LO *Cribrohantkenina inflata*	P17	34.0	2
LO *Globigerapsis index*		34.3	2
FO *Turborotalia cunialensis*	P16	35.2	2
LO *Turborotalia pomeroli*		35.3	2
LO *Globigerinatheka semiinvoluta*		35.3	2
FO *Cribrohantkenina inflata*		35.5	2
LO *Acarinina collactea*		37.7	2
LO *Subbotina linaperta*		37.7	2

Table T2 (continued).

Datum event	Zone (base)	Age (Ma)	Reference
LO *Morozovella spinulosa*		38.1	2
FO *Globigerinatheka semiinvoluta*	P15	38.4	2
LO *Planorotalites*		38.5	2
LO *Acarinina primitiva*		39.0	2
LO *Subbotina frontosa*		39.3	2
LO *Orbulinoides beckmanni*	P14	40.1	2
FO *Orbulinoides beckmanni*	P13	40.5	2
LO *Acarinina bullbrooki*		40.5	2
FO *Turborotalia pomeroli*		42.4	2
FO *Globigerapsis index*		42.9	2
FO *Morozovella lehneri*		43.5	2
LO *Morozovella aragonensis*	P12	43.6	2
FO *Globigerinatheka kugleri*	P11	45.8	2
FO *Turborotalia possagnoensis*		46.0	2
FO *Hantkenina nuttalli*	P10	49.0	2
FO *Planorotalites palmerae*	P9	50.4	2
LO *Morozovella formosa*	P8	50.8	2
FO *Acarinina pentacamerata*		50.8	2
FO *Morozovella aragonensis*	P7	52.3	2
LO *Morozovella marginodentata*		52.5	2
LO *Morozovella lensiformis*		52.7	2
LO *Subbotina velascoensis*		53.5	2
LO *Morozovella aequa*		53.6	2
FO *Morozovella formosa*	P6b	54.0	2
FO *Morozovella lensiformis*		54.0	2
LO *Morozovella velascoensis*	P6a	54.7	2
LO *Morozovella acuta*		54.7	2
FO *Morozovella gracilis*		54.7	2
FO *Igorina broedermanni*		54.7	2
FO *Morozovella marginodentata*		54.8	2
FO *Globanomalina australiformis*		55.5	2
FO *Morozovella subbotinae*		55.9	2
LO *Globanomalina pseudomenardii*	P5	55.9	2
LO *Acarinina nitida* (= *A. acarinata*)		56.3	2
LO *Acarinina mckannai*		56.3	2
FO *Acarinina soldadoensis*	P4c	56.5	2
FO *Acarinina coalingensis* (= *triplex*)		56.5	2
FO *Morozovella aequa*		56.5	2
LO *Acarinina subsphaerica*	P4b	57.1	2
FO *Acarinina mckannai*		59.1	2
FO *Acarinina subsphaerica*		59.2	2
FO *Acarinina nitida*		59.2	2
FO *Globanomalina pseudomenardii*	P4a	59.2	2
LO *Parasubbotina variospira* (= *varianta*?)		59.2	2
FO *Morozovella velascoensis*		60.0	2
FO *Igorina albeari*	P3b	60.0	2
FO *Morozovella conicotruncata*		60.9	2
FO *Morozovella angulata*	P3a	61.0	2
FO *Igorina pusilla*		61.0	2
FO *Praemurica praeangulata*		61.2	2
FO *Praemurica uncinata*	P2	61.2	2
FO *Globanomalina imitata*		61.3	2
FO *Globanomalina compressa*	P1c	63.0	2
FO *Praemurica inconstans*		63.0	2
FO *Parasubbotina varianta*		63.0	2
FO *Subbotina triloculinoides*	P1b	64.5	2
LO *Parvularugoglobigerina eugubina*	P1a	64.9	2
FO *Parvularugoglobigerina eugubina*	Pα	64.97	2

Notes: LO = last occurrence, FO = first occurrence. Reference: 1 = Berggren et al. (1995a), 2 = Berggren et al. (1995b), 3 = Chaisson and Pearson (1997), 4 = Shackleton et al. (1995), 5 = Pearson and Chaisson (1997). Bold = astrochronologically tuned datums.

Table T3. Cretaceous calcareous nannofossil datums.

Datum event	Zone (base)	Age (Ma)	Reference
LO Cretaceous taxa (*Micula prinsii*)		65.0	1
FO *Micula prinsii*		65.4	2
FO *Nephrolithus frequens*	CC26	65.8	2, 3
FO *Micula murus*		66.2	2, 3
FO *Lithraphidites quadratus*	UC20	67.5	2, 4
LO *Reinhardities levis*	CC25/UC19	69.2	2, 3, 4
LO *Tranolithus orionatus*	CC24/UC18	69.6	2, 3, 4
LO *Uniplanarius trifidus*		71.3	2
LO *Aspidolithus parcus constrictus*	UC17	71.4	2, 4, 8
LO *Eiffellithus eximius*	CC23/UC16	75.3	2, 3, 4
FO *Uniplanarius trifidus*	CC22	76.0	2, 3
FO *Uniplanarius sissinghii*	CC21	77.0	2, 3
FO *Ceratolithoides aculeus*	CC20	78.5	2, 3
FO *Misceomarginatus pleniporus*	UC15	79.5	2, 4
LO *Marthasterites furcatus*	CC19	80.6	2, 3
FO *Ceratolithoides verbeekii*		82.0	2
FO *Aspidolithus parcus constrictus*		82.5	2, 8
FO *Aspidolithus parcus*	CC18/UC14	83.4	2, 3, 4, 8
FO *Arkhangelskiella cymbiformis*	UC13	83.5	2, 4
FO *Calculites obscurus*	CC17	84.0	2, 3
LO *Lithastrinus septenarius*	UC12	84.7	2, 4
FO *Lucianorhabdus cayeuxii*	CC16	84.8	2, 3
FO *Reinhardtites anthophorus*	CC15/UC11	85.5	2, 3, 4
FO *Micula decussata*	CC14/UC10	87.2	2, 3, 4
FO *Lithastrinus septenarius*	UC9	89.3	2, 4
FO *Marthasterites furcatus*	CC13	89.3	2, 3
FO *Eiffellithus eximius*	CC12/UC8	91.0	2, 3, 4
FO *Quadrum gartneri*	CC11/UC7	93.2	2, 3, 4
LO *Helenea chiastia*	UC6	93.4	2, 4
LO *Lithraphidites acutus*	UC5	94.0	2, 4
FO *Cylindralithus biarcus*	UC4	94.1	2, 4
FO *Lithraphidites acutus*	CC10/UC3	96.8	2, 3, 4
FO *Gartnerago segmentatum*	UC2	97.0	2, 3, 4
FO *Corollithion kennedyi*	NC10b/UC1	97.6	4, 5, 6
FO *Eiffellithus turriseiffelii*	NC10a	101.7	5, 6
FO *Eiffellithus monechiae*	NC9b	105.0	5, 6
FO *Axopodorhabus albianus*	NC9a	106.1	5, 6
FO *Tranolithus orionatus*	NC8c	107.3	5, 6
FO *Hayesites albiensis*	NC8b	112.5	5, 6
FO *Prediscosphaera columnata*	NC8a	112.6	5, 6
FO *Rhagodiscus achlyostaurion*	NC7c	115.2	5, 6
LO *Micrantholithus hoschulzii*	NC7b	117.3	5, 6
FO *Eprolithus floralis*	NC7a	119.0	5, 6
LO *Conusphaera rothii*	NC6b	119.5	5.6
FO *Hayesites irregularis*	NC6a	121.1	5, 6
FO *Flabellites oblongus*		121.1	2, 5
LO *Calcicalathina oblongata*	NC5d–NC5e	125.1	2, 5
LO *Lithraphidites bollii*	NC5c	126.3	2, 5
LO *Speetonia colligata*	NC5a–NC5b	128.3	9
LO *Cruciellipsis cuvillieri*	NC5a–NC5b	128.3	2, 5
FO *Lithraphidites bollii*	NC4b	129.6	2, 5
LO *Tubodiscus verenae*	NC4a	131.2	2, 5
FO *Eiffellithus striatus*		132.2	2, 7
LO *Rucinolithus wisei*	NK3b	133.1	2, 7
FO *Eiffellithus windii*		134.2	2, 7
FO *Calcicalathina oblongata*	NK3a	135.1	2, 7
FO *Percivalia fenestrata*	NK2b	136.4	2, 7
FO *Cretarhabdus angustiforatus*	NK2a	137.7	2, 7
FO *Nannoconus steinmannii steinmannii*	NK1	140.0	2, 7
FO *Nannoconus steinmannii minor*	NJKd	141.5	2.7
FO *Rotelapillus laffittei*	NJKc	142.3	2, 7
FO *Umbria granulosa*	NJKb	142.7	2, 7
FO *Helenea chiastia*	NJKa	144.6	2, 7
FO *Conusphaera mexicana mexicana*		145.6	2, 7
FO *Polycostella beckmannii*	NJ20b	146.3	2, 7

Notes: LO = last occurrence, FO = first occurrence. Reference: 1 = Berggren et al. (1995b), 2 = Erba et al. (1995), 3 = Sissingh (1977), 4 = Burnett (1999), 5 = Roth (1973), 6 = Bralower et al. (1997), 7 = Bralower et al. (1989), 8 = Gardin et al. (2001), 9 = Applegate and Bergen (1988).

Table T4. Cretaceous planktonic foraminifer datums.

Datum event (LO or FO)	Zone (base)	Age (Ma)	Reference
LO *Abathomphalus mayaroensis*		65.0	1
FO *Abathomphalus mayaroensis*	*A. mayaroensis* (KS31)	68.6	2, 3
FO *Racemiguembelina fructicosa*	*R. fructicosa–C. contusa*	69.6	3
FO *Contusotruncana contusa*	*R. fructicosa–C. contusa*	69.6	3
FO *Gansserina gansseri*	*G. gansseri* (KS30)	72.8	2, 4, 5
FO *Globotruncana aegyptiaca*	*G. aegyptiaca* (KS29)	73.8	2, 4, 5
LO *Radotruncana calcarata*	*G. havanensis* (KS28)	75.2	2, 4, 5
FO *Radotruncana calcarata*	*R. calcarata* (KS27)	75.7	2, 4, 5
FO *Globotruncana ventricosa*	*G. ventricosa* (KS26)	79.5	2, 4, 5
LO *Dicarinella asymetrica*	*G. elevata* (KS25)	83.0	2, 4, 5
FO *Globotruncana elevata*		84.8	5
FO *Dicarinella asymetrica*	*D. asymetrica* (KS24)	85.4	2, 4, 5
FO Large heterohelicids		85.8	3
FO *Contusotruncana fornicata*		88.0	3
FO *Dicarinella concavata*	*D. concavata* (KS23)	89.5	2, 4, 5
LO *Helvetoglobotruncana helvetica*	*M. sigali* (KS22)	90.7	2, 4, 6
FO *Marginotruncana* spp. (*M. renzi*)		92.5	3
FO *Helvetoglobotruncana helvetica*	*H. helvetica* (KS21)	93.0	2, 4, 6
LO *Rotalipora cushmani*	*W. archaeocretacea* (KS20)	94.0	2, 4, 6
FO *Dicarinella algeriana*		95.4	3
FO *Whiteinella* spp. (*W. baltica*)		95.4	3
FO *Rotalipora cushmani*	*R. cushmani* (KS19)	96.6	2, 4, 6
FO *Rotalipora reicheli*	*R. reicheli* (KS18)	96.8	2, 4, 6
FO *Rotalipora globotruncanoides*	*R. globotruncanoides* (KS17)	99.1	2, 4, 6
FO *Planomalina buxtorfi*		100.2	7
FO *Rotalipora appenninica*	*R. appenninica* (KS16)	100.4	2, 4, 6
FO *Rotalipora ticinensis*	*R. ticinensis* (KS15)	101.7	2, 4, 6
FO *Heterohelix* spp. (*H. moremani*)		102.0	3, 7
FO *Rotalipora subticinensis*		102.4	2, 4, 6
FO *Biticinella breggiensis*	*B. breggiensis* (KS14)	105.0	2. 4. 6
FO *Ticinella primula*	*T. primula* (KS13)	109.5	2, 4, 6
LO *Ticinella bejaouaensis*	*H. planispira* (KS12)	112.4	2, 4, 6, 7
LO *Planomalina cheniourensis*		112.6	2, 4, 6, 7
FO *Ticinella bejaouaensis*	*T. bejaouaensis* (KS11)	114.3	2, 4, 6, 7
LO *Globigerinelloides algerianus*	*H. trocoidea* (KS10)	115.2	2, 4, 6
FO *Globigerinelloides algerianus*	*G. algerianus* (KS9)	117.1	2, 4, 6
LO *Leupoldina cabri*	*G. ferreolensis* (KS8)	118.2	2, 4, 6
FO *Leupoldina cabri*	*L. cabri* (KS7)	120.5	2, 4, 6
FO *Globigerinelloides blowi*	*G. blowi* (KS6)	124.0	3
FO *Leupoldina pustulans*		124.9	3
FO Clavihedbergellids		124.9	3
FO *Hedbergella similis*	*H. similis–H. kuznetsovae*	125.1	3
FO *Globigerinelloides* spp.		131.9	3
FO *Hedbergella sigali*		134.9	3
FO *Hedbergella aptica*		134.9	3

Notes: LO = last occurrence, FO = first occurrence. Reference: 1 = Berggren et al. (1995b), 2 = Sliter (1989), 3 = Premoli Silva and Sliter (1999), 4 = Caron (1985), 5 = Erba et al. (1995), 6 = Bralower et al. (1997), 7 = Leckie (1984).

Table T5. Paleogene and Late Cretaceous mid-latitude dinocyst datums for the Northern Hemisphere. (**See table notes.** Continued on next page.)

Dinocyst taxon	Age (Ma)	
	FO	LO
Achilleodinium biformoides (Eisenack 1954b) Eaton 1976	54	30.5?
Achomosphaera alcicornu (Eisenack 1954b) Davey and Williams 1966a	57.65	13
Adnatosphaeridium tutulosum (Cookson and Eisenack 1960) Morgan 1980	94.4	94.06
Alisocysta circumtabulata (Drugg 1967) Stover and Evitt 1978	65	58.53
Alisocysta margarita (Harland 1979a) Harland 1979a	61.68	57.35
Alisocysta reticulata Damassa 1979b	65	61.37
Alisogymnium euclaense (Cookson and Eisenack 1970a) Lentin and Vozzhennikova 1990	87.72	65.00
Apectodinium augustum (Harland 1979c) Lentin and Williams 1981	55.6	55
Apteodinium deflandrei (Clarke and Verdier 1967) Lucas-Clark 1987	98.33	68.80
Areoligera gippingensis Jolley 1992	58	57
Areoligera semicirculata (Morgenroth 1966b) Stover and Evitt 1978	33.73	28.5
Areosphaeridium diktyoplokum (Klumpp 1953) Eaton 1971	50.5	33.3
Biconidinium longissimum Islam 1983c	54.31	50.71
Callaiosphaeridium asymmetricum (Deflandre and Courteville 1939) Davey and Williams 1966b	132.47	78.15
Cannosphaeropsis utinensis O. Wetzel 1933b	83.63	65.70
Carpatella cornuta Grigorovich 1969a	64.75	59.95
Carpodinium obliquicostatum Cookson and Hughes 1964	103.18	93.77
Cassiculosphaeridia reticulata Davey 1969		72.69
Cerebrocysta bartonensis Bujak in Bujak et al. 1980	41	38
Cerodinium diebelii (Alberti 1959b) Lentin and Williams 1987	77.97	59.95
Cereodinium wardenense (Williams and Downie 1966c) Lentin and Williams 1987	56	53.1
Charlesdowniea columna (Michoux 1988) Lentin and Vozzhennikova 1990	51.73	49.88
Charlesdowniea crassiramosa (Williams and Downie 1966b) Lentin and Vozzhennikova 1989	53.75	52.85
Charlesdowniea edwardsii (Wilson 1967c) Lentin and Vozzhennikova 1989	51.32	47.9
Chatangiella verrucosa (Manum 1963) Lentin and Williams 1976	93.50	72.50
Chichaouadinium vestitum (Brideaux 1971) Bujak and Davies 1983	105.00	98.90
Chiropteridium galea (Maier 1959) Sarjeant 1983	33.5	22.36
Conosphaeridium striatoconum (Deflandre and Cookson 1955) Cookson and Eisenack 1969		88.56
Cordosphaeridium cantharellum (Brosius 1963) Gocht 1969	40.8	19.5
Cordosphaeridium funiculatum Morgenroth 1966a	51.16	35?
Corrudinium incompositum (Drugg 1970b) Stover and Evitt 1978	40.8	31.34
Cyclapophysis monmouthensis Benson 1976	67	59.5
Cyclonephelium filoreticulatum (Slimani 1994) Prince et al. 1999	89.51	85.91
Cyclonephelium membraniphorum Cookson and Eisenack 1962b	101.06	88.52
Damassadinium californicum (Drugg 1967) Fensome et al. 1993b	64.75	60.33
Deflandrea oebisfeldensis Alberti 1959b	57.8	52.85
Deflandrea phosphoritica Eisenack 1938b	54	21.9
Dinogymnium spp.	91.69	65.00
Dinopterygium cladoides Deflandre 1935	106.88	72.88
Diphyes colligerum (Deflandre and Cookson 1955) Cookson 1965a	58.88	37
Diphyes ficusoides Islam 1983b	50.24	45.16
Dracodinium? condylos (Williams and Downie 1966b) Costa and Downie 1979	52.5	51.5
Dracodinium politum Bujak et al. 1980	52.1	51.5
Dracodinium varielongitudum (Williams and Downie 1966b) Costa and Downie 1979	53	51.5
Eatonicysta furensis (Heilmann-Clausen in Heilmann-Clausen and Costa 1989) Stover and Williams 1995	51.3	50.2
Eatonicysta pterococcoides (O. Wetzel 1933b) Sarjeant 1985b	77.04	
Eatonicysta ursulae (Morgenroth 1966a) Stover and Evitt 1978	53.61	48.5
Ellipsodinium rugulosum Clarke and Verdier 1967		83.37
Endoscrinium campanula (Gocht 1959) Vozzhennikova 1967	142.60	83.90
Enneadocysta pectiniformis (Gerlach 1961) Stover and Williams 1995	36. 5	29.3
Epelidosphaeridia spinosa Cookson and Hughes 1964 ex Davey 1969a	100.50	93.81
Florentinia mayii Kirsch 1991	79.01	71.86
Gerdiocysta conopeum Liengjarern et al. 1980	33.7	29.3
Glaphyrocysta semitecta (Bujak in Bujak et al. 1980) Lentin and Williams 1981	41.4	32
Heteraulacacysta porosa Bujak in Bujak et al. 1980	41	36.4
Heterosphaeridium difficile (Manum and Cookson 1964) Ioannides 1986	92.15	86.78
Homotryblium tenuispinosum Davey and Williams 1966b	56	14.5
Hystrichokolpoma bulbosum (Ehrenberg 1838) Morgenroth 1968	67	61.58
Hystrichokolpoma cinctum Klumpp 1953	53.51	17
Hystrichosphaeridium tubiferum (Ehrenberg 1838) Deflandre 1937b	119.02	46.33
Hystrichosphaeropsis quasicribrata (O. Wetzel 1961) Gocht 1976	82.33	
Isabelidinium viborgense Heilmann-Clausen 1985	61?	58.79
Kleithriasphaeridium loffrense Davey and Verdier 1976	112.18	76.34
Kleithriasphaeridium readii (Davey and Williams 1966b) Davey and Verdier 1976	100.27	85.8
Laciniadinium biconiculum McIntyre 1975	77.56	
Lentinia serrata Bujak in Bujak et al. 1980	40	33.5
Litosphaeridium siphonophorum (Cookson and Eisenack 1958) Davey and Williams 1966b	101.06	93.81

Table T5 (continued).

Dinocyst taxon	Age (Ma)	
	FO	LO
Manumiella seelandica (Lange 1969) Bujak and Davies 1983	67.1?	60.9?
Melitasphaeridium pseudorecurvatum (Morgenroth 1966a) Bujak et al. 1980	54.2	33?
Odontochitina costata Alberti 1961	99.65	70.43
Odontochitina diversa Pearce 2000 unpublished thesis name	88.96?	69.42?
Odontochitina operculata (O. Wetzel 1933a) Deflandre and Cookson 1955	126.95	70.43
Odontochitina porifera Cookson 1956	84.21	71.29
Oligosphaeridium poculum Jain 1977b		91.88
Oligosphaeridium pulcherrimum (Deflandre and Cookson 1955) Davey and Williams 1966b	129.17	63?
Oligosphaeridium spp.	152.1	48.5
Operculodinium divergens (Eisenack 1954b) Stover and Evitt 1978	41.3	31.97
Ovoidinium verrucosum (Cookson and Hughes 1964) Davey 1970	100	95.84
Palaeocystodinium bulliforme Ioannides 1986	61.6	57.9
Palaeohystrichophora infusorioides Deflandre 1935	99.85	69.42
Palaeoperidinium pyrophorum (Ehrenberg 1838 ex O. Wetzel 1933a) Sarjeant 1967b	73.7	58.04
Palaeotetradinium silicorum Deflandre 1936b	81.54?	73.28
Palynodinium grallator Gocht 1970a	66.77	64.75
Phthanoperidinium amoenum Drugg and Loeblich Jr. 1967	34	29
Phthanoperidinium distinctum Bujak 1994	44.6	42
Raetiaedinium truncigerum (Deflandre 1937b) Kirsch 1991	89.87	75.35
Raphidodinium fucatum Deflandre 1936b	87.07	72.39
Renidinium rigidum Prince et al. 1999	85.61	85.00
Reticulatosphaera actinocoronata (Benedek 1972) Bujak and Matsuoka 1986	35.1	4.18
Rhombodinium draco Gocht 1955	40.5	30.5
Rhombodinium perforatum (Jan du Chêne and Châteauneuf 1975) Lentin and Williams 1977b	37	33.4?
Rhombodinium porosum Bujak 1979	40	33?
Selenopemphix armata Bujak in Bujak et al. 1980	41.8	25.2
Selenopemphix dionaeacysta Head et al. 1989b	17.22	1.92
Senoniasphaera inornata (Drugg 1970b) Stover and Evitt 1978	64.95	62.6
Senoniasphaera protrusa Clarke and Verdier 1967	85.49	81.49
Senoniasphaera rotundata Clarke and Verdier 1967	92.13	73.17
Senoniasphaera rotundata subsp. *alveolata* Pearce et al. 2003	93.07	88.3
Spinidinium echinoideum (Cookson and Eisenack 1960a) Lentin and Williams 1976	87.11	72.49
Spiniferites porosus (Manum and Cookson 1964) Harland 1973		85.14
Spiniferites ramosus subsp. *meandriformis* (Corradini 1973) Lentin and Williams 1975	86.05	74.07
Spiniferites? *velatus* (Clarke and Verdier 1967) Stover and Evitt 1978	83.98	71.86
Spongodinium delitiense (Ehrenberg 1838) Deflandre 1936b	82.57	63.72
Stephodinium coronatum Deflandre 1936a	112.18	87.81
Surculosphaeridium? *longifurcatum* (Firtion 1952) Davey et al. 1966	111.16	81.68
Thalassiphora delicata Williams and Downie 1966c	61	39
Thalassiphora? *spinosa* (Clarke and Verdier 1967) Foucher 1975	82.77	76.89
Triblastula utinensis O. Wetzel 1933b	70.36	68.00
Trichodinium castanea Deflandre 1935 ex Clarke and Verdier 1967	138.60	70.43
Trigonopyxidia ginella (Cookson and Eisenack 1960a) Downie and Sarjeant 1965	89.10	72.34
Trinovantedinium glorianum (Head et al. 1989b) de Verteuil and Norris 1992	11.43	1.97
Trithyrodinium evittii Drugg 1967	65	60?
Trithyrodinium suspectum (Manum and Cookson 1964) Davey 1969b	94.00	71.18?
Unipontidinium aquaeductum (Piasecki 1980) Wrenn 1988	15	13.2
Wetzeliella gochtii Costa and Downie 1976	32.8	26.6
Wetzeliella meckelfeldensis Gocht 1969	53.8	49.4
Xenascus ceratioides (Deflandre 1937b) Lentin and Williams 1973	112.18	72.34
Xiphophoridium alatum (Cookson and Eisenack 1962b) Sarjeant 1966b	98.02?	82.47

Notes: Dinocyst taxon after Williams et al. (2004). LO = last occurrence, FO = first occurrence.

Table T6. Normal polarity intervals for Cenozoic and Cretaceous periods.

Normal polarity interval age (Ma)			
Top	Bottom	Polarity chron	Reference
0.000	0.780	C1n Brunhes	SBP90
0.990	1.070	C1r.1n Jaramillo	SBP90
1.201	1.211	C1r.2n Cobb Mtn.	SBP90
1.770	1.950	C2n Olduvai	SBP90
2.140	2.150	C2r.1n Reunion	CK95
2.581	3.040	C2An.1n Gauss	SPB90/H91
3.110	3.220	C2An.2n	H91
3.330	3.580	C2An.3n	H91
4.180	4.290	C3n.1n Cochiti	H91
4.480	4.620	C3n.2n Nunivak	H91
4.800	4.890	C3n.3n Sidufjall	H91
4.980	5.230	C3n.4n Thvera	H91/SCHPS95
5.875	6.122	C3An.1n	SCHPS95
6.256	6.555	C3An.2n	SCHPS95
6.919	7.072	C3Bn	SCHPS95
7.135	7.170	C3Br.1n	SCHPS95
7.341	7.375	C3Br.2n	SCHPS95
7.406	7.533	C4n.1n	SCHPS95
7.618	8.027	C4n.2n	SCHPS95
8.174	8.205	C4r.1n	SCHPS95
8.631	8.945	C4An	SCHPS95
9.142	9.218	C4Ar.1n	SCHPS95
9.482	9.543	C4Ar.2n	SCHPS95
9.639	9.880	C5n.1n	SCHPS95
9.920	10.839	C5n.2n	SCHPS95
10.943	10.991	C5r.1n	SCHPS95
11.343	11.428	C5r.2n	SCHPS95
11.841	11.988	C5An.1n	SCHPS95
12.096	12.320	C5An.2n	SCHPS95
12.605	12.637	C5Ar.1n	SCHPS95
12.705	12.752	C5Ar.2n	SCHPS95
12.929	13.083	C5AAn	SCHPS95
13.252	13.466	C5ABn	SCHPS95
13.666	14.053	C5ACn	SCHPS95
14.159	14.607	C5ADn	SCHPS95
14.800	14.888	C5Bn.1n	SCHPS95/CK95
15.034	15.155	C5Bn.2n	CK95
16.014	16.293	C5Cn.1n	CK95
16.327	16.488	C5Cn.2n	CK95
16.556	16.726	C5Cn.3n	CK95
17.277	17.615	C5Dn	CK95
18.281	18.781	C5En	CK95
19.048	20.131	C6n	CK95
20.518	20.725	C6An.1n	CK95
20.996	21.320	C6An.2n	CK95
21.768	21.859	C6AAn	CK95
22.151	22.248	C6AAr.1n	CK95
22.459	22.493	C6AAr.2n	CK95
22.588	22.750	C6Bn.1n	CK95
22.804	23.069	C6Bn.2n	CK95
23.353	23.535	C6Cn.1n	CK95
23.677	23.800	C6Cn.2n	CK95
23.999	24.118	C6Cn.3n	CK95
24.730	24.781	C7n.1n	CK95
24.835	25.183	C7n.2n	CK95
25.496	25.648	C7An	CK95
25.823	25.951	C8n.1n	CK95
25.992	26.554	C8n.2n	CK95
27.027	27.972	C9n	CK95
28.283	28.512	C10n.1n	CK95
28.578	28.745	C10n.2n	CK95
29.401	29.662	C11n.1n	CK95
29.765	30.098	C11n.2n	CK95
30.479	30.939	C12n	CK95
33.058	33.545	C13n	CK95
34.655	34.940	C15n	CK95
35.343	35.526	C16n.1n	CK95
35.685	36.341	C16n.2n	CK95
36.618	37.473	C17n.1n	CK95
37.604	37.848	C17n.2n	CK95
37.920	38.113	C17n.3n	CK95
38.426	39.552	C18n.1n	CK95
39.631	40.130	C18n.2n	CK95
41.257	41.521	C19n	CK95
42.536	43.789	C20n	CK95
46.264	47.906	C21n	CK95
49.037	49.714	C22n	CK95
50.778	50.946	C23n.1n	CK95
51.047	51.743	C23n.2n	CK95
52.364	52.663	C24n.1n	CK95
52.757	52.801	C24n.2n	CK95
52.903	53.347	C24n.3n	CK95
55.904	56.391	C25n	CK95
57.554	57.911	C26n	CK95
60.920	61.276	C27n	CK95
62.499	63.634	C28n	CK95
63.976	64.745	C29n	CK95
65.578	67.519	C30n	G95
67.640	68.657	C31n	G95
70.969	71.314	C32n.1n	G95
71.643	73.635	C32n.2n	G95
74.021	74.133	C32r.1n	G95
74.470	79.650	C33n	G95
83.500	120.396	C34n	G95
121.000	123.673	M1n	G95
124.051	124.721	M3n	G95
126.723	127.669	M5n	G95
128.176	128.313	M6n	G95
128.425	128.580	M7n	G95
128.966	129.276	M8n	G95
129.508	129.774	M9n	G95
130.221	130.556	M10n	G95
130.874	131.201	M10Nn.1n	G95
131.252	131.570	M10Nn.2n	G95
131.588	131.880	M10Nn.3n	G95
132.069	132.679	M11n	G95
133.025	133.060	M11r.1n	G95
133.350	133.627	M11An.1n	G95
133.641	133.911	M11An.2n	G95
133.988	134.216	M12n	G95
134.777	134.846	M12r.1n	G95
134.999	135.248	M12An	G95
135.338	135.525	M13n	G95
135.843	136.044	M14n	G95
136.675	137.222	M15n	G95
137.877	139.631	M16n	G95
140.335	140.790	M17n	G95
142.404	143.021	M18n	G95
143.476	143.616	M19n.1n	G95
143.703	144.691	M19n.2n	G95

Notes: SBP90 = Shackleton et al. (1990), H91 = Hilgen (1991a, 1991b), SCHPS95 = Shackleton et al. (1995), CK95 = Cande and Kent (1995), G95 = Gradstein et al. (1995).

Table T7. MST data acquisition parameters, Leg 210.

Measurement	Magnetic susceptibility	GRA bulk density	Natural gamma radiation
Sampling period (s)	—	10	10
Data acquisitions (*N*)	3	—	—
Sampling interval (cm)	2.5	2.5	2.5

Notes: GRA = gamma ray attenuation, MST = multisensor track. *N* = number. — = not applicable.

Table T8. Sediment grain thermal conductivity.

Material	Thermal conductivity (W/[m·K])
Water	0.61
Shale	1.13
Limestone	2.93
Sandstone	4.18

Note: Data from Keen and Beaumont (1990).

CHAPTER NOTE*

N1. Williams, G.L., Boessenkool, K.P., Brinkhuis, H., Pearce, M.A., Fensome, R.A., and Weegink, J.W., unpubl. data. Upper Cretaceous–Neogene dinoflagellate cyst course: morphology, stratigraphy and (paleo)ecology [Urbino, Italy, 4–8 June, 2001].

*Dates reflect file corrections or revisions.